DEVELOPMENT OF A COMBINED PHOTODYNAMIC AND SONODYNAMIC THERAPY FOR THE TREATMENT OF BACTERIAL INFECTIONS

by

Heba Alagha

B.S., in Computer Engineering, University of Jordan, 2005

M.S., in Biomedical Engineering, Boğaziçi University, 2015

Submitted to the Institute of Biomedical Engineering

in partial fulfillment of the requirements

for the degree of

Doctor

of

Philosophy

Boğaziçi University

2023

ACKNOWLEDGMENTS

First and foremost, I would like to express my sincerest gratitude to my thesis supervisor Prof. Dr. Murat Gülsoy for his constant guidance, support, and motivation throughout my entire post-graduate education. Besides, I would like to thank the members of my thesis committee: Prof. Dr. Hale Saybaşılı, Prof. Dr. Bora Garipcan, Assoc. Prof. Dr. Nermin Topaloğlu, and Asst. Prof. Dr. Burcu Güleryüz for their valuable insights and contributions.

I would also like to thank all my colleagues and friends in the Biophotonics laboratory for their help, and for making this journey enjoyable and full of nice memories.

Finally, I am grateful to my family for their continuous help, support, and encouragement throughout my PhD journey.

This research was funded by Boğaziçi University Research Fund Grant Number 15121.

ACADEMIC ETHICS AND INTEGRITY STATEMENT

I, Heba Alagha, hereby certify that I am aware of the Academic Ethics and Integrity Policy issued by the Council of Higher Education (YÖK) and I fully acknowledge all the consequences due to its violation by plagiarism or any other way.

Name :

Signature:

Date:

ABSTRACT

DEVELOPMENT OF A COMBINED PHOTODYNAMIC AND SONODYNAMIC THERAPY FOR THE TREATMENT OF BACTERIAL INFECTIONS

Antimicrobial resistance is one of the biggest threats to global health. Developing new treatment modalities that can eradicate pathogens without inducing drug resistant strains, is of great necessity. Photodynamic therapy (PDT) is such a promising modality that aims to destroy pathogens using light-activated drugs, but is limited by the light penetration depth in tissues. Its close relative, sonodynamic therapy (SDT), has the capability to overcome this limitation, due to the superior tissue penetration of low-intensity ultrasound compared to light, but the full potential of this therapy has not been realized yet. The aim of this PhD research was to develop an efficient antimicrobial therapy via the combination of PDT and SDT. For this purpose, IR780 iodide loaded mesoporous silica nanoparticles were synthesized, and their antimicrobial photodynamic and sonodynamic potentials against gram-positive *Staphylococcus aureus* and methicillin resistant *Staphylococcus aureus*, and gram-negative *Pseudomonas aeruginosa* and multi drug resistant Pseudomonas aeruginosa, were investigated. The antimicrobial photodynamic and sonodynamic potentials of free IR780 iodide were also investigated. The outcomes of the conducted studies demonstrated that both IR780 iodide and IR780 iodide loaded mesoporous silica nanoparticles can be utilized as photo/sono therapeutic agents, for the effective inactivation of drug resistance bacteria. However, IR780 iodide loaded mesoporous silica nanoparticles are more suitable for clinical application.

Keywords: Photodynamic therapy, Sonodynamic therapy, Antimicrobial resistance, IR780 iodide, Mesoporous silica nanoparticles, methicillin resistant *Staphylococcus aureus*, multi drug resistant *Pseudomonas aeruginosa*.

ÖZET

BAKTERİYEL ENFEKSİYONLARIN TEDAVİSİ İÇİN FOTODİNAMİK VE SONODİNAMİK KOMBİNE TERAPİ

Antimikrobiyal direnç, küresel sağlığa yönelik en büyük tehditlerden biridir. İlaca dirençli suşları indüklemeden patojenleri ortadan kaldırabilecek yeni tedavi yöntemleri geliştirmek büyük bir zorunluluktur. Fotodinamik tedavi (FDT), ışık ile aktive edilen ilaçları kullanarak patojenik yapıları yok etmeyi amaçlayan, umut vadedici bir yöntemdir, ancak dokulardaki ışık penetrasyon derinliği ile sınırlıdır. Yakın bağıl, sonodinamik tedavisi (SDT), ışığa kıyasla düşük yoğunluklu ultrasonun üstün doku penetrasyonu nedeniyle bu sınırlamanın üstesinden gelme yeteneğine sahiptir, ancak bu tedavinin tam potansiyeli henüz gerçekleştirilmemiştir. Bu doktora araştırmasının amacı, FDT ve SDT kombinasyonu ile etkili bir antimikrobiyal tedavi geliştirmekti. Bu amaçla, IR780 iyodür yüklü mezopor silika nanopartiküller sentezlendi, gram-pozitif *Staphylococcus aureus* ve metisiline dirençli *Staphylococcus aureus* ve gram-negatif *Pseudomonas aeruginosa* ve çok ilaca dirençli *Pseudomonas aeruginosa*'ya karşı antimikrobiyal fotodinamik ve/ veya sonodinamik potansiyelleri araştırıldı. Serbest IR780 iyodürün antimikrobiyal fotodinamik ve/ veya sonodinamik potansiyelleri de araştırıldı. Yapılan çalışmaların sonuçları, IR780 iyodür ve IR780 iyodür yüklü mezopor silika nanopartiküllerin, ilaç direnci bakterilerinin etkili inaktivasyonu için foto/ sono terapötik ajanlar olarak kullanılabileceğini göstermiştir. Bununla birlikte, IR780 iyodür yüklü mezopor silika nanopartiküller klinik uygulama için daha uygundur.

Anahtar Sözcükler: Fotodinamik tedavi, Sonodinamik tedavi, Antimikrobiyal direnç, IR780 iyodür, Mezopor silika nanopartiküller, metisiline dirençli *Staphylococcus aureus*, çok ilaca dirençli *Pseudomonas aeruginosa*.

TABLE OF CONTENTS

LIST OF FIGURES

LIST OF TABLES

LIST OF SYMBOLS

$^{\circ}C$	Degree Celsius
μg	Microgram
μl	Microlitre
μM	Micromolar
mM	Millimolar
nm	Nanometer
$^1O_2$	Singlet state oxygen
cm^2	Square centimeter
h	Hour
min	Minute
pH	Potential of hydrogen
W	Watt
Δ	Delta

LIST OF ABBREVIATIONS

ANOVA	Analysis of variance
CDC	Center for Disease Control and Prevention
CFU	Colony forming unit
CTAB	Hexadecyl-trimethyl-ammonium bromide
CV	Crystal violet
DMSO	Dimethyl sulfoxide
DPBF	1,3-diphenylisobenzofuran
E. coli	Escherichia coli
NaN3	Sodium azide
Eq.	Equation
ESBL	Extended spectrum beta-lactamase
HMME	Hematoporphyrin monomethyl ether
ICG	Indocyanine green
Laser	Light Amplification by Stimulated Emission of Radiation
MB	Methylene blue
MDR	Multi-drug resistant
MRSA	Methicillin-resistant Staphylococcus aureus
MSN	Mesoporous silica nanoparticles
MSN@IR780	IR780 iodide loaded mesoporous silica nanoparticle
MTT	3-(4,5-dimethylthiazol-2-yl)-2,5-diphenyltetrazolium bromide
NIR	Near infrared
OD	Optical density
P. aeruginosa	*Pseudomonas aeruginosa*
PBS	Phosphate buffered saline
PDT	Photodynamic therapy
pL-ce6	poly-L-lysine chlorin (e6) conjugate
PS	Photosensitizer
PTT	Photothermal therapy

ROS	Reactive oxygen species
S. aureus	*Staphylococcus aureus*
SD	Standard deviation
SEM	Scanning electron microscopy
STEM	Scanning transmission electron microscopy
TBO	Toluidine blue O
TEOS	Tetraethyl orthosilicate
TSA	Tryptic soy agar
TSB	Tryptic soy broth
UCNP	Up-conversion nanoparticles
US	Ultrasound
UV	Ultraviolet
VIS	Visible
HCL	Hydrochloric acid
NH_4OH	Ammonium hydroxide

1. INTRODUCTION

1.1 Motivation

Antimicrobial resistance poses a global serious threat to public health. Infections caused by drug resistant microorganisms including soft-tissue infections, oral infections, burn infection, and surgical wound infections, often fail to respond to antimicrobial drugs, resulting in prolonged illness, increased risk of spreading resistant microorganisms to others, and a greater risk of death [1],[2],[3]. This problem has motivated researchers to search for and develop alternative treatments to combat microbial infections, such as photodynamic therapy (PDT), sonodynamic therapy (SDT), and photothermal therapy (PTT).

PDT is a promising treatment. It is based on the use of light and a drug called photosensitizer (PS) in the presence of oxygen to produce cytotoxicity of target tissues or microorganisms. SDT is a close relative to PDT that involves the use of ultrasound instead of light to activate the photosensitizers. Photothermal therapy (PTT) on the other hand, relies on the generation of hyperthermia to destroy target tissues and microorganisms. These therapies have advantages over conventional therapies, such as the unlikelihood of developing resistance to therapy after repeated use, which is the case with the repeated use of antibiotics [4],[5],[6]. Also, the treatments are non-toxic and easy to apply. However, the full promise of these therapies has not been realized yet, and each therapy suffers from low treatment efficiency. An approach to combine multiple therapies is expected to result in enhanced cytotoxic effect, and improved efficiency.

The aim of this research is to develop an efficient combined therapy for the treatment of bacterial infections caused by resistant bacteria. For this purpose, two separate studies are conducted, one employing IR780 iodide, and the second employing IR780 iodide loaded mesoporous silica nanoparticles, for a combined photodynamic and son-

odynamic therapy against *Staphylococcus aureus*, methicillin resistant *Staphylococcus aureus*, *Pseudomonas aeruginosa*, and multi drug resistant *Pseudomonas aeruginosa*. To our knowledge, this is the first study to combine PDT and SDT using IR780 iodide or IR780 iodide loaded mesoporous silica nanoparticles on reference and resistant strains of gram-positive *Staphylococcus aureus*, and gram-negative *Pseudomonas aeruginosa*.

1.2 Objectives

1. Synthesizing IR780 iodide loaded mesoporous silica nanoparticles, characterizing the nanoparticles, and assessing their photothermal, photodynamic and sonodynamic potentials.

2. Assessing the main parameters (power density, irradiation time, photosensitizer dose) of photodynamic therapy with near-infrared laser (785nm) and its appropriate photosensitizer (IR780 iodide, IR780 iodide loaded mesoporous silica nanoparticles).

3. Assessing the main parameters (US power density, irradiation time, US duty cycle, sonosensitizer dose) of sonodynamic therapy with IR780 iodide or IR780 iodide loaded mesoporous silica nanoparticles.

4. Investigating the photodynamic, sonodynamic, and combined photodynamic and sonodynamic potentials of IR780 iodide against reference and resistant strains of gram-positive Staphylococcus aureus and gram-negative Pseudomonas aeruginosa in vitro, and testing for any thermal effect involved.

5. Investigating the photodynamic, sonodynamic, and combined photodynamic and sonodynamic potentials of IR780 iodide loaded mesoporous silica nanoparticles against reference and resistant strains of gram-positive Staphylococcus aureus and gram-negative Pseudomonas aeruginosa in vitro, and testing for any thermal effect involved.

1.3 Outline

Chapter 2 presents background on infections, common infection causing bacteria, photodynamic therapy, and sonodynamic therapy, with latest research in the field.

Chapter 3 presents the preliminary studies that were conducted to determine the nontoxic doses of ultrasound and 785nm laser light on gram-positive *Staphylococcus aureus* and gram- negative *Pseudomonas aeruginosa*.

Chapter 4 presents the *in vitro* studies conducted to investigate the photodynamic, sonodynamic and combined photodynamic and sonodynamic potentials of IR780 iodide on reference and resistant strains of gram- positive *Staphylococcus aureus* and gram- negative *Pseudomonas aeruginosa*.

Chapter 5 presents the *in vitro* studies conducted to investigate the photodynamic, sonodynamic and combined photodynamic and sonodynamic potentials of IR780 iodide loaded mesoporous silica nanoparticles on reference and resistant strains of gram- positive *Staphylococcus aureus* and gram- negative *Pseudomonas aeruginosa*.

Chapter 6 gives overall discussion and conclusion of the thesis.

2. BACKGROUND

2.1 Microbes and Infections

Infections are caused by microbes that enter the body, multiply, and cause harm, illness, or even death. There are many types of microbes: bacteria, viruses, fungi, and parasites. Infections caused by microbes include soft-tissue infections, oral infections, burn infections, and surgical wound infections which account for almost 25% of nosocomial infections [7]. *Staphylococcus aureus* (*S. aureus*) and *Pseudomonas aeruginosa* (*P. aeruginosa*) are common wound infecting bacteria.

S. aureus is a gram-positive bacterium present in the human microbiota of the nasal mucosa in about 20-40% of the general population [8]. Meanwhile, it is shown to be a potential pathogenic causing skin infections, respiratory tract infections, and post-operative wound infections. *S. aureus* has a high ability to adapt to, and hence develop resistance to antibiotics. Methicillin-resistant *S. aureus* (MRSA) has emerged in 1961 shortly after methicillin was introduced into clinical practice [8]. MRSA is one of the most common causes of community and hospital acquired infections that are becoming very difficult to treat due to the increasing resistance of MRSA to almost all existing classes of antibiotics [9]. If left untreated, MRSA infections can become severe, and may cause life-threatening sepsis.

P. aeruginosa is a gram-negative bacterium that is usually found in soil and water. It is a leading nosocomial pathogen that is responsible for about 10% of hospital acquired infections [10], including pneumonias, urinary tract infections, and surgical site infections [11]. Infections caused by *P. aeruginosa* are associated with high morbidity and mortality compared to infections caused by other pathogens [11]. In addition to having intrinsic resistance to many antibiotics, *P. aeruginosa* is capable of developing resistance to many antibiotics after therapy [11], leading to the emergence of multi drug resistance (MDR) *P. aeruginosa* strains. Multidrug resistant is defined as

resistance to at least three different classes of antimicrobials [12]. According to the Centers for Disease Control and Prevention (CDC), MDR *P. aeruginosa* pose serious threat to public health [13].

2.2 Conventional Treatments and the Emergence of Antimicrobial Resistance

Infections are usually treated with antimicrobial drugs (antibacterial, antifungal, antiviral, and antiparasitic drugs). Each time one takes antimicrobial drugs, he increases the chances that microbes in his body will learn to resist these drugs by adapting their structure or function, in some way that prevents them from being killed by the antimicrobial drugs, causing antimicrobial resistance. The development of antimicrobial resistance, and the evolution of resistant strains is a natural phenomenon, however, some human actions, such as the misuse of antimicrobial drugs, accelerate the emergence of drug resistant strains.

Infections caused by drug resistant strains often fail to respond to antimicrobial drugs that may have worked effectively before the resistance occurred, leading to prolonged illness, delayed healing, and could even become life threatening, especially to patients with diabetes or who take cancer chemotherapy, and need to undergo a surgery, since they are at increased risk of post-surgical wound infections [7]. This problem has become a serious threat to public health that there is urgent need for the development of innovative and efficient alternative antimicrobial treatments for infections.

2.3 Alternative Therapies to Address the Antimicrobial Resistance

In the search for new alternative therapies to fight against microbial infections that can overcome the problem of developing resistance to therapy after repeated use,

non-conventional therapies such as photodynamic therapy, photothermal therapy, and sonodynamic therapy stand as promising alternatives.

2.3.1 Photodynamic Therapy (PDT)

Photodynamic therapy (PDT) involves the use of a drug called a photosensitizer (PS), along with light of appropriate wavelength, in the presence of oxygen to destroy target cells or microorganisms. The treatment starts with the administration of a photosensitizer, either topically or intravenously, followed by the uptake of this compound, and a selective accumulation in the target cells or microorganisms. Then, the photosensitizer is irradiated with light of the appropriate wavelength. Upon absorption of light energy, the photosensitizer gets excited to the first excited singlet state, from which it can relax to the more long-lived triplet state. This triplet PS can interact with molecular oxygen in two pathways, type I reaction (electron transfer), and type II reaction (photon-induced energy transfer), leading to the formation of oxygen radicals and singlet oxygen, respectively. The generated reactive oxygen species (ROS) oxidize intracellular molecules and thereby destroy target cells or microorganisms [14].

The concept of photodynamic therapy as a treatment modality to eradicate microorganisms has been around for more than a century [15]. However, the potential of PDT against microbial infections was not utilized for several decades, mainly due to the discovery of antibiotics. Nevertheless, the rapid emergence of resistance to even those antibiotics which initially appeared to be highly effective, has revived the interest in PDT as an antimicrobial therapy. Within the past decade, it has become clear that PDT has a good potential for the treatment of microbial infections [16],[17],[18],[19]. The suggested mechanisms to account for the lethal damage caused to bacteria by PDT include: oxidation of membrane lipids, cross-linking of proteins, and oxidative damage to nucleic acids (Figure 2.1), which result in the disruption of the normal functioning of the microorganism [20].

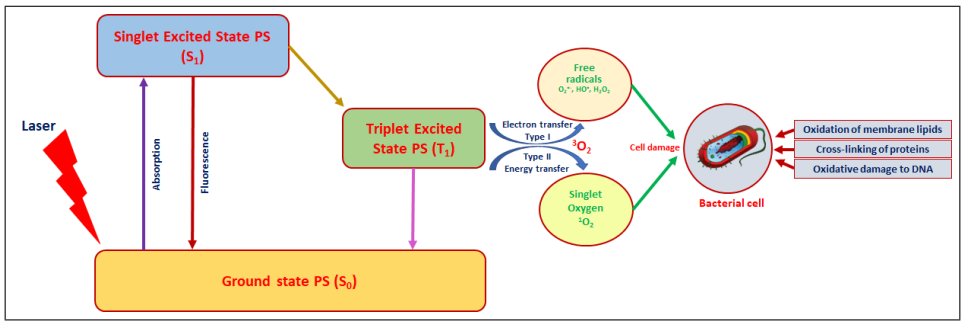

Figure 2.1 Schematic illustration of photodynamic therapy on bacteria.

PDT possesses several favorable features such as:

- Broad spectrum of action, since one photosensitizer can act on bacteria, fungi, yeasts, and parasitic protozoa.
- Small probability to promote the onset of mutagenicity.
- Localized treatment with minimal toxicity to healthy tissue.
- Ease of application.
- And most important in the treatment of microbial infections, is that chances that microorganisms can develop resistance to PDT are highly unlikely, which means that repeated administrations of PDT can be applied [21].

The main limitation of PDT is that the light needed to activate most photosensitizers cannot pass more than about one centimeter through the tissue, which limits the application of PDT to superficial areas on or just under the skin, or on the lining of internal organs [22],[23]. To overcome this issue, ultrasound has been suggested as an alternative energy source to excite the photosensitizers, as it has superior tissue penetration. Besides, most of the photosensitizers can be excited by ultrasound as well, and thus ca be used as sonosensitizers [24],[25].

2.3.2 Sonodynamic Therapy (SDT)

Similar to PDT, SDT starts by the administration of a sonosensitizer, followed by uptake of this compound, and a selective retention in the target tissue. The target tissue is then irradiated by ultrasound. Ultrasound interacts with surrounding aqueous environment, and results in the presence of a unique phenomenon known as acoustic cavitation [24]. As a result of acoustic cavitation, ROS will be generated. Although the exact mechanism by how ROS are generated by acoustic cavitation is not fully understood, there are two accepted hypotheses to explain that; the first hypothesis suggests that the high energy release associated with acoustic cavitation can lead to sonolysis of water molecules and/or the sonosensitizer molecules. The formed radicals can then react with oxygen, triggering the production of ROS. The second hypothesis suggests the involvement of sonoluminescence (light generated as a result of enormous concentration of energy associated with acoustic cavitation), in the generation of ROS by triggering a purely photodynamic process [26]. According to this hypothesis, the sonosensitizer can be activated to an excited state upon absorption of the emitted sonoluminescent light, and can experience the two types of reactions as in PDT (Figure 2.2) [27]. SDT has been recently investigated as an antimicrobial therapy [28],[29],[30],[31],[32],[33],[34],[35].

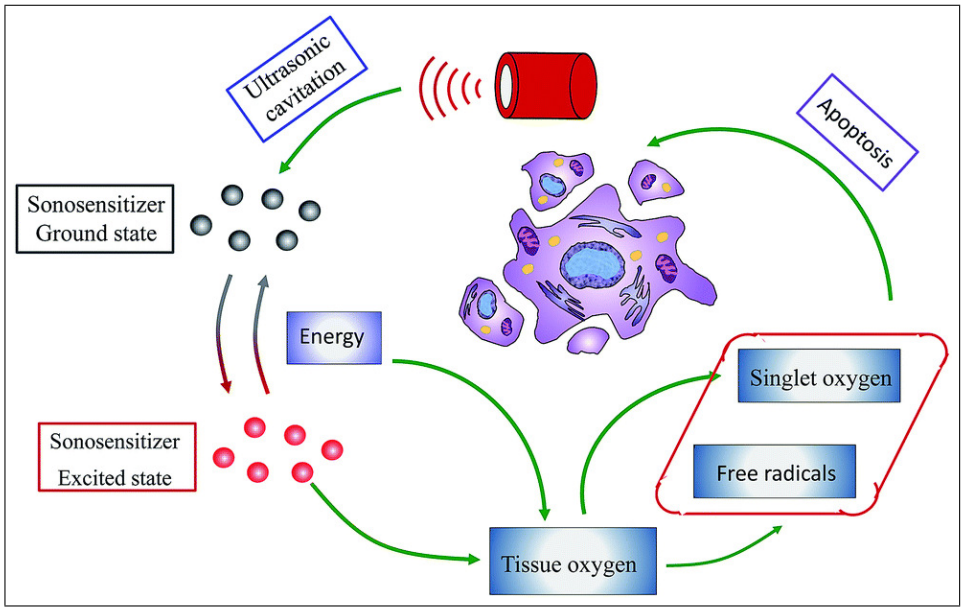

Figure 2.2 Schematic illustration of mechanism of sonodynamic therapy [27].

2.3.3 Photosensitizers, Sonosensitizers, and Nanocarriers

The choice of the photo/sonosensitizer plays an important role in the success of PDT and SDT. The prerequisites for an ideal sensitizer include chemical purity, chemical and physical stability, activation at wavelengths with optimal tissue penetration (for PDT), low dark toxicity, solubility in water, high quantum yield of the long-lived triplet state, selectivity for target cells, short time interval between administration and maximal accumulation within target tissues, and rapid clearance from the body [36],[37].

IR780 iodide is a near-infrared (NIR) dye with a peak absorption of 780 nm in human plasma, which coincides with the therapeutic window (600-1000 nm) [38], allowing relatively deeper tissue penetration. IR780 iodide has some favorable characteristics that make it desirable for use in medical diagnosis and therapy: Its high fluorescence intensity and preferential accumulation in tumor cells, make it a desirable dye for medical imaging [39],[40],[41], its ability to generate heat upon laser irradiation, enables its utilization as a photothermal agent in photothermal therapy [41],[42] and its capability of producing reactive oxygen species, makes it a promising agent for use as a photosensitizer in PDT [43],[44],[45], and as a sonosensitizer in SDT [46].

Despite the favorable characteristics of IR780 iodide, its hydrophobicity and toxicity limit its clinical application [44],[45]. To overcome these limitations, the use of nanoparticles to encapsulate and deliver IR780 iodide to target cells, stands as a promising approach [44],[45],[47],[48],[49],[50],[51].

The use of nanoparticles as photo/sonosensitizer carriers in PDT/SDT can resolve some of the challenges associated with classical PDT/SDT such as:

- Increasing the amount of photo/sonosensitizer that can be delivered to target cells (cancer cells, microbial cells), due to their large surface to volume ratios.
- Preventing the premature release of photo/sonosensitizer and potential inactiva-

tion of the drug by plasma components, which reduce the efficacy of conventional PDT/SDT.

- Their surface can be further modified with functional groups or targeting agents, thereby improving the biodistribution pharmacokinetics, cell uptake, and targeting abilities. [52],[53],[54],[55],[56],[57],[58],[59].

In recent years, mesoporous silica nanoparticles (MSN) have received high attention for their potential biomedical applications, especially as nanocarriers, due to their unique properties such as ease of synthesis, controllable particle size, good biocompatibility, easy functionalization, and large specific surface area and pore volume, enabling high loading capacity of drugs [60],[61],[62],[63],[64],[65].

The anticancer and antimicrobial photodynamic potentials of MSN encapsulating different PSs have been investigated so far with promising results [66],[67],[68],[69], [70],[71],[72],[73],[74],[75],[76],[77]. It was only recently that the anticancer photodynamic potential of MSNs loaded with IR780 iodide was investigated in a study conducted by Yu et al. [78]. In the study, manganese doped MSNs were synthesized, loaded with IR780, further coated with manganese, and their anticancer effect was investigated on mouse oral cancer (MOC2) and Lewis lung carcinoma (LLC) cells *in vitro*, and MOC2 injected mice in vivo. The results of the in vitro studies indicated that the designed nanoplatform induced a higher cell-killing effect than IR780 iodide alone, while the results of the *in vivo* studies demonstrated that the designed nanoplatform inhibited tumor growth and tumor metastasis.

The anticancer and antimicrobial sonodynamic potentials of MSN loaded with sonosensitizers were investigated in few studies [79],[80].

2.3.4 Antimicrobial combined photodynamic and sonodynamic therapy

The scientific basis of both PDT and SDT relies on the generation of ROS, and the fact that both PDT and SDT trigger similar events and induce similar biological responses has motivated researchers to investigate the combined effect of the two therapies for cancer treatment [81],[82],[83],[84],[85]. Xu et al. reported the first integrative use of PDT and SDT for the treatment of antibiotic resistant bacteria. In his study, hematoporphyrin monomethyl ether (HMME) was enclosed into the core of yolk-structured multifunctional up-conversion nanoparticles (UCNPs). The combined PDT and SDT efficacy of these UCNPs for the inhibition of MRSA and extended spectrum beta-lactamase (ESBL)-producing *E. coli* strains, was tested *in vitro*. Results revealed that the combined PDT and SDT resulted in a greater inhibition rate (100%) as compared with either PDT (74.2%) or SDT (70%) alone [86]. Few studies have recently investigated the combined effect of PDT and SDT for bacterial infections [87],[88].

To our knowledge, the antimicrobial photodynamic and sonodynamic potentials of MSN encapsulating IR780 iodide has not been investigated so far.

In the light of this background, we report the investigation of the antimicrobial photodynamic, sonodynamic, and combined photodynamic and sonodynamic potentials of IR780 iodide, and IR780 iodide loaded mesoporous silica nanoparticles on *S. aureus*, MRSA, *P. aeruginosa*, and MDR *P. aeruginosa* for the first time, in addition to the evaluation of the post treatment antibiofilm efficacy of IR780 iodide loaded mesoporous silica nanoparticles mediated PDT, SDT, and combined PDT and SDT on MRSA and MDR *P. aeruginosa*.

3. PRELIMINARY STUDIES

3.1 Introduction

Preliminary studies were conducted to determine the suitable laser and ultrasound doses on *S. aureus* (ATCC 25923) and *P. aeruginosa* (ATCC 27853).

3.2 Materials and Methods

3.2.1 Materials

Tryptic soy agar (TSA) and Tryptic soy broth (TSB) were purchased from Merck KGaA (Darmstadt, Germany). Phosphate buffer saline (PBS, pH 7.4) was purchased from AppliChem GmbH (Darmstadt, Germany).

3.2.2 Bacterial Strains

The bacterial strains used were *S. aureus* (ATCC 25923) and *P. aeruginosa* (ATCC 27853). Working in the biosafety cabinet, 10 ml of Sterile TSB was added to a sterile 50 ml falcon tube. An isolated colony from a freshly prepared agar plate was picked with a sterile loop, and used to inoculate the sterile TSB by submerging the loopful of bacteria into the sterile TSB. After overnight incubation at 37 °C in a shaking incubator (rpm=225 for *S. aureus*, and rpm=200 for *P. aeruginosa*), the bacterial suspension was centrifuged at 3000 rpm for 10 min at room temperature, and the pellet was resuspended in PBS (pH 7.4) to a final concentration of 10^7-10^8 CFU/ml.

3.2.3 Laser Source

Laser irradiation was provided by an infrared diode laser system at 785 nm (MDL-III-785, Changchun, China) in a continuous wave mode. The distance from the tip of the laser output to the bottom of the 12-well plate was adjusted so that the diameter of the laser beam matches exactly with the diameter of the wells of the 12-well plate, in order to maximize the irradiated surface covered. The laser output power was changed to give five different light intensities (100, 200, 300, 400, and 500 mW/cm^2).

3.2.4 Effect of 785 nm Laser Light on Bacterial Cell Viability

800 μl aliquots of bacterial suspensions were transferred into the wells of 12-well plate and mixed with 800 μl of PBS (pH 7.4) in each well. The wells were then exposed to laser light (except for a control group) at five different intensities (100, 200, 300, 400, and 500 mW/cm^2), for a duration of 5 min. One well was irradiated at a time. Following laser irradiation, the bacterial suspensions in all groups were diluted according to serial dilution method. Diluted samples were plated on tryptic soy agar plates, and incubated in the dark for 24 h. The number of CFU was counted with the naked eye and multiplied by the dilution factor to determine viable bacteria. Experiments were conducted in triplicate.

3.2.5 Ultrasound Source

Ultrasound (US) irradiation was provided by a therapeutic ultrasound unit (Sonoplus 190, Enraf-Nonius B.V., Rotterdam, Netherlands), which has a frequency of 1 MHz and a maximum intensity of 2 W/cm^2. The US probe was placed in contact with the 12-well plate. Adequate contact between the bottom of the multi-well plate and the surface of the US probe was facilitated by using an ultrasound gel.

3.2.6 Effect of Ultrasound on Bacterial Cell Viability

To test the effect of US, 800 μl aliquots of bacterial suspensions were transferred into the wells of 12-well plates and mixed with 800 μll of PBS (pH 7.4) in each well. The wells (except for a control group) were then exposed to US at different doses. Following US irradiation, the bacterial suspensions in all groups were diluted according to serial dilution method. Diluted samples were plated on tryptic soy agar plates and incubated in the dark for 24 h. The number of CFU was counted with the naked eye and multiplied by the dilution factor to determine viable bacteria. Experiments were conducted in triplicate.

3.2.7 Temperature Measurements

Infrared thermal thermometer (Raytek, Raynger ST, CA, USA) was used to record temperature before and after each laser or US application. Results are means of three independent experiments (n=3).

3.2.8 Statistical Analysis

All data were expressed as mean ± standard deviation (SD). Comparison among the different groups was assessed by one-way analysis of variance (ANOVA) followed by the Tukey test. A ($p \leq 0.05$) was used to indicate statistical significance.

3.3 Results

3.3.1 Effect of 785 nm Laser Light on Bacterial Cell Viability

No decrease in bacterial cell viability was observed in any group compared to the control group, for both tested strains *S. aureus* (ATCC 25923) and *P. aeruginosa*

(ATCC 27853) ($P > 0.05$). The highest dose (500 mW/cm^2, 5 min) was selected to be used in PDT studies for *S. aureus*, MRSA, *P. aeruginosa*, and MDR. *P. aeruginosa*. The results are plotted in Figure 3.1 for *S. aureus*, and Figure 3.2 for *P. aeruginosa*.

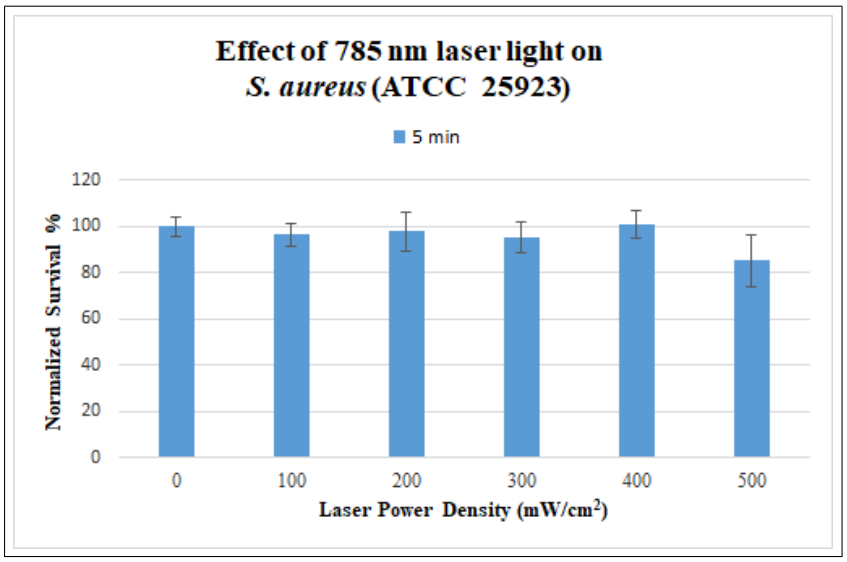

Figure 3.1 Effect of 785 nm laser light (5 min) on *S. aureus* (ATCC 25923) viability. Data are mean values ± SD of triplicate experiments (n=3).

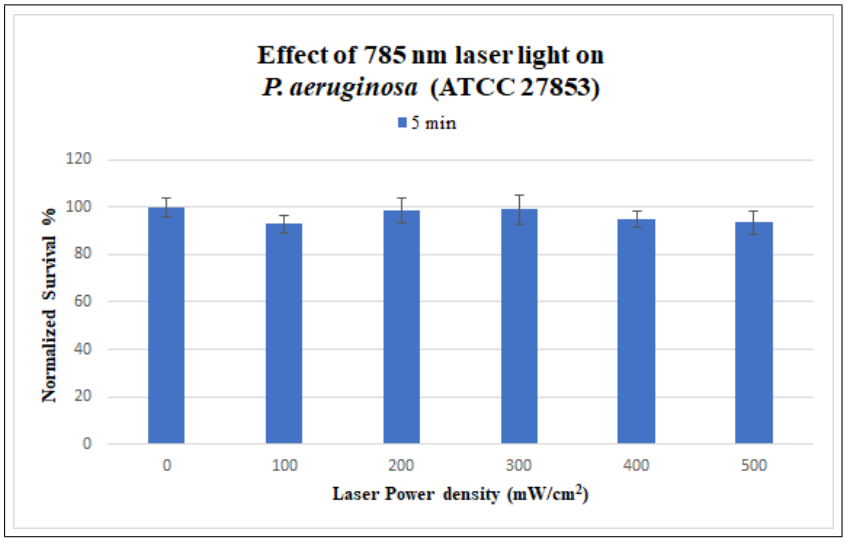

Figure 3.2 Effect of 785 nm laser light (5 min) on *P. aeruginosa* (ATCC 27853) viability. Data are mean values ± SD of triplicate experiments (n=3).

3.3.2 Effect of Ultrasound on Bacterial Cell Viability

Power densities up to 2W/cm^2, exposure times up to 5 min, and duty cycles (20%, 50%, and 100%) were tested. 2 W/cm^2 and continuous wave (100% duty cycle) caused heating of the probe and frequent stops during irradiation, so they were excluded. The combination of 1.5 W/cm^2 with 50% duty cycle was tested for different irradiation times. For *S. aureus* (ATCC 25923), exposure times 4 min and 5 min showed some decrease in cell viability compared to the control group ($p \leq 0.05$). Therefore, the US dose of (1.5 W/cm^2, 50% duty cycle, 3 min) was chosen to be used in SDT experiments for *S. aureus* (ATCC 25923) and MRSA. For *P. aeruginosa* (ATCC 27853), no decrease in bacterial cell viability was observed in any group compared to the control group ($P > 0.05$). However, and for comparative reasons, the US dose of (1.5 W/cm^2, 50% duty cycle, 3 min) was chosen to be used in SDT experiments for *P. aeruginosa* (ATCC 27853) and MDR *P. aeruginosa*. The results are plotted in Figure 3.3 for *S. aureus*, and Figure 3.4 for *P. aeruginosa*.

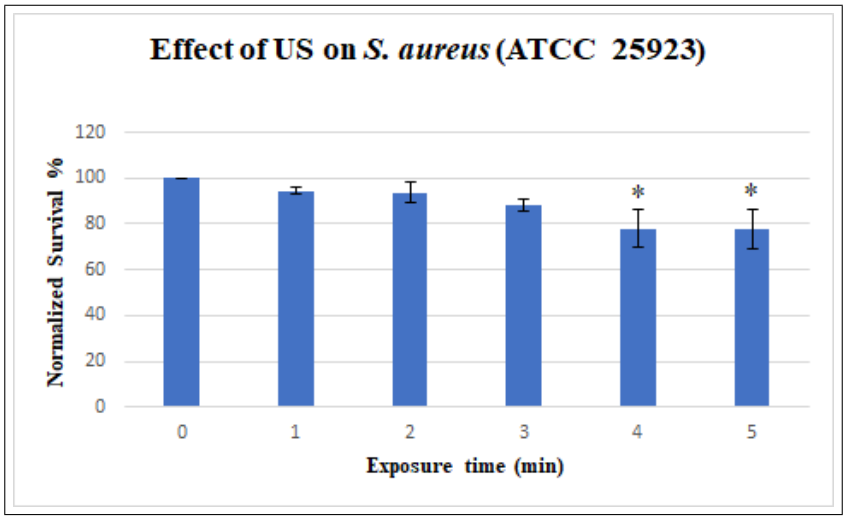

Figure 3.3 Effect of US (1.5 W/cm^2, 50% duty cycle, 1-5 min) on *S. aureus* (ATCC 25923) viability. $*$ indicates statistical significance ($p \leq 0.05$) compared to the control group. Data are mean values $\pm$ SD of triplicate experiments (n=3).

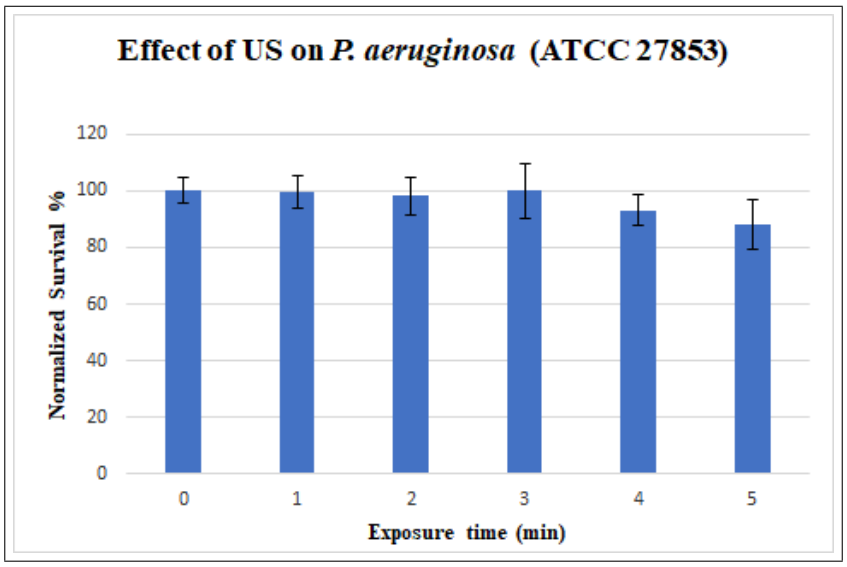

Figure 3.4 Effect of US (1.5 W/cm^2, 50% duty cycle, 1-5 min) on *P. aeruginosa* (ATCC 27853) viability. $*$ indicates statistical significance ($p \leq 0.05$) compared to the control group. Data are mean values $\pm$ SD of triplicate experiments (n=3).

3.3.3 Temperature Measurements

Figures 3.5 and 3.6 show the increase in temperature during laser light (500 mW/cm^2, 5 min) and US (1.5 Wcm^2, 50% duty cycle, 3 min) irradiations on *S. aureus* (ATCC 25923) and *P. aeruginosa* (ATCC 27853), as recorded by an infrared thermometer. No statistically significant difference was found between *S. aureus* and *P. aeruginosa*, in response to laser light or US irradiations ($P > 0.05$). Temperature increase in response to laser light irradiation was about 2 °C, while it was about 6 °C in response to US irradiation.

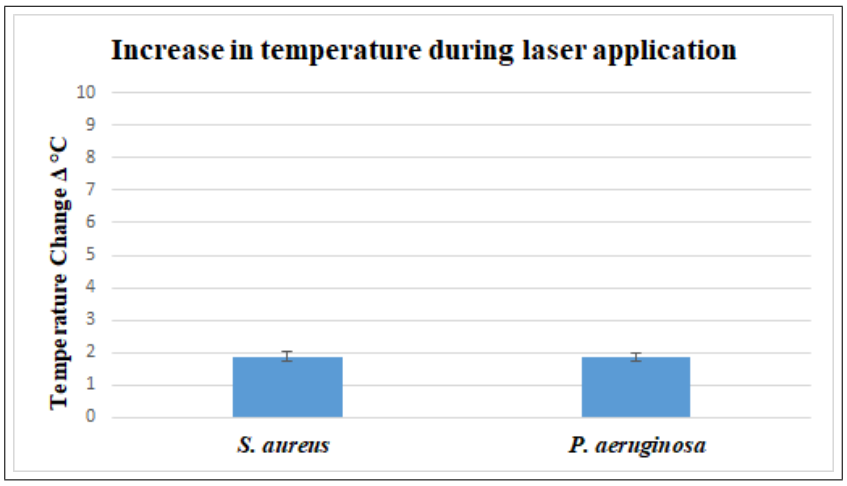

Figure 3.5 Temperature increase during laser light exposure (500 mW/cm^2, 5 min) on *S. aureus (ATCC 25923)* and *P. aeruginosa* (ATCC 27853). Data are mean values ± SD of triplicate experiments (n=3).

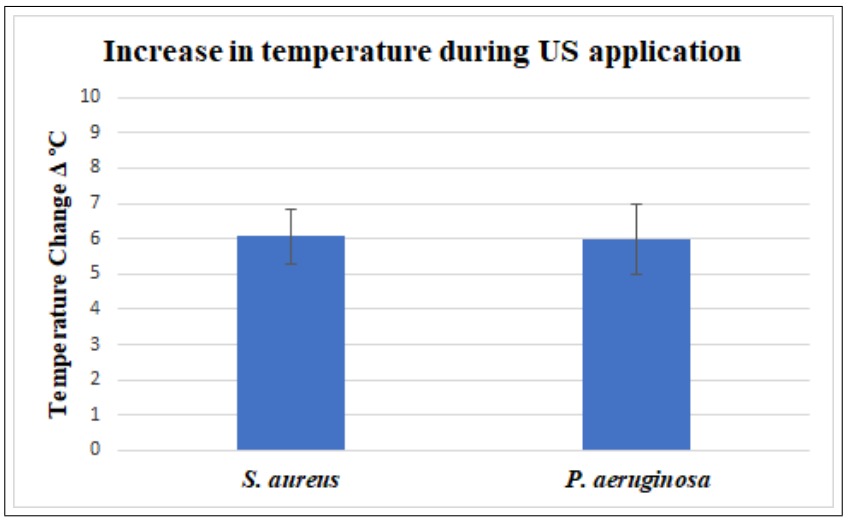

Figure 3.6 Temperature increase during US exposure (1.5 W/cm^2, 50% duty cycle, 3 min) on *S. aureus (ATCC 25923)* and *P. aeruginosa* (ATCC 27853). Data are mean values ± SD of triplicate experiments (n=3).

3.4 Discussion and Conclusion

It is important to optimize the laser parameters (power density, irradiation time, etc.), and US parameters (power density, irradiation time, duty cycle, etc.), to achieve optimal PDT and SDT effects. The aim of this study was to determine the suitable laser and US doses on *S. aureus* (ATCC 25923) and *P. aeruginosa* (ATCC 27853). The highest nontoxic doses of laser and US were selected to be used for upcoming PDT,

SDT, and combined PDT and SDT studies, because this would give higher treatment efficiencies at the same photo/sonosensitizer doses.

4. ANTIMICROBIAL PDT, SDT, AND COMBINED PDT AND SDT USING IR780 IODIDE: *IN VITRO STUDY*

4.1 Introduction

IR780 iodide is a NIR dye with a peak absorption of 780 nm in human plasma, which coincides with the therapeutic window (600-1000 nm) [38], allowing relatively deeper tissue penetration. IR780 iodide has some favorable characteristics that make it desirable for use in medical diagnosis and therapy: Its high fluorescence intensity and preferential accumulation in tumor cells, make it a desirable dye for medical imaging [39],[40],[41], its ability to generate heat upon laser irradiation, enables its utilization as a photothermal agent in photothermal therapy [41],[42], and its capability of producing reactive oxygen species, makes it a promising agent for use as a photosensitizer in PDT [43],[44],[45], and as a sonosensitizer in SDT [46].

The aim of this study is to investigate the photodynamic, sonodynamic, and combined photodynamic and sonodynamic potentials of IR780 iodide on gram-positive *S. aureus* and MRSA, and gram-negative *P. aeruginosa* and MDR *P. aeruginosa in vitro*.

4.2 Materials and Methods

4.2.1 Materials

IR-780 iodide (≥95%), Absolute ethanol (≥99.9%), and 1,3 Diphenylisobenzofuran (DPBF, 97%) were purchased from Sigma-Aldrich (Darmstadt, Germany). Tryptic soy agar and Tryptic soy broth were purchased from Merck KGaA (Darmstadt, Germany). Phosphate buffer saline (PBS, pH 7.4) was purchased from AppliChem GmbH (Darmstadt, Germany). Sodium Azide (NaN3, ≥99%) was purchased from Biomatik

Corporation (Ontario, Canada). All chemicals were used without further purification.

4.2.2 Bacterial Strains

The bacterial strains used in this study were methicillin susceptible *S. aureus* (ATCC 25923), methicillin-resistant *S. aureus* (MRSA, clinically isolated), *P. aeruginosa* (ATCC 27853), and multi-drug resistant *P. aeruginosa* (MDR *P. aeruginosa*, clinically isolated). Working in the biosafety cabinet, 10 ml of sterile TSB was added to a sterile 50 ml falcon tube. An isolated colony from a freshly prepared agar plate was picked with a sterile loop and used to inoculate the sterile TSB by submerging the loopful of bacteria into the sterile TSB. After overnight incubation at 37 $^{\circ}C$ in a shaking incubator (rpm=225 for *S. aureus* and MRSA, and rpm=200 for *P. aeruginosa* and MDR *P. aeruginosa*), the bacterial suspension was centrifuged at 3000 rpm for 10 min at room temperature, and the pellet was resuspended in PBS (pH 7.4) to a final concentration of 10^7-10^8 CFU/ml.

4.2.3 Laser Source

Laser irradiation was provided by an infrared diode laser system at 785 nm (MDL-III-785, Changchun, China) in a continuous wave mode with an output laser power of 1.95 W. The distance from the tip of the laser output to the bottom of the multi-well plate was fixed to give laser irradiation of 500 mW/cm^2. Laser exposure time was 5 min, based on the preliminary studies conducted. The experimental setup is shown in Figure 4.1.

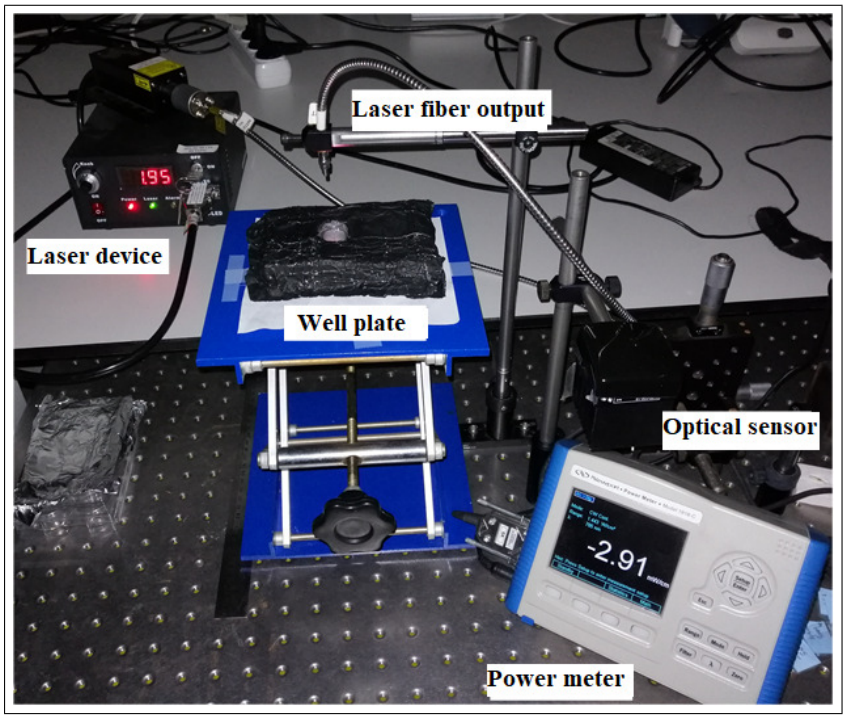

Figure 4.1 Experimental setup for PDT studies using 785 nm diode laser. The distance from the tip of the laser output to the bottom of the multi-well plate was fixed to give laser irradiation of 500 mW/cm^2.

4.2.4 Ultrasound Source

US irradiation was provided by a therapeutic ultrasound unit (Sonoplus 190, Enraf-Nonius B.V., Rotterdam, Netherlands) at a frequency of 1 MHz, intensity of 1.5 W/cm^2, 50% duty cycle, and 3 min exposure time. US parameters were selected based on the preliminary studies conducted. The US probe was placed in contact with the 12-well plate. Adequate contact between the bottom of the multi-well plate and the surface of the US probe was facilitated by using an ultrasound gel. The experimental setup is shown in Figure 4.2.

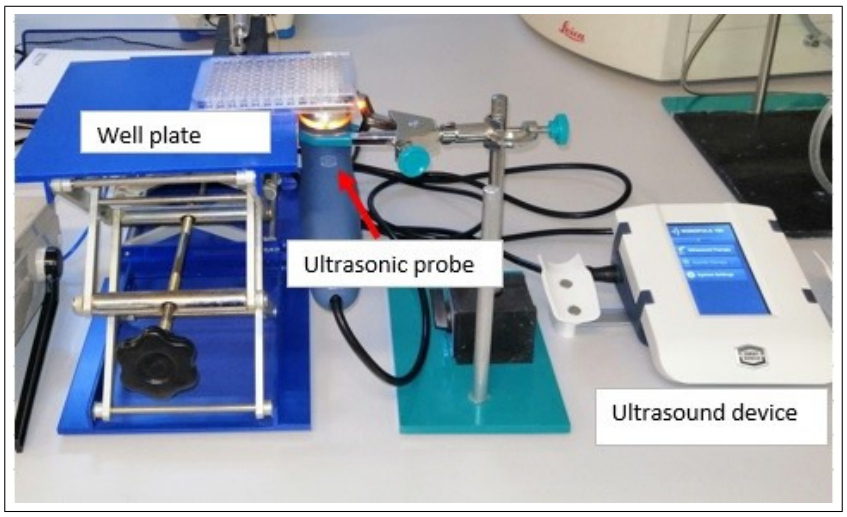

Figure 4.2 Experimental setup for SDT studies using therapeutic ultrasound unit (Sonoplus 190, Enraf-Nonius B.V., Rotterdam, Netherlands). Adequate contact between the bottom of the multi-well plate and the surface of the US probe was facilitated by using an ultrasound gel.

4.2.5 PDT Studies

The following groups were tested for each bacterial strain:

- G1: control; no laser, no PS.
- G2: IR780 iodide only (1-3 μM).
- G3: PDT; IR780 iodide (1-3 μM) + laser (500 mW/cm^2, 5 min).

12-well plates were used for the experiments, as the diameter of the wells matched well with the laser beam diameter, thus maximizing the irradiated surface covered. 800 μl aliquots of bacterial suspensions were transferred into the wells of 12-well plates. For groups G2 and G3, 800 μl of IR780 iodide solutions (1-3 μM) were added to each well, mixed with bacteria, and incubated in the dark for 30 min. In G1 group, the bacterial suspension in the well was mixed with equal volume (800 μl) of PBS (pH 7.4). The bacterial suspensions in PDT groups were exposed to laser light (500 mW/cm^2, 5 min). Following laser light exposure, the bacterial suspensions in all groups were diluted according to serial dilution method. Diluted samples were plated

on tryptic soy agar plates and incubated at 37 $^{\circ}C$ for 24 h. The number of CFU was counted with the naked eye and multiplied by the dilution factor to determine viable bacteria. Experiments were conducted in triplicate.

4.2.6 SDT Studies

The following groups were tested for each bacterial strain:

- G1: control; no US, no sonosensitizer.
- G2: IR780 iodide only (1-3 μM).
- G3: SDT; IR780 iodide (1-3 μM) + US (1.5 W/cm^2, 50% duty cycle, 3 min).

12-well plates were used for the experiments. 800 μl aliquots of bacterial suspensions were transferred into the wells of 12-well plates. For groups G2 and G3, 800 μl of IR780 iodide solutions (1-3 μM) were added to each well, mixed with bacteria, and incubated in the dark for 30 min. In G1 group, the bacterial suspension in the well was mixed with equal volume (800 μl) of PBS (pH 7.4). The bacterial suspensions in G2 and G3 groups were exposed to US irradiation (1.5 W/cm^2, 50% duty cycle, 3 min). One well was irradiated at a time. Following ultrasound exposure, the bacterial suspensions in all groups were diluted according to serial dilution method. Diluted samples were plated on tryptic soy agar plates and incubated at 37 $^{\circ}C$ for 24 h. The number of CFU was counted with the naked eye and multiplied by the dilution factor to determine viable bacteria. Experiments were conducted in triplicate.

4.2.7 Combined PDT and SDT studies

Based on the results of PDT and SDT studies, The concentration of 2 μM IR780 iodide was chosen to be applied in the combined treatment, as it showed no

dark toxicity and best PDT and SDT results. The following groups were tested for each bacterial strain:

- G1: control; No laser, no US, no PS.
- G2: IR780 iodide only (2 μM)
- G3: PDT; IR780 iodide (2 μM) + laser (500 mW/cm^2, 5 min).
- G4: SDT; IR780 iodide (2 μM) + US (1.5 W/cm^2, 50% duty cycle, 3 min).
- G5: SPDT; SDT followed by PDT.
- G6: PSDT; PDT followed by SDT.

12-well plates were used for the experiments. 800 μl aliquots of bacterial suspensions were transferred into the wells of 12-well plates. For groups G2-G6, 800 μl of IR780 iodide solutions (2 μM) were added to each well, mixed with bacteria, and incubated in the dark for 30 min. In G1 group, the bacterial suspension in the well was mixed with equal volume (800 μl) of PBS (pH 7.4). The bacterial suspension in G3 group was exposed to laser light (500 mW/cm^2, 5 min). The bacterial suspension in G4 group was exposed to US irradiation (1.5 W/cm^2, 50% duty cycle, 3 min). The bacterial suspension in G5 group was exposed to US irradiation (1.5 W/cm^2, 50% duty cycle, 3 min) followed by laser light (500 mW/cm^2, 5 min). The bacterial suspension in G6 group was exposed to laser light (500 mW/cm^2, 5 min), followed by US irradiation (1.5 W/cm^2, 50% duty cycle, 3 min). Following light and US exposures, the bacterial suspensions in all groups were diluted according to serial dilution method. Diluted samples were plated on tryptic soy agar plates and incubated at 37 $^\circ C$ for 24 h. The number of CFU was counted with the naked eye and multiplied by the dilution factor to determine viable bacteria. Experiments were conducted in triplicate.

4.2.8 Bacterial Cell Viability in the Presence of ROS Quenchers

For MRSA and MDR *P. aeruginosa*, the photodynamic and sonodynamic effects of IR780 iodide were tested utilizing NaN3 as a singlet oxygen quencher. For MRSA, the following groups were tested:

- G1: control.
- G2: control + NaN3.
- G3: PDT.
- G4: PDT + NaN3.

For MDR *P. aeruginosa*, the following groups were tested:

- G1: control.
- G2: control + NaN3.
- G3: PDT.
- G4: PDT + NaN3.
- G5: SDT.
- G6: SDT + NaN3.

12-well plates were used for the experiments. 800 μl aliquots of bacterial suspensions were transferred into the wells of 12-well plates. In groups G3 and G5, 800 μl of IR780 iodide solutions (specific concentration for each bacterial strain) were added to each well, mixed with bacteria, and incubated in the dark for 30 min. In groups G4, and G6, 800 μl of IR780 iodide and NaN3 were added to each well, mixed with bacteria (final concentration of NaN3 was 50 mM), and incubated in the dark for 30 min. In G1 group, the bacterial suspension in the well was mixed with 800 μl of PBS. In G2

group, the bacterial suspension in the well was mixed with 800 μl of PBS and NaN3 (final concentration of NaN3 was 50 mM). The bacterial suspensions in G3 and G4 groups were exposed to laser light (500 mW/cm^2, 5 min). The bacterial suspensions in G5 and G6 groups were exposed to US irradiation (1.5 W/cm^2, 50% duty cycle, 3 min). Following light and US exposures, the bacterial suspensions in all groups were diluted according to serial dilution method. Diluted samples were plated on tryptic soy agar plates and incubated at 37 $°C$ for 24 h. The number of CFU was counted with the naked eye and multiplied by the dilution factor to determine viable bacteria. Experiments were conducted in triplicate.

4.2.9 Temperature Measurements

An infrared thermal thermometer (Raytek, Raynger ST, CA, USA) was used to record the temperature before and after each laser or US application. Also, an infrared thermal camera (Flir E5, Teledyne FLIR, Täby, Sweden) was used to detect the temperature change during 785 nm laser irradiation (500 mW/cm^2, 5min), and US irradiation (1.5 W/cm^2, 50% duty cycle, 3 min) of IR780 iodide solution (2 μM). Results are means of three independent experiments (n=3).

4.2.10 Reactive Oxygen Species (ROS) Detection

1,3-Diphenylisobenzofuran (DPBF) was used to detect the ability of by IR780 iodide to produce ROS in response to laser or US irradiation, indirectly. Briefly, 10 mM stock solution of DPBF was prepared in ethanol, and kept in the dark. 1 μl of the stock solution was mixed with 1 ml of either IR780 iodide (0.25, 1.5, and 2 μM) or PBS (pH 7.4) in 10 mm cuvettes, and the solutions in the cuvettes were exposed to either laser or US. For laser irradiations, 785 nm laser light (500 mW/cm^2) was applied for 5 min, and the absorbance intensity at 410 nm was recorded initially and after every 1 min of laser irradiation. For US irradiations, US (1.5 W/cm^2, 50% duty cycle) was applied for 3 min, and the absorbance intensity at 410 nm was recorded initially and after every 1

min of US irradiation. Results are means of three independent experiments (n=3).

4.2.11 Statistical Analysis

All data were expressed as mean ± SD. Comparison among the different groups was assessed by one-way analysis of variance (ANOVA) followed by the Tukey test. A ($p \leq 0.05$) was used to indicate statistical significance.

4.3 Results

4.3.1 PDT Studies

4.3.1.1 PDT application on *S. aureus*. It was observed that IR780 iodide did not cause bacterial cell death at 1 and 2 μM concentrations, however, at 3 μM concentration, it caused bacterial cell death, which was statistically significantly different from the control group ($P \leq 0.05$). All PDT groups caused significant decrease in bacterial cell viability with respect to the control group (93%, 99.8%, and 99.95% for PDT (1 μM), PDT (2 μM), and PDT (3 μM), respectively). The results are plotted in Figure 4.3 normalized to the control group.

4.3.1.2 PDT application on *P. aeruginosa*. It was observed that IR780 iodide did not cause bacterial cell death at 1 and 2 μM concentrations, however, at 3 μM concentration, it caused bacterial cell death which was statistically significantly different from the control group ($P \leq 0.05$). All PDT groups caused significant decrease in bacterial cell viability with respect to the control group (96.5%, 99.8%, and 99.96% for PDT (1 μM), PDT (2 μM), and PDT (3 μM), respectively). The results are plotted in Figure 4.4 normalized to the control group.

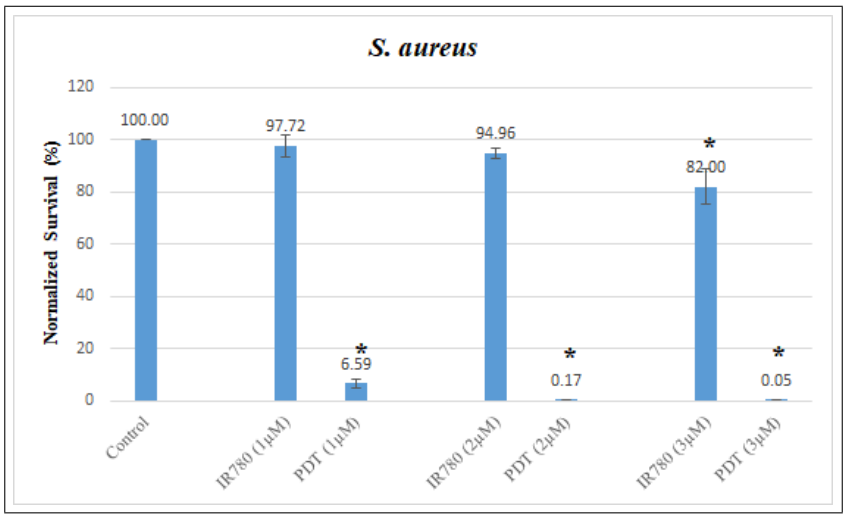

Figure 4.3 Viability of *S. aureus* (ATCC 25923) after PDT using 785 nm diode laser (500 mW/cm^2, 5 min). $*$ indicates statistical significance ($P \leq 0.05$) compared to the control group. Data represent mean values $\pm$ SD of triplicate experiments (n=3).

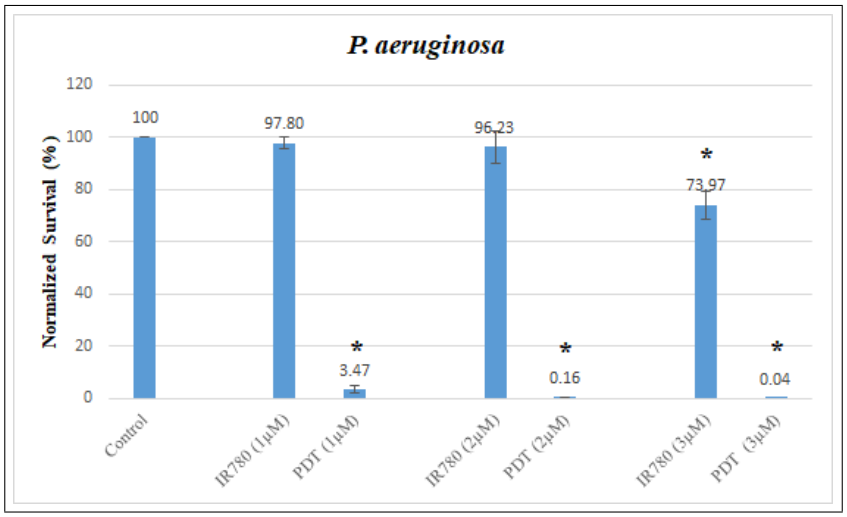

Figure 4.4 Viability of *P. aeruginosa* (ATCC 27853) after PDT using 785 nm diode laser (500 mW/cm^2, 5 min). $*$ indicates statistical significance ($P \leq 0.05$) compared to the control group. Data represent mean values $\pm$ SD of triplicate experiments (n=3).

4.3.1.3 PDT application on MRSA.

The concentrations of IR780 iodide tested on *S. aureus* (ATCC 25923) were so toxic on MRSA, therefore, dark toxicity of IR780 iodide with concentrations less than 1 μM were tested on MRSA first, then, the highest concentration with no dark toxicity was selected to be applied in PDT studies.

The results are shown in Figure 4.5. IR780 iodide concentrations more than 0.25 μM caused significant bacterial cell death with respect to the control group ($P \leq$

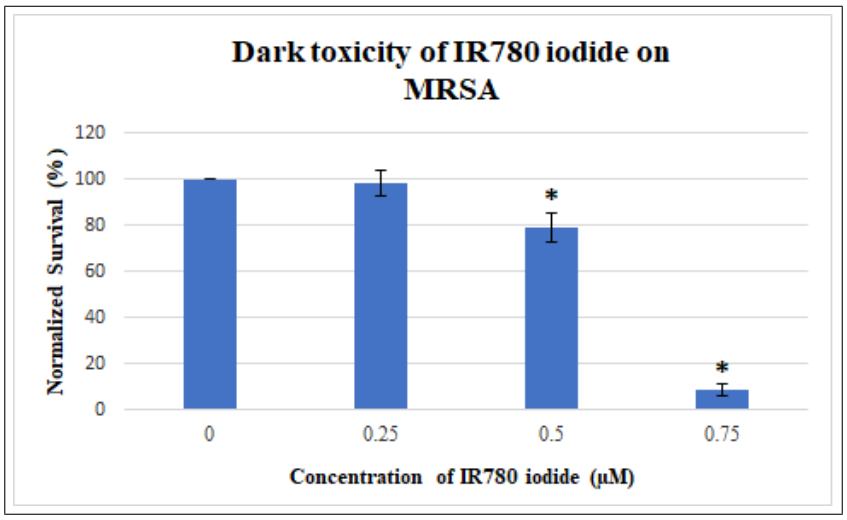

Figure 4.5 Dark toxicity of IR780 iodide on MRSA. $*$ indicates statistical significance with respect to the control group. Data represent mean values $\pm$ SD of triplicate experiments (n=3).

0.05).Based on these results, the concentration of IR780 iodide (0.25 μM) was applied in PDT studies. The results indicated that there was a significant decrease in bacterial cell viability (98.31%) in PDT group with respect to the control group ($P \leq$ *0.05*). The results are plotted in Figure 4.6 normalized to the control group.

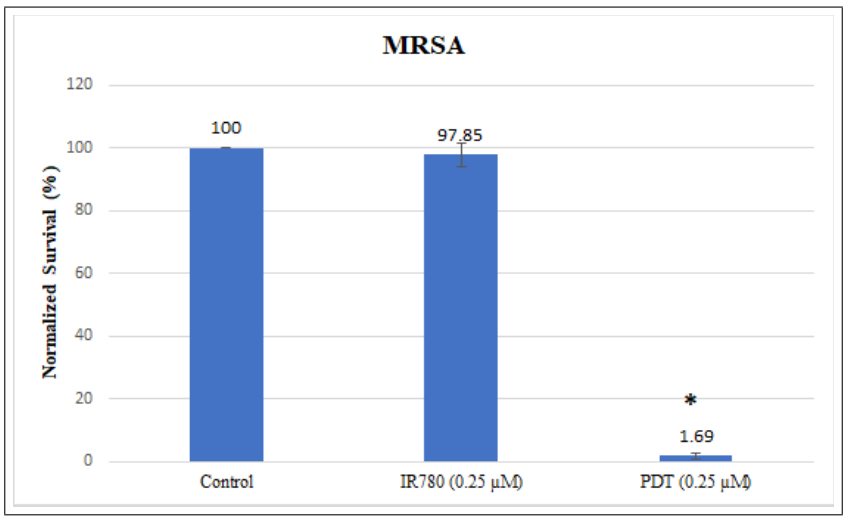

Figure 4.6 Viability of MRSA after PDT using 785 nm diode laser (500 mW/cm^2, 5 min). $*$ indicates statistical significance ($P \leq$ *0.05*) compared to the control group. Data represent mean values $\pm$ SD of triplicate experiments (n=3).

4.3.1.4 PDT application on MDR *P. aeruginosa.* The concentrations of IR780 iodide (2 and 3 μM) tested on *P. aeruginosa* (ATCC 27853) were toxic on MDR *P. aeruginosa*, therefore, dark toxicity of IR780 iodide with concentrations less than 2 μM were tested on MDR *P. aeruginosa* first, then, the highest concentration with no dark toxicity was selected to be applied in PDT studies. The results are shown in Figure 4.7. IR780 iodide concentrations more than 1.5 μM caused significant bacterial cell death with respect to the control group ($P \leq 0.05$). Based on these results, the concentration of IR780 iodide (1.5 μM) was applied in PDT studies. The results indicated that there was a significant decrease in bacterial cell viability (97.76%) in PDT group with respect to the control group ($P \leq 0.05$). The results are plotted in Figure 4.8 normalized to the control group.

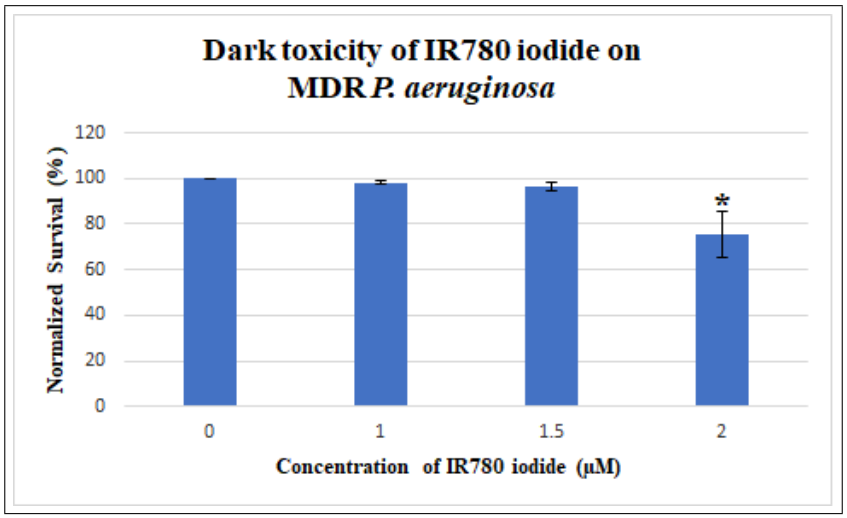

Figure 4.7 Dark toxicity of IR780 iodide on MDR *P. aeruginosa*. $*$ indicates statistical significance with respect to the control group. Data represent mean values $\pm$ SD of triplicate experiments (n=3).

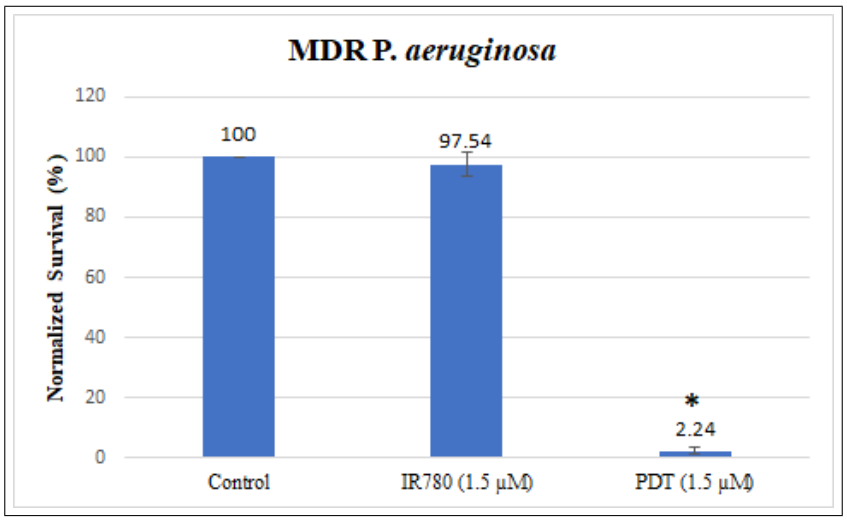

Figure 4.8 Viability of MDR *P. aeruginosa* after PDT using 785 nm diode laser (500 mW/cm^2, 5 min). $*$ indicates statistical significance ($P \leq 0.05$) compared to the control group. Data represent mean values $\pm$ SD of triplicate experiments (n=3).

4.3.2 SDT Studies

4.3.2.1 SDT application on *S. aureus*. It was observed that IR780 iodide did not cause bacterial cell death at 1 and 2 μM) concentrations, however at 3 μM) concentration, it caused bacterial cell death, which was significantly different from the control group ($P \leq 0.05$). After exposure to US, IR780 iodide at concentrations of 2 and 3 μM), caused significant decrease in bacterial cell viability (10.76% and 30.77%, respectively), with respect to the control group. The results are plotted in Figure 4.9 normalized to the control group.

4.3.2.2 SDT application on *P. aeruginosa*. It was observed that IR780 iodide did not cause bacterial cell death at 1 and 2 μM concentrations, however at 3 μM) concentration, it caused bacterial cell death, which was significantly different from the control group ($P \leq 0.05$). After exposure to US, IR780 iodide at concentrations of 2 and 3 μM), caused significant decrease in cell viability (19.79% and 38%, respectively) with respect to the control group. The results are plotted in Figure 4.10 normalized to the control group.

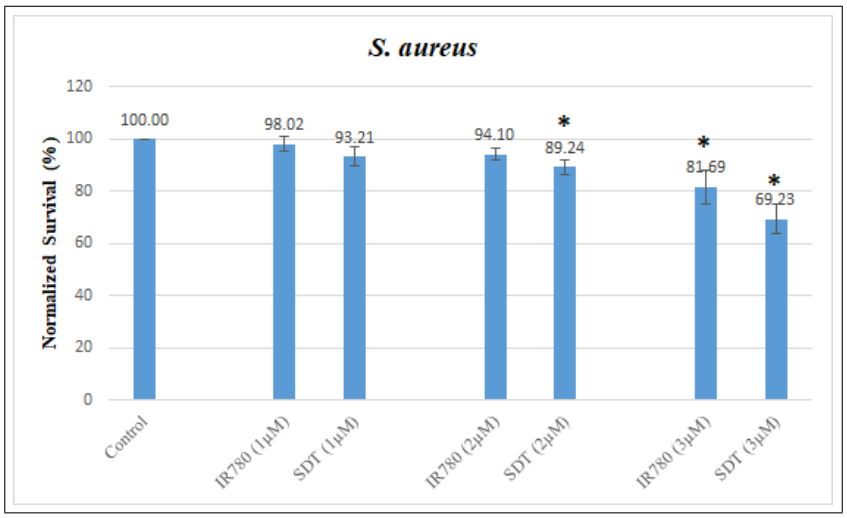

Figure 4.9 Viability of *S. aureus* (ATCC 25923) after SDT using 1-MHz US unit (1.5 W/cm^2, 50% duty cycle, 3 min). $*$ indicates statistical significance ($P \leq 0.05$) compared to the control group. Data represent mean values ± SD of triplicate experiments (n=3).

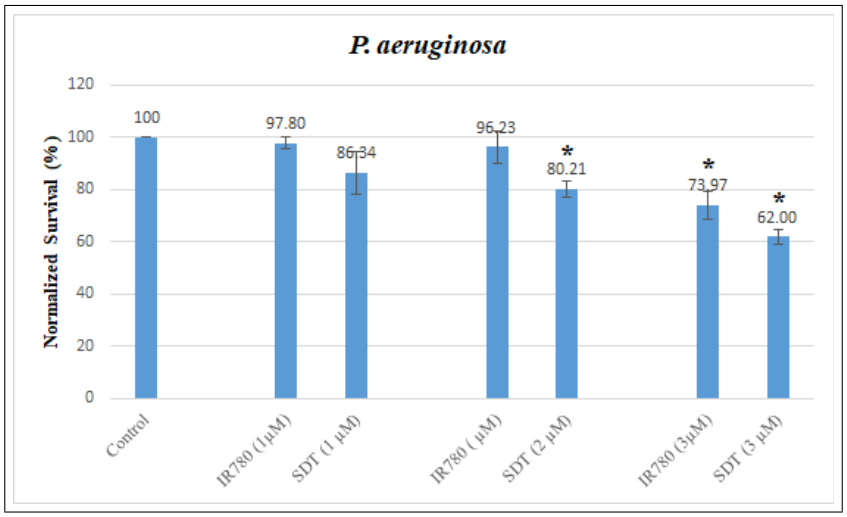

Figure 4.10 Viability of *P. aeruginosa* ATCC 27853 after SDT using 1-MHz US unit (1.5 W/cm^2, 50% duty cycle, 3 min). $*$ indicates statistical significance ($P \leq 0.05$) compared to the control group. Data represent mean values ± SD of triplicate experiments (n=3).

4.3.2.3 SDT application on MRSA. Based on the dark toxicity results shown in Figure 4.5, the concentration of IR780 iodide (0.25 μM)) was applied in SDT studies. The results indicated that there was no significant difference in bacterial cell viability between SDT group and the control group ($P > 0.05$). The results are plotted in Figure 4.11 normalized to the control group.

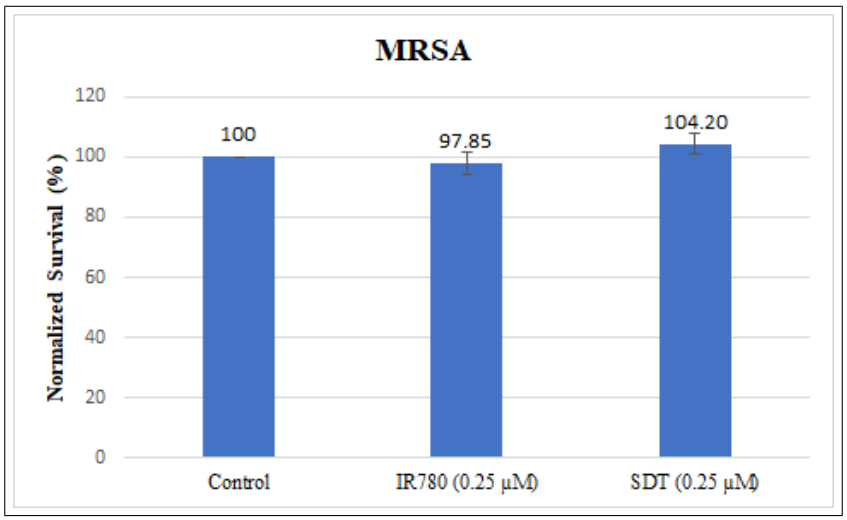

Figure 4.11 Viability of MRSA after SDT using 1-MHz US unit (1.5 W/cm^2, 50% duty cycle, 3 min). Data represent mean values ± SD of triplicate experiments (n=3).

4.3.2.4 SDT application on MDR *P. aeruginosa*. Based on the dark toxicity results shown in Figure 4.7, the concentration of IR780 iodide (1.5 μM)) was applied in SDT studies. The results indicated that there was a significant difference in bacterial cell viability (9.43%) between SDT group and the control group ($P \leq 0.05$). The results are plotted in Figure 4.12 normalized to the control group.

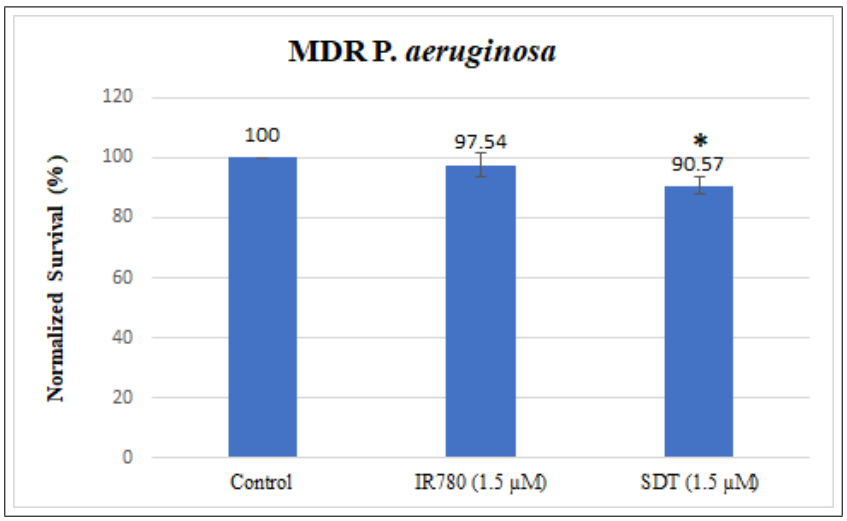

Figure 4.12 Viability of MDR *P. aeruginosa* after SDT using 1-MHz US unit (1.5 W/cm^2, 50% duty cycle, 3 min). $*$ indicates statistical significance ($P \leq 0.05$) compared to the control group. Data represent mean values ± SD of triplicate experiments (n=3).

4.3.3 Combined PDT and SDT Studies

4.3.3.1 Combined PDT and SDT application on *S. aureus*. It was observed that SDT, PDT, SPDT, and PSDT caused significant decrease in bacterial cell viability with respect to the control group (10.76%, 99.85%, 99.87%, and 99.94%, respectively). There was no statistically significant difference between the last three groups, but they were statistically significantly different from SDT group ($P \leq 0.05$). The results are plotted in Figure 4.13 normalized to the control group.

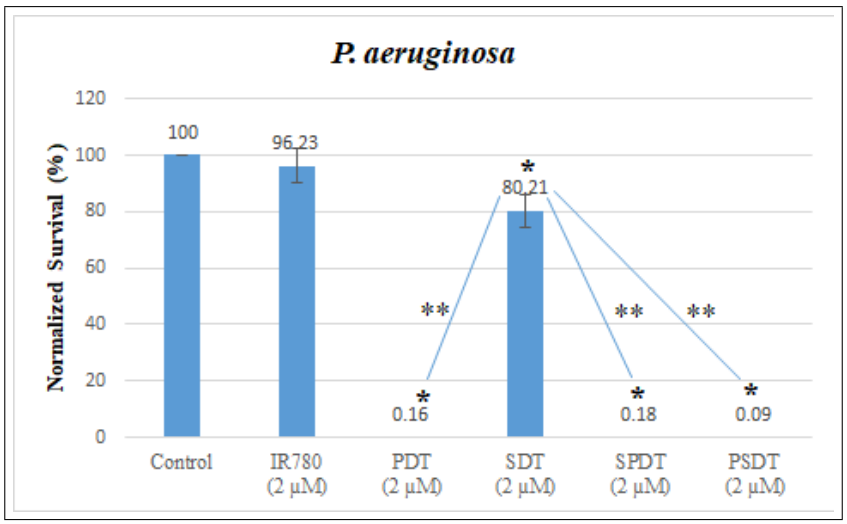

Figure 4.13 Viability of *S. aureus* (ATCC 25923) after combined PDT and SDT using 785 nm diode laser (500 mW/cm^2, 5 min), and 1-MHz US unit (1.5 W/cm^2, 50% duty cycle, 3 min). SPDT: SDT followed by PDT. PSDT: PDT followed by SDT. $*$ indicates statistical significance ($P \leq 0.05$) compared to the control group.$**$ indicates statistical significance ($P \leq 0.05$) compared to SDT group. Data represent mean values $\pm$ SD of triplicate experiments (n=3).

4.3.3.2 Combined PDT and SDT application on *P. aeruginosa*. It was observed that SDT, PDT, SPDT, and PSDT caused significant decrease in bacterial cell viability with respect to the control group (19,79%, 99.84%, 99.82%, and 99.91%, respectively). There was no statistically significant difference between the last three groups, but they were statistically significantly different from SDT group ($P \leq 0.05$). The results are plotted in Figure 4.14 normalized to the control group.

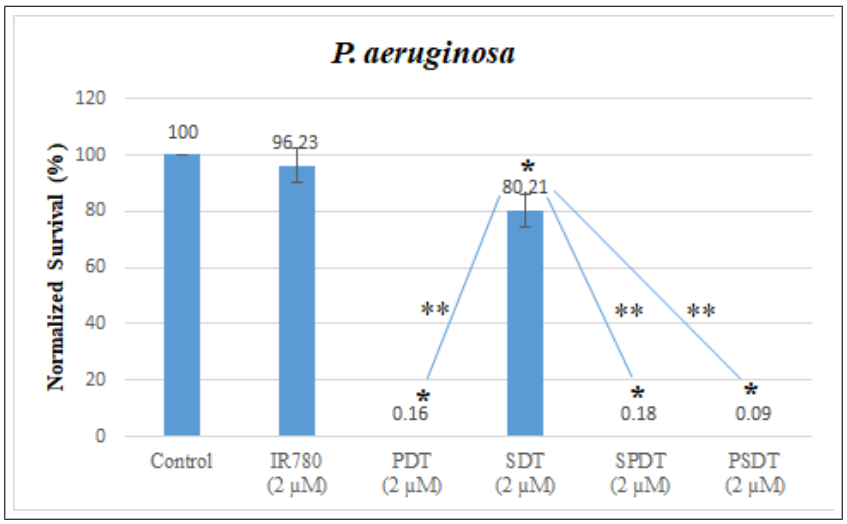

Figure 4.14 Viability of *P. aeruginosa* (ATCC 27853) after combined PDT and SDT using 785 nm diode laser (500 mW/cm^2, 5 min), and 1-MHz US unit (1.5 W/cm^2, 50% duty cycle, 3 min). SPDT: SDT followed by PDT. PSDT: PDT followed by SDT. $*$ indicates statistical significance ($P \leq 0.05$) compared to the control group.$**$ indicates statistical significance ($P \leq 0.05$) compared to SDT group. Data represent mean values $\pm$ SD of triplicate experiments (n=3).

4.3.3.3 Combined PDT and SDT application on MRSA. It was observed that SDT did not cause bacterial cell death. PDT, SPDT, and PSDT caused significant decrease in bacterial cell viability with respect to the control group (98.54%, 98.70%, and 98.79%, respectively). The results are plotted in Figure 4.15 normalized to the control group. There was no statistically significant difference between PDT, SPDT and PSDT groups, but they were statistically significantly different from SDT group ($P \leq 0.05$).

4.3.3.4 Combined PDT and SDT application on MDR *P. aeruginosa*. It was observed that SDT, PDT, SPDT, and PSDT caused significant decrease in bacterial cell viability with respect to the control group (9.43%, 97.76%, 99.44%, and 99.54%, respectively). There was no statistically significant difference between the last three groups, but they were statistically significantly different from SDT group ($P \leq 0.05$). The results are plotted in Figure 4.16 normalized to the control group.

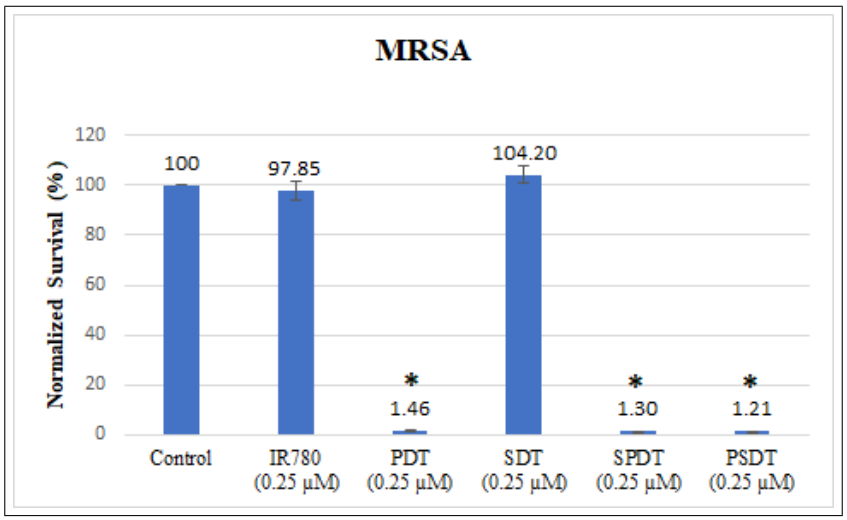

Figure 4.15 Viability of MRSA after combined PDT and SDT using 785 nm diode laser (500 mW/cm^2, 5 min), and 1-MHz US unit (1.5 W/cm^2, 50% duty cycle, 3 min). SPDT: SDT followed by PDT. PSDT: PDT followed by SDT. $*$ indicates statistical significance ($P \leq 0.05$) compared to the control group. Data represent mean values ± SD of triplicate experiments (n=3).

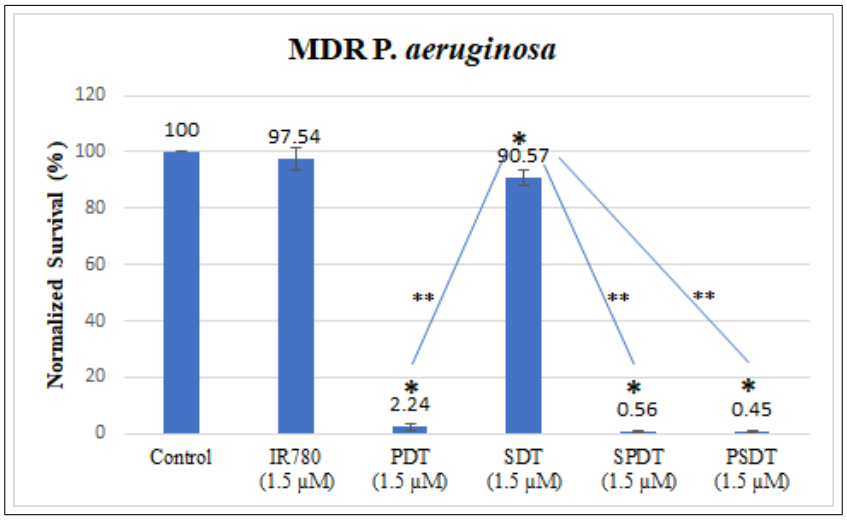

Figure 4.16 Viability of MDR *P. aeruginosa* after combined PDT and SDT using 785 nm diode laser (500 mW/cm^2, 5 min), and 1-MHz US unit (1.5 W/cm^2, 50% duty cycle, 3 min). SPDT: SDT followed by PDT. PSDT: PDT followed by SDT. $*$ indicates statistical significance ($P \leq 0.05$) compared to the control group.$**$ indicates statistical significance ($P \leq 0.05$) compared to SDT group. Data represent mean values ± SD of triplicate experiments (n=3).

4.3.4 Bacterial Cell Viability in the Presence of ROS Quenchers

The effects of the presence of NaN3, as a singlet oxygen quencher, on bacterial cell viability with or without IR780 iodide are shown in Figure 4.17 for MRSA, and Figure 4.18 for MDR *P. aeruginosa*. Control groups involve bacterial cells incubated

with 0 or 50 mM of NaN3 for 30 min, to test for its toxicity (without laser or US irradiation). No decrease in cell viability associated with NaN3 dissolved in PBS (pH 7.4), was observed.

For MRSA, the second cluster of bars in figure 4.17 corresponds to the groups incubated with 0.25 μM of IR780 iodide with 0 or 50 mM of NaN3 for 30 min, before laser irradiation. Addition of NaN3 caused a significant increase in bacterial cell viability due to laser irradiation (99% survival), compared to PDT group without the addition of NaN3 (1.5% survival). The effect of the presence of NaN3 on bacterial cell viability due to US irradiation was not tested for MRSA, since US irradiation without NaN3 did not cause any decrease in bacterial cell viability as indicated in section 4.3.2.3 and Figure 4.11.

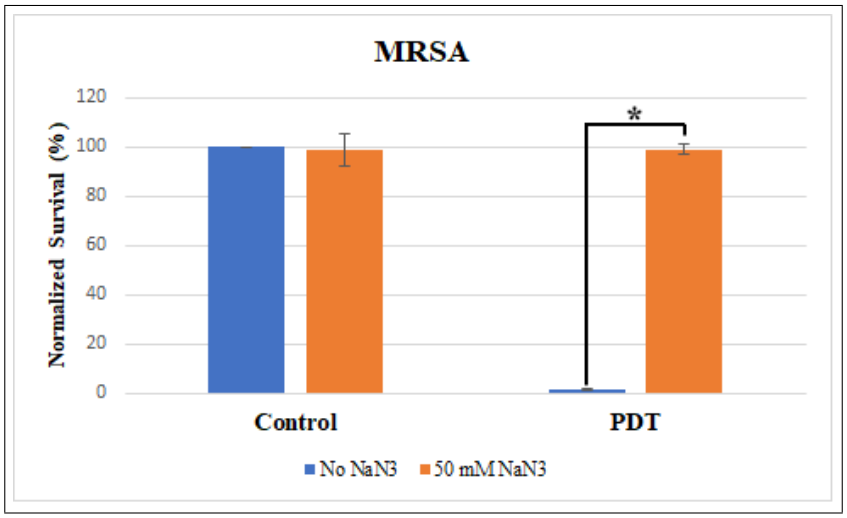

Figure 4.17 Viability of MRSA after PDT (500 mW/cm^2, 5 min) in the presence and absence of NaN3 (50 mM). IR780 iodide concentration used was 0.25 μM. $*$ indicates statistical significance ($P \leq 0.05$) compared to the control group. Data represent mean values $\pm$ SD of triplicate experiments (n=3).

For MDR *P. aeruginosa*, the second cluster of bars in Figure 4.18 corresponds to the groups incubated with 1.5 μM of IR780 iodide with 0 or 50 mM of NaN3 for 30 min, before laser irradiation. The third cluster of bars corresponds to the groups incubated with 1.5 μM of IR780 iodide with 0 or 50 mM of NaN3 for 30 min, before US irradiation. Addition of NaN3 caused a significant increase in bacterial cell viability due to laser and US irradiations, compared to PDT and SDT groups without the addition

of NaN3 ($P \leq 0.05$).

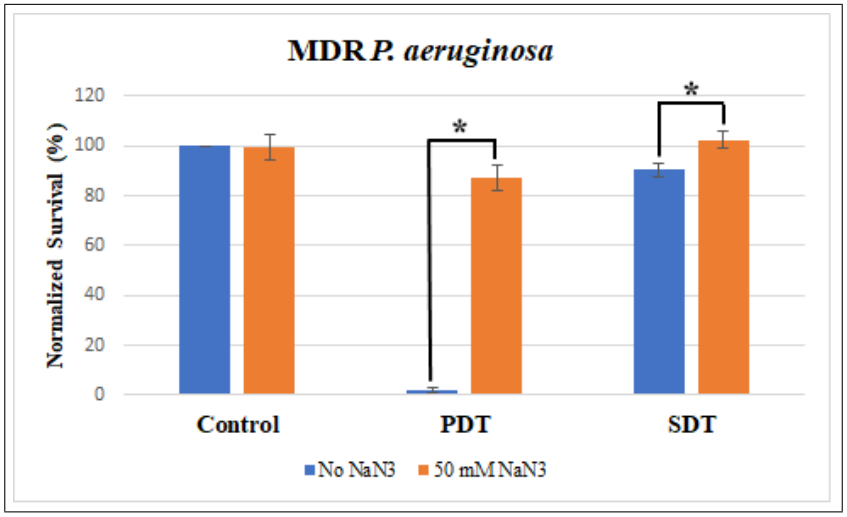

Figure 4.18 Viability of MDR *P. aeruginosa* after PDT (500 mW/cm^2, 5 min) and SDT (1.5 W/cm^2, 50% duty cycle, 3 min), in the presence and absence of NaN3 (50 mM). IR780 iodide concentration used was 1.5 μM. $*$ indicates statistical significance ($P \leq 0.05$) compared to the control group. Data represent mean values $\pm$ SD of triplicate experiments (n=3).

4.3.5 Temperature Measurements

Thermal changes of IR780 iodide solutions (2 μM) during 785 nm laser irradiation (500 mW/cm^2, 5 min), and US irradiation (1.5 W/cm^2, 50% duty cycle, 3 min) were recorded.

For laser irradiation, the increase in temperature after 5 min irradiation of IR780 iodide (2 μM) and PBS (control), was about 1.5 °C and 2 °C, respectively. The results are plotted in Figure 4.19. For US irradiation, the increase in temperature after 3 min irradiation of IR780 iodide (2 μM) and PBS (control), was about 5 °C and 7 °C, respectively. The results are plotted in Figure 4.20.

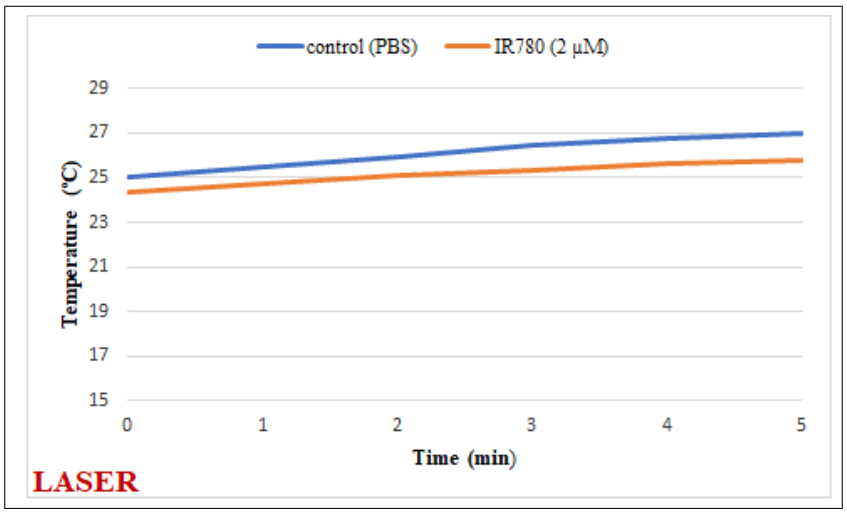

Figure 4.19 Thermal change analysis obtained using an infrared thermal camera for the control (PBS, pH 7.4) and IR780 iodide (2 μM), under 785 nm laser light irradiation (500 mW/cm^2, 5 min). Data represent mean values ± SD of triplicate experiments (n=3).

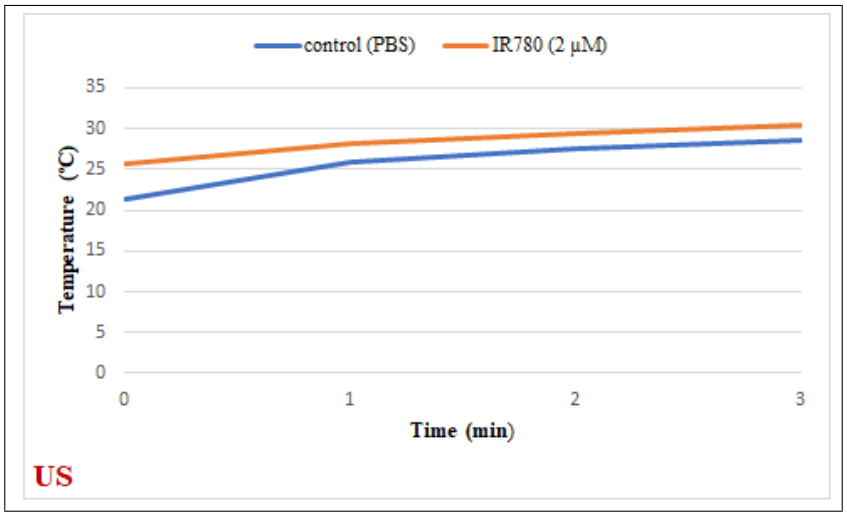

Figure 4.20 Thermal change analysis obtained using an infrared thermal camera for the control (PBS, pH 7.4) and IR780 iodide (2 μM), under 1-MHz US irradiation (1.5 W/cm^2, 50% duty cycle, 3 min). Data represent mean values ± SD of triplicate experiments (n=3).

These results are consistent with the results obtained using an infrared thermal thermometer before and after each laser and US application in PDT and SDT experiments. The results are shown in Figure 4.21 for PDT, and Figure 4.22 for SDT.

As can be seen in Figure 4.21, the maximum temperature increase during PDT was about 1.5 $°C$, and there was no statistically significant difference between the different bacterial strains examined ($P > 0.05$).

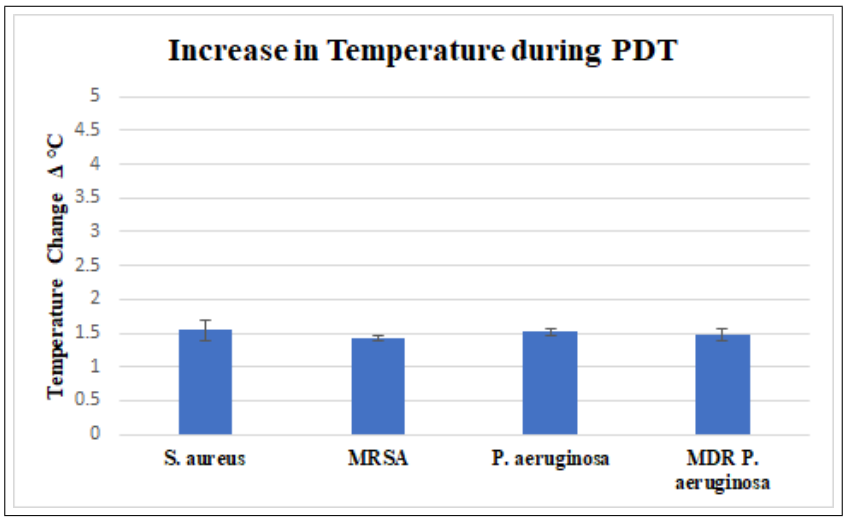

Figure 4.21 Thermal change during PDT (785 nm laser light, 500 mW/cm^2, 5 min), for the different tested bacterial strains, obtained using an infrared thermal thermometer. IR780 iodide concentrations used were 2 μM, 2 μM, 0.25 μM, and 1.5 μM for *S. aureus* (ATCC 25923), *P. aeruginosa* (ATCC 27853), MRSA, and MDR *P. aeruginosa*, respectively. Data represent mean values ± SD of triplicate experiments (n=3).

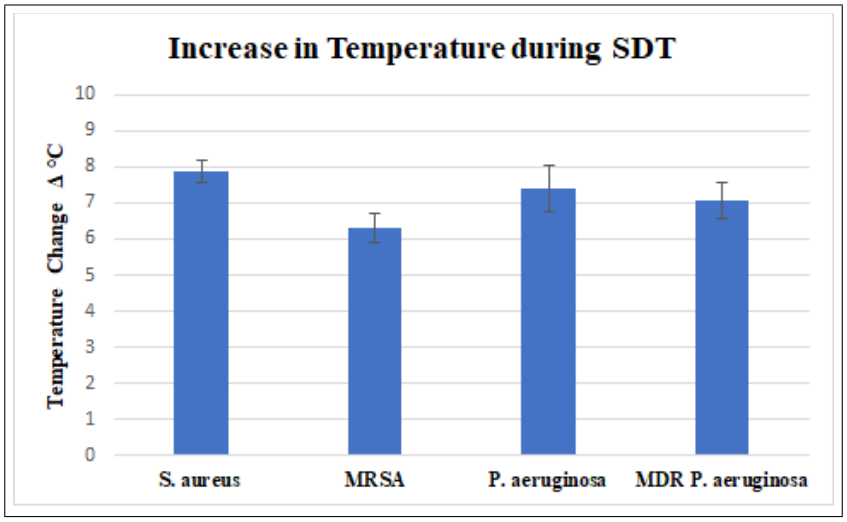

Figure 4.22 Thermal change during SDT (1.5 W/cm^2, 50% duty cycle, 3 min), for the different tested bacterial strains, obtained using an infrared thermal thermometer. IR780 iodide concentrations used were 2 μM, 2 μM, 0.25 μM, and 1.5 μM for *S. aureus* (ATCC 25923), *P. aeruginosa* (ATCC 27853), MRSA, and MDR *P. aeruginosa*, respectively. Data represent mean values ± SD of triplicate experiments (n=3).

As can be seen in Figure 4.22, the maximum temperature increase during SDT was about 8 $°C$, and there was no statistically significant difference between the different bacterial strains examined ($P > 0.05$).

4.3.6 Reactive Oxygen Species (ROS) Detection

DPBF reacts with ROS causing absorbance bleaching of the probe near 410 nm, and the change in the absorbance can be measured using a spectrophotometer [89]. By utilizing this method, the ability of IR780 iodide to generate ROS under 785 nm laser light irradiation (500 mW/ cm^2), and US (1.5 W/cm^2, 50% duty cycle), was monitored via absorption reduction of DPBF at 410 nm. For laser irradiation, the absorbance intensity of DPBF was observed over a period of 5 min, and the decrease in absorbance, , after every 1 min of laser irradiation, was plotted versus time. For US irradiation, the absorbance intensity of DPBF was observed over a period of 3 min, and the decrease in absorbance, after every 1 min of US irradiation, was plotted versus time. The results are shown in Figure 4.23 and Figure 4.24. As can be seen, IR780 iodide caused significant DPBF bleaching (reduction in absorbance intensity) under laser and US irradiations, indicating ROS production. The reduction in absorbance intensity was concentration dependent. The figures also show that the bleaching caused under laser irradiation (40%, 50%, and 72% for IR780 (0.25 μM), IR780 (1.5 μM), and IR780 (2 μM), respectively) was more than the bleaching caused under US irradiation (13%, 19%, and 26% for IR780 (0.25 μM), IR780 (1.5 μM), and IR780 (2 μM), respectively).

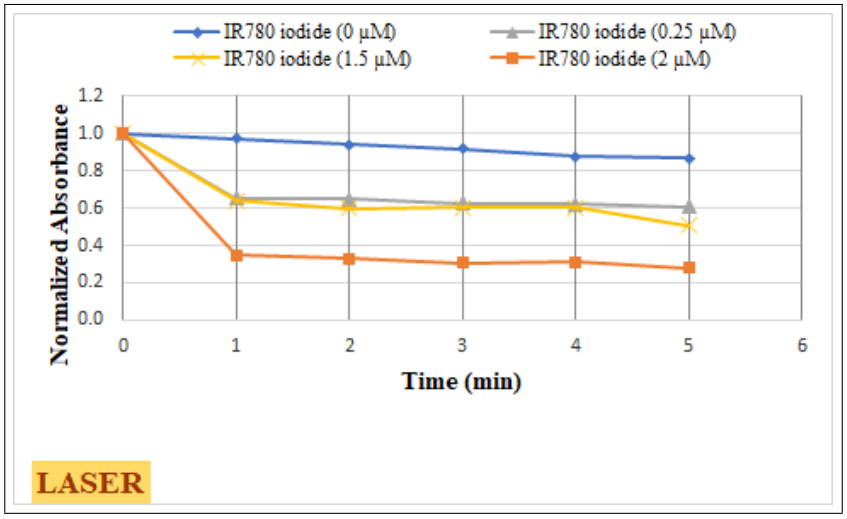

Figure 4.23 ROS production shown as a decrease in DPBF absorbance at 410 nm, under 785 nm laser light irradiation (500 mW/cm^2) for a duration of 5 min, in the presence of IR780 iodide (0, 0.25, 1.5, and 2 μM). Data represent mean values of triplicate experiments (n= 3).

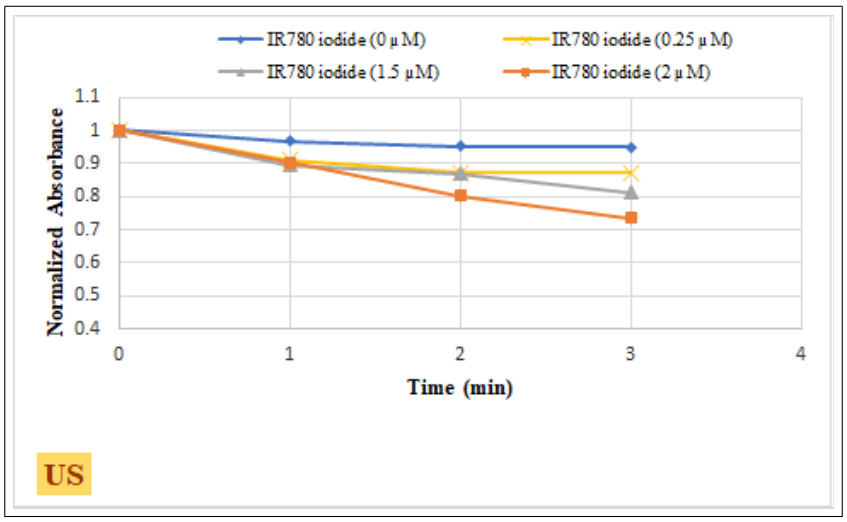

Figure 4.24 ROS production shown as a decrease in DPBF absorbance at 410 nm under US irradiation (1.5 W/cm^2, 50% duty cycle) for a duration of 3 min, in the presence of IR780 iodide (0, 0.25, 1.5, and 2 μM). Data represent mean values of triplicate experiments (n= 3).

A summary of the results obtained in PDT, SDT, SPDT, and PSDT studies is presented in Table 4.1.

Table 4.1

Summary of the results obtained in PDT, SDT, SPDT, and PSDT studies using IR780 iodide. SDT; IR780 iodide with US (1.5 W/cm^2, 50% duty cycle, 3 min), PDT; IR780 iodide with laser light (500 mW/cm^2, 5 min); SPDT; SDT followed by PDT. PSDT; PDT followed by SDT. IR780 iodide concentrations used were 2 μM, 2 μM, 0.25 μM, and 1.5 μM for *S. aureus*, *P. aeruginosa*, MRSA, and MDR *P. aeruginosa*, respectively. Temperature measurements were obtained using an infrared thermal thermometer. Data represent mean values ± SD of triplicate experiments (n = 3).

Normalized survival of planktonic bacteria with respect to the control group % (control =100%)						
	SDT	**PDT**	**SPDT**	**PSDT**	**SDT+NaN3**	**PDT+NaN3**
***S. aureus* (ATCC 25923)**	89.24±4.43	0.15±0.04	0.13±0.05	0.06±0.03	-	-
***P. aeruginosa* (ATCC 27853)**	80.21±5.92	0.16±0.07	0.18±0.05	0.09±0.03	-	-
MRSA	104.20±3.36	1.46±0.41	1.30±0.08	1.21±0.09	-	98.91±2.26
MDR *P. aeruginosa*	90.57±2.77	2.24±1.15	0.56±0.40	0.45±0.37	102.49±3.26	87.13±4.98
Increase in Temperature $\Delta\ ^\circ C$						
	SDT	**PDT**				
***S. aureus* (ATCC 25923)**	7.87±0.29	1.54±0.16				
***P. aeruginosa* (ATCC 27853)**	7.40±0.63	1.52±0.05				
MRSA	6.30±0.41	1.43±0.04				
MDR *P. aeruginosa*	7.06±0.51	1.47±0.09				

4.4 Discussion

The choice of the photo/sonosensitizer plays an important role in the success of PDT and SDT. Identification of novel photo/sonosensitizers is one of the approaches taken by researchers to enhance PDT and SDT. This study aimed to investigate the photodynamic, sonodynamic, and combined photodynamic and sonodynamic potentials of IR780 iodide on reference and resistant strains of gram-positive and gram-negative bacteria. To our best knowledge, there are no studies in literature reporting the use of IR780 iodide as a photo/sonosensitizer in PDT or SDT of bacterial infections.

The results of our study suggest that IR780 iodide can function both, as a photosensitizer and as a sonosensitizer, in PDT and SDT of gram-positive *S. aureus* (ATCC 25923) and MRSA, and gram-negative *P. aeruginosa* (ATCC 27853) and MDR *P. aeruginosa*.

The results of PDT indicated that IR780 iodide effectively reduced the number of living bacterial cells after irradiation with 785 nm laser light (500 mW/cm^2, 5 min) for all the tested strains.

For the same laser dose and IR780 iodide concentration (2 μM), no difference was observed between gram-positive *S. aureus* (ATCC 25923) and gram-negative *P. aeruginosa* (ATCC 27853), in their sensitivity to PDT. In various studies, gram-positive bacteria were shown to be more sensitive to PDT than gram-negative bacteria [19],[28],[90],[91]. The reason for that could be the nature of the photosensitizer. According to George et al. (2009), gram-negative bacteria are less sensitive to PDT than gram-positive bacteria, due to the membrane barrier that prevents uptake of anionic and neutral photosensitizers, and this can be overcome by using cationic photosensitizers, or by coupling anionic photosensitizers with positively charged entities [92]. This can explain why our photosensitizer IR780 iodide, which is a cationic dye, was equally effective on gram-positive *S. aureus* (ATCC 25923) and gram-negative *P. aeruginosa* (ATCC 27853).

Resistant strains of *S. aureus* and *P. aeruginosa* were less sensitive to PDT than their reference strains. This is probably due to the lower concentrations of IR780 iodide used (0.25 μM and 1.5 μM for MRSA and MDR. *P. aeruginosa*, respectively) compared to the 2 μM concentration used for both *S. aureus* (ATCC 25923) and *P. aeruginosa* (ATCC 27853). The fact that IR780 iodide was more toxic on resistant strains of *S. aureus* and *P. aeruginosa* can be linked to a phenomenon termed "collateral sensitivity", which makes resistant strains more sensitive to specific drugs or chemicals [88],[93]. Lower concentrations of IR780 iodide, as expected, were less efficient in ROS production in response to laser light irradiation, as was confirmed by the DPBF bleaching results. Less ROS, in turn, would result in lower PDT efficiency.

The results of SDT studies indicated that SDT was less effective than PDT for all the tested strains. This is consistent with studies [28],[86]. This can be explained by the less ROS production in SDT compared to PDT, as confirmed by DPBF bleaching results, which showed that ROS production in response to US, was less than ROS production in response to laser light (Figures 4.23 and 4.24).

For the same US dose and IR780 iodide concentration (2 μM), gram-negative *P. aeruginosa* (ATCC 27853) was more sensitive to SDT than gram-positive *S. aureus* (ATCC 25923). Again, this could be due to the use of a cationic sonosensitizer. The positive charge of the photo/sonosensitizer can enhance the uptake of the photo/sonosensitizer by gram-negative bacteria. In a study by Costley et al., it was shown that gram-positive *S. aureus* was more sensitive to sonodynamic treatment by Rose Bengal (anionic dye), than gram-negative *P. aeruginosa*. However, when using a Rose Bengal-antimicrobial peptide conjugate (Rose Bengal-C(KLAKLAK)2), the gram-negative *P. aeruginosa* was more sensitive to SDT (7 log reduction) than the gram-positive *S. aureus* (5 log reduction). It was suggested that the net positive charge on the peptide, could enhance the uptake of the Rose Bengal-C(KLAKLAK)2 by the bacteria [94].

Similar to PDT results, resistant strains of *S. aureus* and *P. aeruginosa* were less sensitive to SDT than their reference strains, due to the lower concentrations of

IR780 iodide used. For MRSA, SDT treatment with 0.25 μM IR780 iodide, did not induce any reduction in bacterial cell viability compared to the control group. Lower concentrations of IR780 iodide, were less efficient in ROS production in response to US irradiation, as confirmed by the DPBF bleaching results. Less ROS, in turn, would result in lower SDT efficiency.

For the combined treatment of SDT and PDT, the order by which SDT or PDT was applied (SPDT or PSDT), did not have an effect on the results. Both treatments resulted in significant reduction in bacterial cell viability compared to SDT, but not PDT, for all the tested strains. This could be due to the lower treatment efficiency of SDT compared to PDT, especially for MRSA, where SDT didn't kill any bacteria.

The photodynamic, sonodynamic, and photothermal properties of IR780 iodide were evaluated by measuring the temperature rise, and ROS production during laser and US irradiations.

The ability of IR780 iodide to generate ROS upon laser radiation was confirmed by the significant decrease in absorbance intensity of DPBF at 410 nm after laser irradiation. The temperature rise in response to PDT was about 1.5 $°C$. These results indicate that the killing caused by IR780 iodide, in response to laser irradiation, was mainly due to photodynamic effect, and no photothermal effect was involved. This was also confirmed by the results obtained from testing the photodynamic effect of IR780 iodide in the presence of NaN3, a singlet oxygen quencher, on MRSA and MDR *P. aeruginosa*. The addition of NAN3 caused a significant increase in bacterial cell viability after laser irradiation, as compared to PDT groups without the addition of NaN3, for both strains, excluding any photothermal effect involved.

In response to US irradiation, IR780 iodide was also able to generate ROS, as confirmed by the decrease in absorbance intensity of DPBF at 410 nm after US irradiation. The temperature rise in response to SDT reached a maximum of about 8 $°C$ in *S. aureus*. Although US alone didn't cause any bacterial cell death in any of the tested strains, investigating the effect of the presence of NaN3 on bacterial

cell viability of MDR *P. aeruginosa*, was utilized to test if there was any thermal effect involved in the killing caused by IR780 iodide and US. The results revealed that the addition of NaN3 caused a significant increase in bacterial cell viability after US irradiation, as compared to SDT without the addition of NaN3, excluding any thermal effect involved. These results indicate that the killing caused by IR780 iodide, in response to US irradiation, was mainly due to sonodynamic effect. The results also indicate that the killing was caused specifically by singlet oxygen ($^1O_2$), and this is consistent with the study conducted by Huang et al. [50].

4.5 Conclusion

In conclusion, IR780 Iodide was investigated as a photo/sonosensitizer for antibacterial PDT, SDT, and combined PDT and SDT of *S. aureus* (ATCC 25923), *P. aeruginosa* (ATCC 27853), MRSA, and MDR *P. aeruginosa*, for the first time. The results confirmed that IR780 iodide, possesses high photodynamic and sonodynamic potentials for antimicrobial therapy. However, the hydrophobicity of IR780 iodide could limit its application *in vivo*. Therefore, encapsulating it within nanoparticles, could be a right choice to overcome this limitation, while benefitting from its potentials for PDT and SDT. In the next chapter, this choice is investigated.

5. ANTIMICROBIAL PDT, SDT, AND COMBINED PDT AND SDT USING IR780 IODIDE LOADED MESOPOROUS SILICA NANOPARTICLES: *IN VITRO STUDY*

5.1 Introduction

Mesoporous silica nanoparticles (MSN) have received high attention for their potential biomedical applications, especially as nanocarriers, due to their unique properties such as ease of synthesis, controllable particle size, good biocompatibility, easy functionalization, and large specific surface area and pore volume, enabling high loading capacity of drugs [60],[61],[62],[63],[64],[65].

The anticancer and antimicrobial photodynamic potential of MSN encapsulating different PSs has been investigated so far with promising results [66],[67],[68],[69],[70],[71], [72],[73],[74],[75],[76],[77], while their sonodynamic potential was investigated in few studies [79],[80]. To our knowledge, the antimicrobial photodynamic and sonodynamic potentials of MSN encapsulating IR780 iodide have not been investigated so far. The results of the studies conducted in Chapter 4, revealed that IR780 iodide has a potential to be used as a photo/sonosensitizer in antimicrobial PDT and SDT, however, its hydrophobicity could limit its clinical application [44],[45]. Using MSN to encapsulate IR780 iodide is expected to overcome this limitation, while benefiting from its high potentials for PDT and SDT.

The aim of this study is to investigate the antimicrobial photodynamic, sonodynamic, and combined photodynamic and sonodynamic potentials of mesoporous silica nanoparticles encapsulating IR780 iodide on gram-positive *S. aureus* and MRSA, and gram-negative *P. aeruginosa* and MDR *P. aeruginosa in vitro*.

5.2 Materials and Methods

5.2.1 Materials

IR-780 iodide (≥95%), Absolute ethanol (≥99.9%), Crystal Violet (≥90%), 1,3-Diphenylisobenzofuran (DPBF, 97%), Hexadecyl-trimethyl-ammonium bromide (CTAB), NH4OH, Tetraethyl orthosilicate (TEOS), Dimethyl sulfoxide (DMSO), Hydrochloric acid (HCL, 36.5-38%), and 3-(4,5-dimethylthiazol-2-yl)-2,5-diphenylte-trazolium bromide (MTT) were purchased from Sigma-Aldrich (Darmstadt, Germany). Tryptic soy agar and Tryptic soy broth were purchased from Merck KGaA (Darmstadt, Germany). Phosphate buffer saline (PBS, pH 7.4) was purchased from AppliChem GmbH (Darmstadt, Germany). Sodium Azide (NaN3, ≥99%) was purchased from Biomatik Corporation (Ontario, Canada). RPMI 1640, fetal bovine serum (FBS), penicillin/streptomycin solution and trypsin/EDTA solution were purchased from Biosera (Nuaille, France). All chemicals were used without further purification.

5.2.2 Bacterial strains

The Bacterial strains used in this study were methicillin-susceptible *S. aureus* (ATCC 25923), methicillin-resistant *S. aureus* (MRSA, clinically isolated), *P. aeruginosa* (ATCC 27853) and multidrug-resistant (MDR) *P. aeruginosa* (clinically isolated). All strains were provided by Dr. Nermin Topaloğlu Avşar from Izmir Katip Çelebi University in Turkey. Working in the biosafety cabinet, 10 ml of sterile TSB was added to a sterile 50 ml falcon tube. An isolated colony from a freshly prepared agar plate was picked with a sterile loop and used to inoculate the sterile TSB by submerging the loopful of bacteria into the sterile TSB. After overnight incubation at 37 $^{\circ}C$ in a shaking incubator (rpm 225 for *S. aureus* and MRSA, and rpm=200 for *P. aeruginosa* and MDR *P. aeruginosa*), the bacterial suspension was centrifuged at 3000 rpm for 10 min at room temperature, and the pellet was resuspended in PBS (pH 7.4) to a final concentration of 10^7-10^8 CFU/ml.

5.2.3 Nanoparticles Synthesis and Characterization

5.2.3.1 MSN synthesis. MSN were synthesized using a modified Stöber method [95]. Briefly, 1.057 ml of NH_4OH was added to 7.5 ml of distilled water under magnetic stirring at 500 rpm. 21.44 ml of distilled water was then added to complete the volume to 30 ml. Temperature of the solution was raised to 40 $°C$, and 0.058 g CTAB was added. When CTAB was fully dissolved, the temperature of the solution was raised to 60 $°C$. After that, 118 μl TEOS and 482 μl Ethanol were added, and kept 2 hours under magnetic stirring at 500 rpm. The solution was then centrifuged (14800 rpm, 15 min), supernatant collected, and the pellet was washed thrice by resuspending in ethanol. To remove CTAB, the pellet was dissolved in 20 ml ethanol, the temperature of the solution was raised to 60 $°C$, and 20 μl HCL was added. The solution was kept under magnetic stirring at 500 rpm for 3 h. The solution was then centrifuged, supernatant collected, and the pellet was washed thrice by resuspending in ethanol. The nanoparticles pellet was dried in an incubator (EN 025, Nüve Laboratory and Sterilization Technology, Ankara, Turkey) at 60 $°C$ overnight, weighted, and dissolved in distilled water to get a final concentration of 10 mg/ml.

5.2.3.2 IR780 iodide loaded MSN (MSN@IR780) synthesis. As synthesized MSN (15 mg) were dissolved in 22 ml ethanol, and 2 ml of IR780 iodide solution -prepared in ethanol (1 mg/ml)- was then added to the solution and kept in the dark for 24 h under magnetic stirring (500 rpm). The solution was then centrifuged, supernatant collected, and the pellet was resuspended in distilled water, washed one time, then resuspended in distilled water to a final concentration of 10 mg/ml.

5.2.3.3 Characterization of nanoparticles. STEM images of MSN were obtained using Scanning Transmission Electron Microscopy (Quattro ESEM, Thermos Fisher Scientific, MA, USA). The absorption spectrums of MSN, IR780 iodide, and MSN@IR780 were measured with a UV-VIS spectrophotometer (NanoDrop 2000c, Thermo Fisher Scientific, MA, USA) to confirm the loading of IR780 iodide into MSN.

The loading efficiency of IR780 iodide into MSN was determined spectrophotometrically. Briefly, the absorption spectrum of the supernatant following the loading step in nanoparticles synthesis, was measured at 780 nm. Then, by using established calibration curve for IR780 iodide, the concentration of IR780 iodide in the supernatant was determined, and the loading efficiency was calculated according to Eq. 5.1:

$$LoadingEfficiency = \frac{IR780(Initial) - IR780(Supernatant)}{IR780(Initial)} \times 100 \qquad (5.1)$$

where IR 780 (Initial) = Initial concentration of IR780 iodide in nanoparticle solution, IR 780 (Supernatant) = concentration of IR780 iodide in supernatant.

5.2.4 Laser Source

Laser irradiation was provided by an infrared diode laser system at 785 nm (MDL-III-785, Changchun, China) in a continuous wave mode with output laser power of 1.95 W. The distance from the tip of the laser output to the bottom of the multi well plate was fixed to give laser irradiation of 500 mW/cm^2. Laser exposure time was 5 min, based on the preliminary studies conducted. The experimental setup is shown in Figure 4.1.

5.2.5 Ultrasound Source

US irradiation was provided by a therapeutic ultrasound unit (Sonoplus 190, Enraf-Nonius B.V., Rotterdam, Netherlands) at a frequency of 1 MHz, intensity of 1.5 W/cm^2, 50% duty cycle, and 3 min exposure time. US parameters were selected based on the preliminary studies conducted. The US probe was placed in contact with the 12-well plate. Adequate contact between the bottom of the multi-well plate and the surface of the US probe was facilitated by using an ultrasound gel. The experimental setup is shown in Figure 4.2.

5.2.6 Dark Toxicity Studies

The dark toxicity of IR780 iodide loaded MSN on *S. aureus* (ATCC 25923) and *P. aeruginosa* (ATCC 27853) was investigated to determine the nontoxic concentrations to be used in PDT, SDT, and combined PDT and SDT studies. The concentrations (50, 100, 150, 200, 250 and 300 μg/ml) were tested.

5.2.7 Cytotoxicity of MSN@IR780 on Mammalian Cells

The MTT assay was used to assess the cytotoxicity of MSN@IR780 on mouse fibroblast L929 cells. L929 cells were cultured in 25 cm^2 flasks in RPMI-1640 medium, supplemented with 10% fetal bovine serum and 1% Penicillin-Streptomycin Solution, at 37 $^{\circ}C$ in a humidified 5% CO_2 atmosphere. Culture medium was changed every 24 h and cells were sub cultured upon reaching confluence. The cells were detached using 0.25% (w/v) trypsin/EDTA solution, and counted in a cell counter (TC20 Automated Cell Counter, Bio-Rad Laboratories, Inc., California, USA). L929 cells were seeded at a density of 5000 cells/well in a 96-well polystyrene plate, in a culture medium consisting of RPMI supplemented with 10% FBS and 1% penicillin-streptomycin, in a total volume of 100 μl, and incubated for 24 h at 37 $^{\circ}C$ with 5% CO2 in air. The medium was replaced with either fresh medium (Control group), or fresh medium with MSN@IR780 solution (150 and 250 μg/ml), and incubated for 2 h at 37 $^{\circ}C$ with 5% CO_2 in air. The culture medium was removed and replaced with fresh medium and 10% MTT in a total volume of 100 μl, and incubated for 1 h at 37 $^{\circ}C$, which led to the formation of Formazan dye. The medium was then removed and 100 μl DMSO was added to each well to solubilize the dye. The Formazan product was dissolved after 10 min shaking. Finally, a microplate reader (iMark Microplate Reader, Bio-Rad Laboratories, Inc., California, USA) was used to measure the absorbance at a wavelength of 570 nm against 750 nm, and the viability of cells was determined by comparing the absorbance of MSN@IR780 groups and control group. Experiments were conducted in triplicate.

5.2.8 PDT Studies

The following groups were tested for each bacterial strain:

- G1: control; no laser, no nanoparticles.
- G2: Laser ONLY; (500 mW/cm^2, 5 min).
- G3: (MSN@IR780); IR780 iodide loaded MSN only (150, 250 μg/ml).
- G4: (MSN@IR780 PDT); IR780 iodide loaded MSN + laser.

12-well plates were used for the experiments, as the diameter of the wells matched with laser beam diameter, thus maximizing the irradiated surface covered. 800 μl aliquots of bacterial suspensions were transferred into the wells of 12-well plates. For groups G3 and G4, 800 μl of MSN@IR780 solutions were added to each well, mixed with bacteria, and incubated in the dark for 30 min. In G1 and G2 groups, the bacterial suspensions in the wells were mixed with equal volumes of PBS (800 μl). The bacterial suspensions in PDT groups were exposed to laser light (500 mW/cm^2, 5 min). Following light exposure, the bacterial suspensions in all groups were diluted according to serial dilution method. Diluted samples were plated on tryptic soy agar plates and incubated at 37 $°C$ for 24 h. The number of CFU was counted with the naked eye and multiplied by the dilution factor to determine viable bacteria. Experiments were conducted in triplicate.

5.2.9 SDT Studies

The following groups were tested for each bacterial strain:

- G1: control; no US, no nanoparticles.
- G2: (MSN@IR780); IR780 iodide loaded MSN only (150, 250 μg/ml).

- G3: (MSN@IR780 SDT); IR780 iodide loaded MSN + US (1.5 W/cm^2, 50% duty cycle, 3 min).

12-well plates were used for the experiments. 800 μl aliquots of bacterial suspensions were transferred into the wells of 12-well plates. For groups G2 and G3, 800 μl of MSN@IR780 solutions were added to each well, mixed with bacteria, and incubated in the dark for 30 min. In G1 group, the bacterial suspension in the well was mixed with 800 μl of PBS (pH 7.4). The bacterial suspensions in G2 and G3 groups were exposed to US irradiation (1.5 W/cm^2, 50% duty cycle, 3 min). One well was irradiated at a time. Following US exposure, the bacterial suspensions in all groups were diluted according to serial dilution method. Diluted samples were plated on tryptic soy agar plates and incubated at 37 $^{\circ}C$ for 24 h. The number of CFU was counted with the naked eye, and multiplied by the dilution factor to determine viable bacteria. Experiments were conducted in triplicate.

5.2.10 Combined PDT and SDT studies

The following groups were tested for each bacterial strain:

- G1: control; no laser, no US, no nanoparticles.
- G2: (MSN@IR780 PDT); IR780 iodide loaded MSN + laser.
- G3: (MSN@IR780 SDT); IR780 iodide loaded MSN + US.
- G4: MSN@IR780 SPDT; SDT followed by PDT.

12-well plates were used for the experiments. 800 μl aliquots of bacterial suspensions were transferred into the wells of 12-well plates. For groups G2-G4, 800 μl of MSN@IR780 solutions (150 and 250μg/ml) were added to each well, mixed with bacteria, and incubated in the dark for 30 min. In G1 group, the bacterial suspension

in the well was mixed with equal volume of PBS (800 μl). The bacterial suspension in G2 group was exposed to laser light (500 mW/cm^2, 5 min). The bacterial suspension in G3 group was exposed to US irradiation (1.5 W/cm^2, 50% duty cycle, 3 min). The bacterial suspension in G4 group was exposed to US irradiation (1.5 W/cm^2, 50% duty cycle, 3 min) followed by laser light (500 mW/cm^2, 5 min). Following light and US exposures, the bacterial suspensions in all groups were diluted according to serial dilution method. Diluted samples were plated on tryptic soy agar plates, and incubated at 37 $°C$ for 24 h. The number of CFU was counted with the naked eye, and multiplied by the dilution factor to determine viable bacteria. Experiments were conducted in triplicate.

5.2.11 Bacterial Cell Viability in the Presence of ROS Quenchers

The photodynamic and sonodynamic effects of MSN@IR780 were tested utilizing NaN3 as a singlet oxygen quencher on resistant strains (MRSA and MDR P. aeruginosa). The concentrations of MSN@IR780 used were 150 μg/ml and 250 μg/ml for MRSA and MDR P. aeruginosa, respectively. The following groups were tested for each bacterial strain:

- G1: control.
- G2: control + NaN3.
- G3: MSN@IR780 PDT.
- G4: MSN@IR780 PDT + NaN3.
- G5: MSN@IR780 SDT.
- G6: MSN@IR780 SDT + NaN3.

12-well plates were used for the experiments. 800 μl aliquots of bacterial suspensions were transferred into the wells of 12-well plates. In groups G3 and G5, 800 μl

of MSN@IR780 solutions were added to each well, mixed with bacteria, and incubated in the dark for 30 min. In groups G4, and G6, 800 μl of MSN@IR780 and NaN3 were added to each well, mixed with bacteria (final concentration of NaN3 was 50mM), and incubated in the dark for 30 min. In G1 group, the bacterial suspension in the well was mixed with equal volume of PBS (800 μl). In G2 group, the bacterial suspension in the well was mixed with 800 μl of PBS and NaN3 (final concentration of NaN3 was 50 mM). The bacterial suspensions in G3 and G4 groups were exposed to laser light (500 mW/cm^2, 5 min). The bacterial suspensions in G5 and G6 groups were exposed to US irradiation (1.5 W/cm^2, 50% duty cycle, 3 min). Following light and US exposures, the bacterial suspensions in all groups were diluted according to serial dilution method. Diluted samples were plated on tryptic soy agar plates and incubated at 37 $^{\circ}C$ for 24 h. The number of CFU was counted with the naked eye and multiplied by the dilution factor to determine viable bacteria. Experiments were conducted in triplicate.

5.2.12 Temperature Measurements

An infrared thermal thermometer (Raytek, Raynger ST, CA, USA) was used to record temperature before and after each laser or US application. Also, an infrared thermal camera (Flir E5, Teledyne FLIR, Täby, Sweden) was used to detect the temperature change during 785 nm laser irradiation (500 mW/cm^2, 5 min), or US irradiation (1.5 W/cm^2, 50% duty cycle, 3 min) of MSN@IR780 solution (250 μg/ml). Results are means of three independent experiments (n=3).

5.2.13 Reactive Oxygen Species (ROS) Detection

1,3-Diphenylisobenzofuran (DPBF) was used to detect the ability of MSN@IR780 to produce ROS in response to laser or US irradiation, indirectly. Briefly, 10 mM stock solution of DPBF was prepared in ethanol, and kept in the dark. 1 μl of the stock solution was mixed with 1 ml of either MSN@IR780 (150 and 250 μg/ml) or PBS in 10 mm cuvettes, and the solutions in the cuvettes were exposed to either laser or US.

For laser irradiations, 785 nm laser light (500 mW/cm^2) was applied for 5 min, and the absorbance intensity at 410 nm was recorded initially and after every 1 min of laser irradiation. For US irradiations, US (1.5 W/cm^2, 50% duty cycle) was applied for 3 min, and the absorbance intensity at 410 nm was recorded initially and after every 1 min of US irradiation. Results are means of three independent experiments (n=3).

5.2.14 Post-treatment Biofilm Formation Assay

For MRSA and MDR *P. aeruginosa*, the post-treatment (after PDT, SDT, and SPDT) biofilm formation, was assessed. Briefly, an overnight culture of bacteria was diluted to 10^7-10^8 CFU/ml in fresh TSB. 800 μl aliquots of bacterial suspensions were transferred into the wells of 12-well plates. In MSN@IR780 PDT group, the bacterial suspension was incubated with 800 μl of MSN@IR780 (150 and 250 μg/ml, for MRSA and MDR *P. aeruginosa*, respectively), for 30 min in the dark, then exposed to laser light (500 mW/cm^2, 5 min). In MSN@IR780 SDT group, the bacterial suspension was incubated with 800 μl of MSN@IR780 (150 and 250 μg/ml, for MRSA and MDR *P. aeruginosa*, respectively), for 30 min in the dark, then exposed to US irradiation (1.5 W/cm^2, 50% duty cycle, 3 min). In MSN@IR780 SPDT group, the bacterial suspension was incubated with 800 μl of MSN@IR780 (150 and 250 μg/ml, for MRSA and MDR *P. aeruginosa*, respectively), for 30 min in the dark, then exposed to US irradiation (1.5 W/cm^2, 50% duty cycle, 3 min), followed by laser light (500 mW/cm^2, 5 min). In the control group, the bacterial suspension was mixed with 800 μl of PBS. Plates were incubated for 24 h at 37 $^\circ C$ for biofilm formation. After incubation, the broth containing unattached bacterial cells was discarded, and biofilms were washed twice with PBS. Next, Crystal Violet (CV) (0.2% w/v) was added to the biofilms, and allowed to sit for 15 min. After staining, excess CV was removed, and the wells were washed with PBS again to remove any remaining planktonic bacteria. The wells were then air-dried, and 95% ethanol was added to them. Then, the well plate was left on a shaker for 5 min, in order to lyse all bacteria and remove excess CV. Finally, 100 μl aliquots were transferred into 96-well plates, and their Optical Density at 570 nm (OD_{570}) was measured using a microtiter plate reader (iMark Microplate Reader,

Bio-Rad Laboratories, Inc., California, USA). Results are means of three independent experiments (n= 3).

5.2.15 SEM Examination of Post-treatment Biofilms

Scanning Electron Microscopy (SEM) images were obtained to examine the morphology of MRSA and MDR *P. aeruginosa* biofilms 72 h after PDT, SDT, and SPDT treatments. Biofilms were let to grow at the bottom of 12-well plates as described in section 5.2.14. After 72 h of growth, the biofilms were rinsed with sterile PBS and washed with sterile deionized water. The samples were then fixed using 2.5% glutaraldehyde solution for 16 h at 4 $°C$. The plates were washed further with deionized water before being dehydrated by successive insertion in solutions containing 25%, 50%, 75%, and 100% ethanol. The wells were then left to dry in an incubator at 37 $°C$ for 24 h. After incubation, the bottoms of the experimental wells were cut out, platinum sputtered, and scanned with SEM (Quattro ESEM, Thermos Fisher Scientific, MA, USA).

5.2.16 Statistical Analysis

All data were expressed as mean ± SD. Comparison among the different groups was assessed by one-way analysis of variance (ANOVA) followed by the Tukey test. A ($p \leq 0.05$) was used to indicate statistical significance.

5.3 Results

5.3.1 Nanoparticles Synthesis and Characterization

Mesoporous silica nanoparticles were successfully synthesized. STEM images confirmed the synthesis of spherical nanoparticles with a diameter of around 60 nm

(Figure 5.1A and B). MSN were then loaded with IR780 iodide. The loading was confirmed by UV-VIS absorption spectrum of MSN@IR780 as shown in Figure 5.1C.

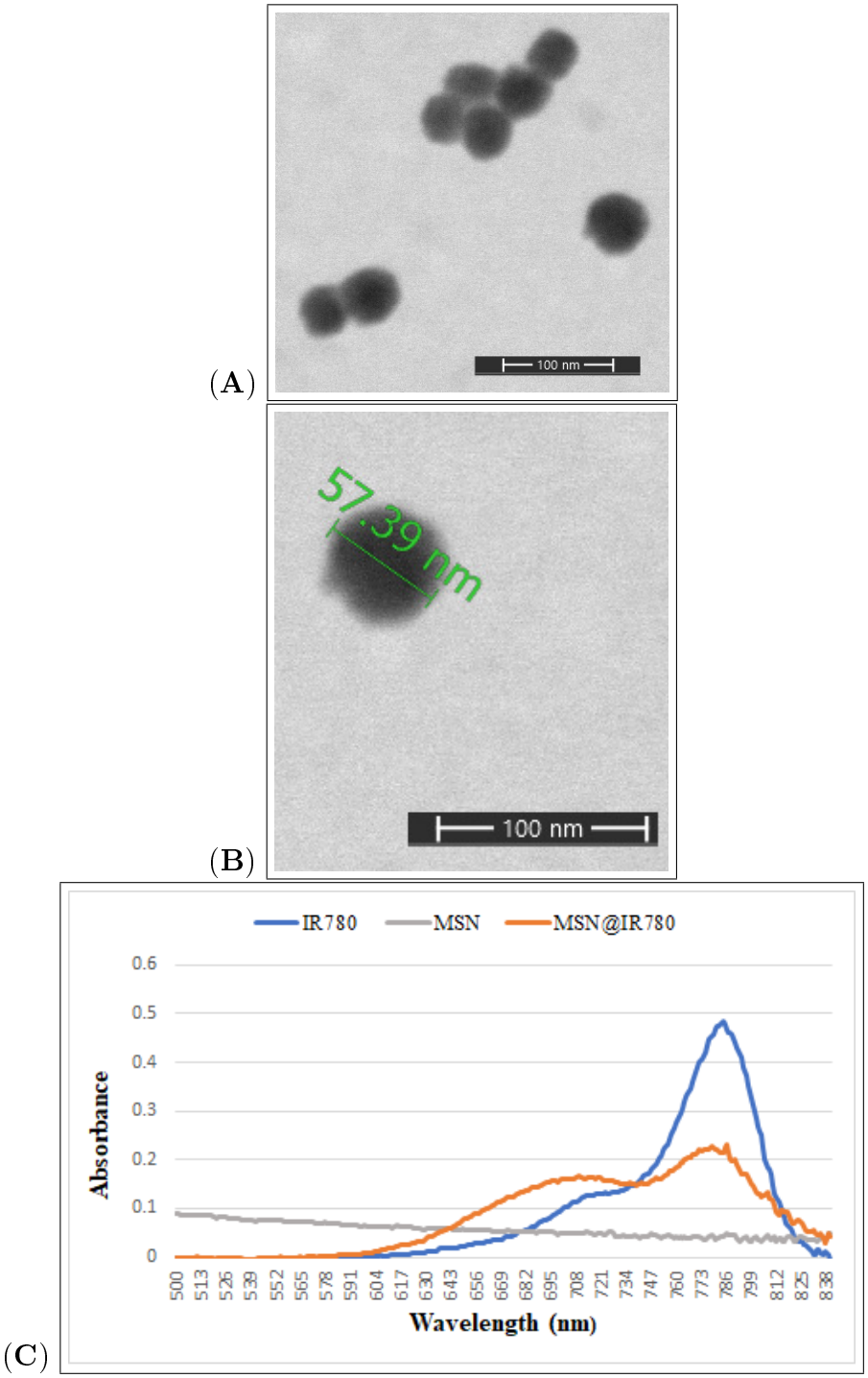

Figure 5.1 STEM images of MSN showing (A) Successful synthesis of spherical MSN, (B) Size of synthesized MSN. (C) UV-VIS spectrum of MSN, IR780 iodide, and MSN@IR780 confirming the loading of IR780 iodide into MSN.

To be able to determine the amount of IR780 iodide loaded into MSN, a calibration curve for IR780 iodide was established first: Briefly, solutions of IR780 iodide

were prepared in ethanol at different concentrations, and their absorbances were measured at 780 nm and plotted versus concentration values. Then, the absorbance of the supernatant following the loading step in nanoparticles synthesis was measured at 780 nm. From this value and the calibration curve, the concentration of IR780 iodide in the supernatant was determined. By subtracting this value from the concentration of IR780 iodide initially added into nanoparticle solution, the concentration of IR780 iodide loaded into MSN was determined, and the loading efficiency was calculated from Eq. 5.1 The results are shown in Table 5.1.

Table 5.1
Loading amount and efficiency of IR780 iodide into MSN

Concentration in preparation solution	83,33 μg/ml
Concentration in supernatant	3.93 μg/ml
Concentration loaded into MSN	79.4 μg/ml
Loading Efficiency	**95%**

5.3.2 Dark Toxicity of IR780 Iodide Loaded MSN

To determine the nontoxic doses for MSN@IR780, six different concentrations (50, 100, 150, 200, 250, and 300 μg/ml) were tested on *S. aureus* (ATCC 25923), and *P. aeruginosa* (ATCC 27853). For *S. aureus*, no cytotoxicity was observed for up to 150 μg/ml, so this concentration was selected to be applied in PDT, SDT, and SPDT studies of *S. aureus* and MRSA. For *P. aeruginosa*, no cytotoxicity was observed for up to 250 μg/ml, so this concentration was selected to be applied in PDT, SDT, and SPDT studies of *P. aeruginosa* and MDR *P. aeruginosa*. The results are shown in Figure 5.2 for *S. aureus* and Figure 5.3 for *P. aeruginosa*.

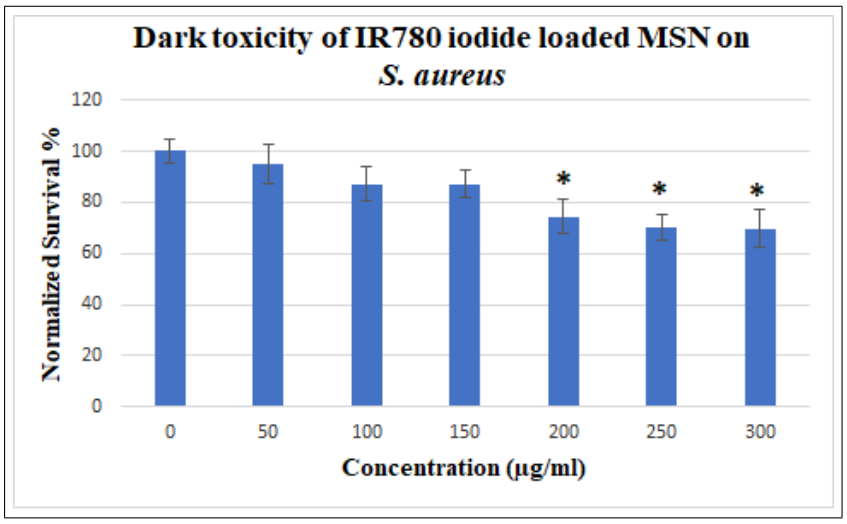

Figure 5.2 Dark toxicity of IR780 iodide loaded MSN on *S. aureus* (ATCC 25923). $*$ indicates statistical significance with respect to the control group. Data represent mean values $\pm$ SD of triplicate experiments (n=3).

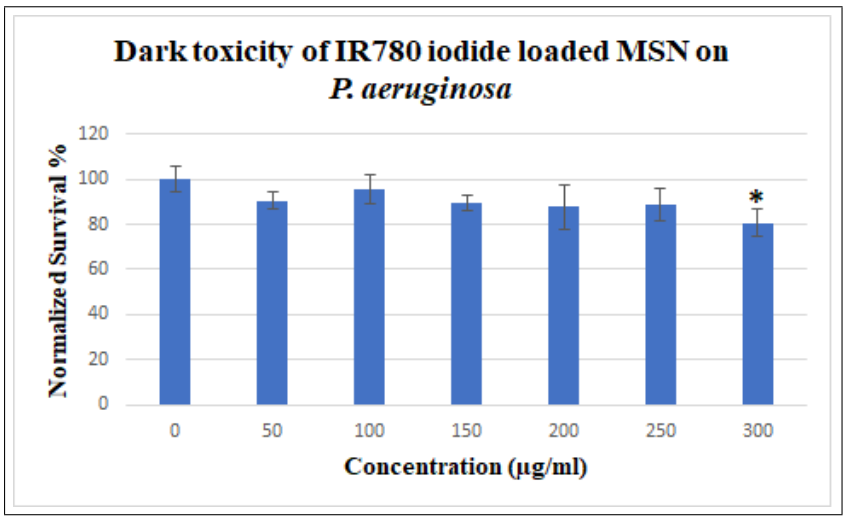

Figure 5.3 Dark toxicity of IR780 iodide loaded MSN on *P. aeruginosa* (ATCC 27853). $*$ indicates statistical significance with respect to the control group. Data represent mean values $\pm$ SD of triplicate experiments (n=3).

5.3.3 Cytotoxicity of MSN@IR780 on L929 cells

The cytotoxic effect of MSN@IR780 at concentrations of 150 and 250 μg/ml (the concentrations used in PDT, SDT, and SPDT studies), on L929 cells was evaluated. No cytotoxicity was observed at the tested concentrations, compared to the control group ($P > 0.05$). The results are plotted in Figure 5.4.

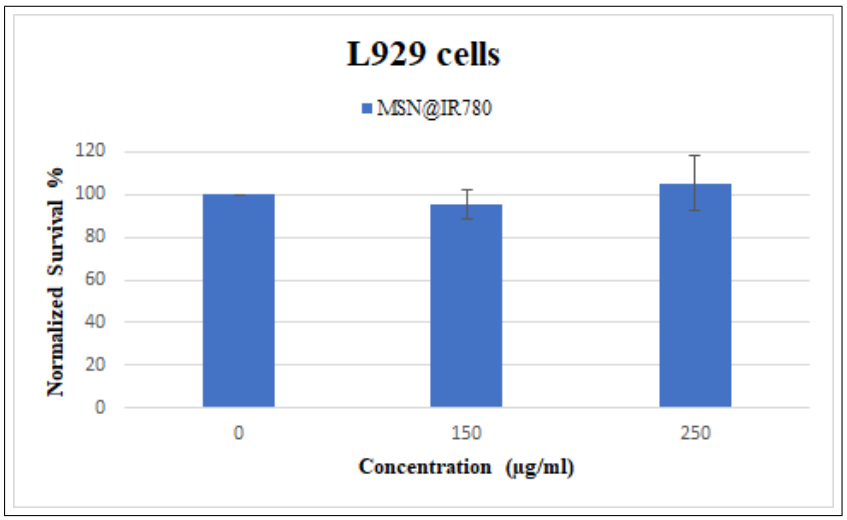

Figure 5.4 Cytotoxicity of IR780 iodide loaded MSN on L929 cells. Data represent mean values ± SD of triplicate experiments (n=3).

5.3.4 PDT Studies

5.3.4.1 PDT application on *S. aureus*. It was observed that there was a significant decrease in bacterial cell viability in MSN@IR780 PDT group with respect to the control group ($P \leq 0.05$). Almost 74% of the bacteria in MSN@IR780 PDT group were killed. The results are plotted in Figure 5.5 normalized to the control group. There was no statistically significant difference between laser ONLY and MSN@IR780 groups, and the control group.

5.3.4.2 PDT application on *P. aeruginosa*. The results of PDT application on *P. aeruginosa* are plotted in Figure 5.6 normalized to the control group. In MSN@IR780 PDT group, it was observed that there was about 32% decrease in bacterial cell viability with respect to the control group ($P \leq 0.05$). Laser ONLY and MSN@IR780 had no effect on bacterial cell viability.

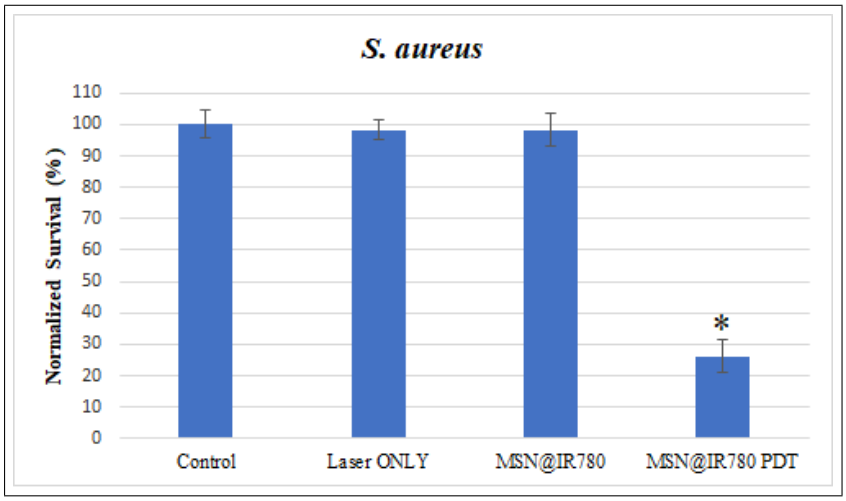

Figure 5.5 Viability of *S. aureus* (ATCC 25923) after PDT using 785 nm diode laser (500 mW/cm^2, 5 min) and MSN@IR780 (150 μg/ml). $*$ indicates statistical significance ($P \leq 0.05$) compared to the control, laser ONLY, and MSN@IR780 groups. Data represent mean values $\pm$ SD of triplicate experiments (n=3).

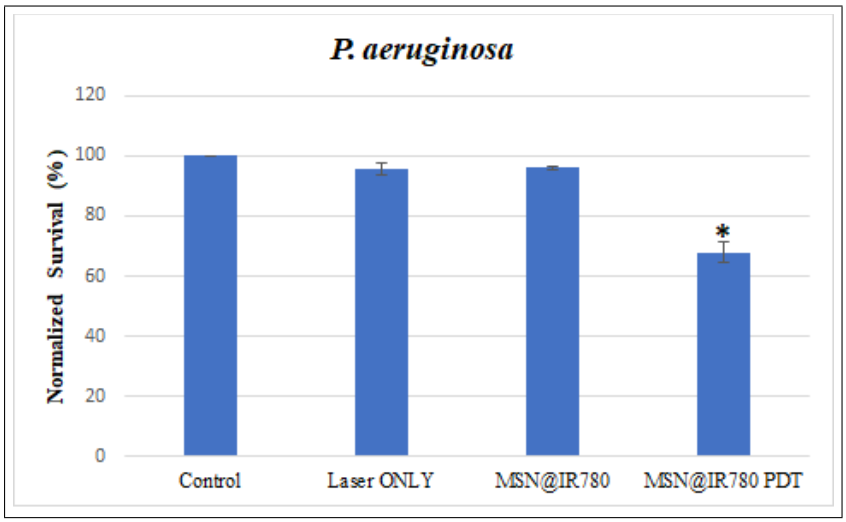

Figure 5.6 Viability of *P. aeruginosa* (ATCC 27853) after PDT using 785 nm diode laser (500 mW/cm^2, 5 min) and MSN@IR780 (250 μg/ml). $*$ indicates statistical significance ($P \leq 0.05$) compared to the control, laser ONLY, and MSN@IR780 groups. Data represent mean values $\pm$ SD of triplicate experiments (n=3).

5.3.4.3 PDT application on MRSA. For MRSA, it was observed that 99.97% of the bacteria in MSN@IR780 PDT group were killed. The results are plotted in Figure 5.7 normalized to the control group. It was observed that there was no statistically significant difference between laser ONLY and MSN@IR780 groups, and the control group.

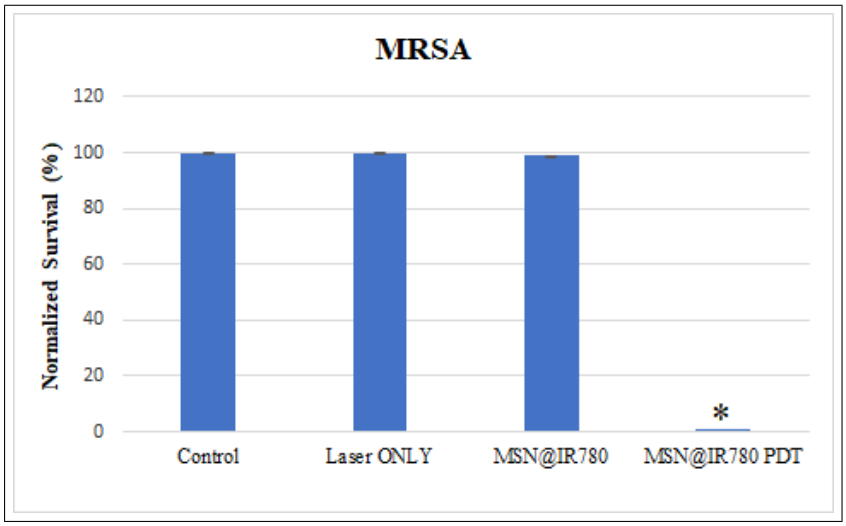

Figure 5.7 Viability of MRSA after PDT using 785 nm diode laser (500 mW/cm^2, 5 min) and MSN@IR780 (150 μg/ml). $*$ indicates statistical significance ($P \leq 0.05$) compared to the control, laser ONLY, and MSN@IR780 groups. Data represent mean values ± SD of triplicate experiments (n=3).

5.3.4.4 PDT application on MDR *P. aeruginosa*. The results of PDT application on MDR *P. aeruginosa* are plotted in Figure 5.8 normalized to the control group. In MSN@IR780 PDT group, it was observed that there was about 36% decrease in bacterial cell viability, with respect to the control group ($P \leq 0.05$). Laser ONLY and MSN@IR780 had no effect on bacterial cell viability.

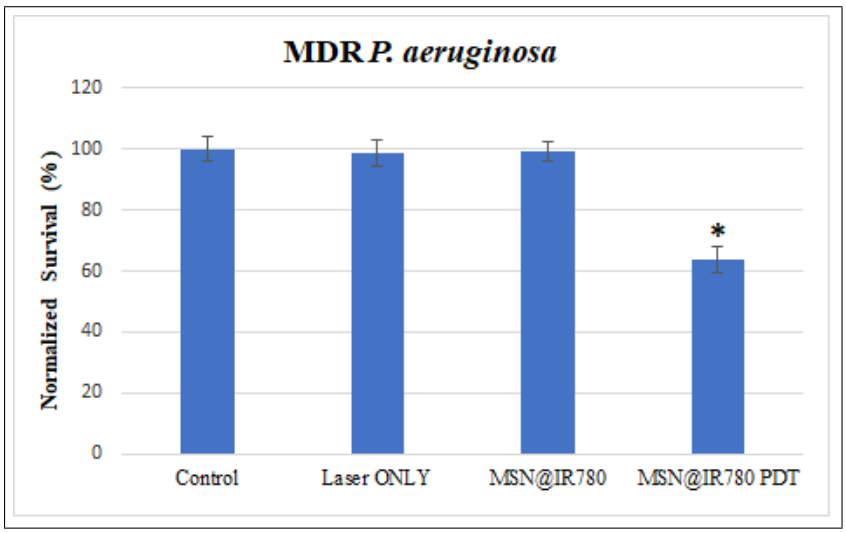

Figure 5.8 Viability of MDR *P. aeruginosa* after PDT using 785 nm diode laser (500 mW/cm^2, 5 min) and MSN@IR780 (250 μg/ml). $*$ indicates statistical significance ($P \leq 0.05$) compared to the control, laser ONLY, and MSN@IR780 groups. Data represent mean values ± SD of triplicate experiments (n=3).

5.3.5 SDT Studies

5.3.5.1 SDT application on *S. aureus*. It was observed that there was a significant decrease in bacterial cell viability in MSN@IR780 SDT group with respect to the control group. About 15% of the bacteria in MSN@IR780 SDT group were killed. The results are plotted in Figure 5.9 normalized to the control group. There was no statistically significant difference between MSN@IR780 group and the control group.

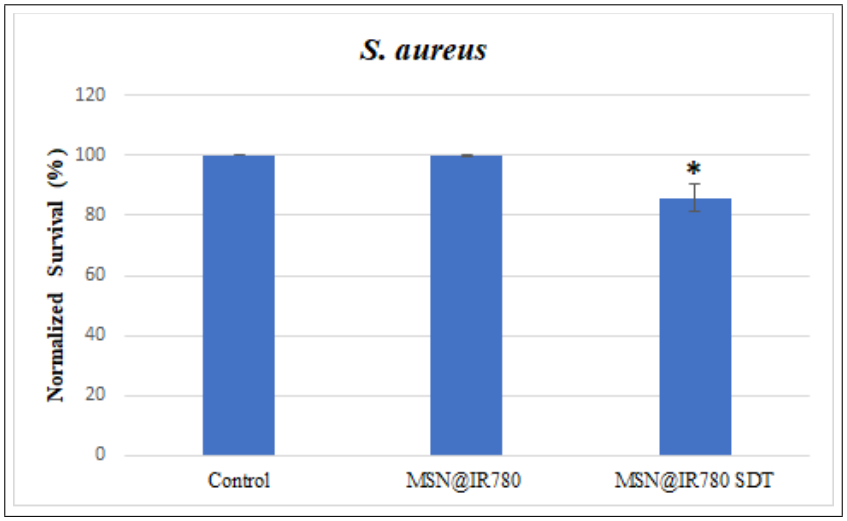

Figure 5.9 Viability of *S. aureus* (ATCC 25923) after SDT using using 1-MHz ultrasound unit (1.5 W/cm^2, 50% duty cycle, 3 min) and MSN@IR780 (150 μg/ml). $*$ indicates statistical significance ($P \leq 0.05$) compared to the control group. Data represent mean values $\pm$ SD of triplicate experiments (n=3).

5.3.5.2 SDT application on *P. aeruginosa*. The results of SDT application on *P. aeruginosa* are plotted in Figure 5.10 normalized to the control group. In MSN@IR780 SDT group, it was observed that there was about 18% decrease in bacterial cell viability with respect to the control group ($P \leq 0.05$).

5.3.5.3 SDT application on MRSA. For MRSA, it was observed that 21% of the bacteria in MSN@IR780 SDT group were killed. The results are plotted in Figure 5.11 normalized to the control group. No statistically significant difference was found between MSN@IR780 group and the control group.

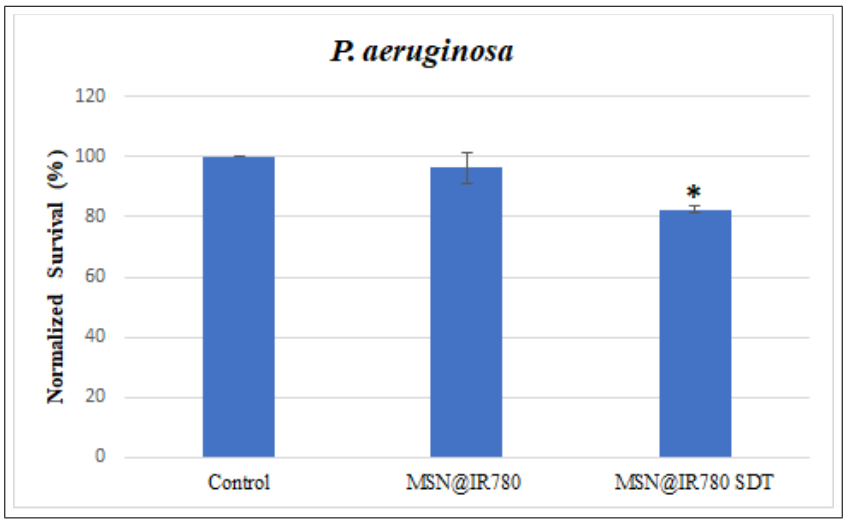

Figure 5.10 Viability of *P. aeruginosa* (ATCC 27853) after SDT using using 1-MHz ultrasound unit (1.5 W/cm^2, 50% duty cycle, 3 min) and MSN@IR780 (250 μg/ml). $*$ indicates statistical significance ($P \leq 0.05$) compared to the control group. Data represent mean values $\pm$ SD of triplicate experiments (n=3).

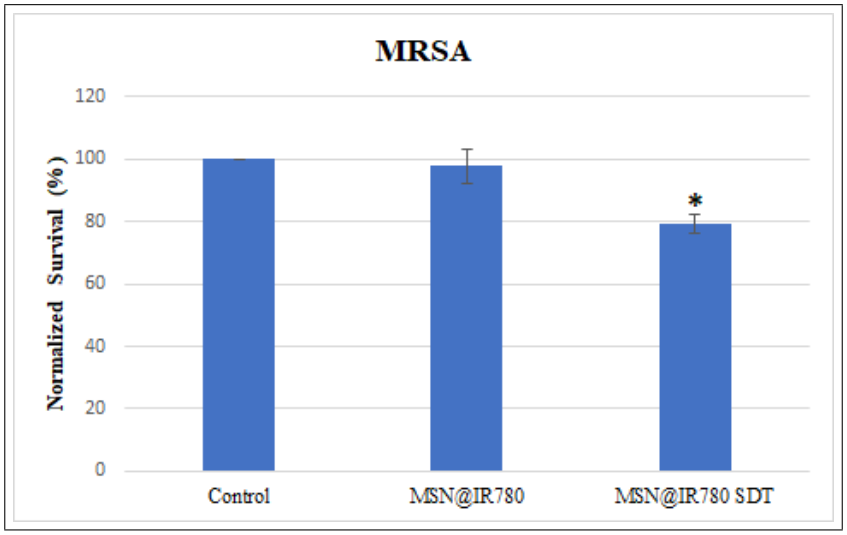

Figure 5.11 Viability of MRSA after SDT using using 1-MHz ultrasound unit (1.5 W/cm^2, 50% duty cycle, 3 min) and MSN@IR780 (150 μg/ml). $*$ indicates statistical significance ($P \leq 0.05$) compared to the control group. Data represent mean values $\pm$ SD of triplicate experiments (n=3).

5.3.5.4 SDT application on MDR *P. aeruginosa*. The results of SDT application on MDR *P. aeruginosa* are plotted in Figure 5.12 normalized to the control group. In MSN@IR780 SDT group, it was observed that there was about 14% decrease in bacterial cell viability with respect to the control group ($P \leq 0.05$).

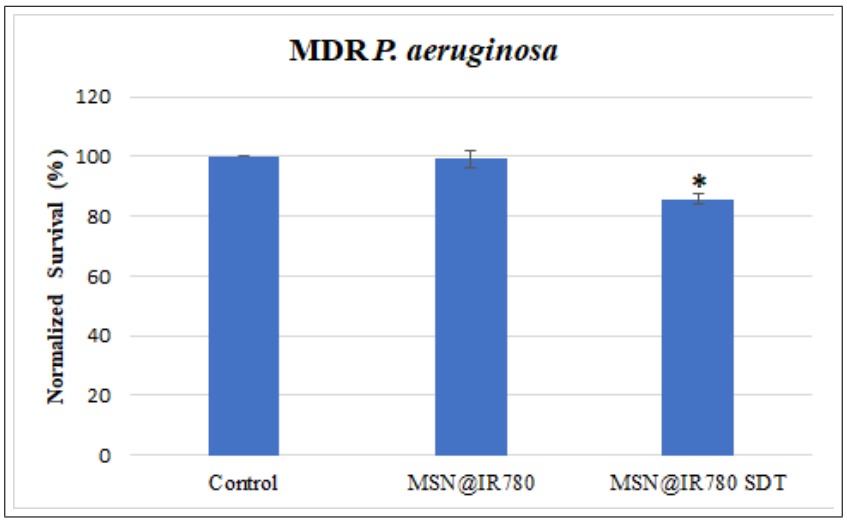

Figure 5.12 Viability of MDR *P. aeruginosa* after SDT using using 1-MHz ultrasound unit (1.5 W/cm^2, 50% duty cycle, 3 min) and MSN@IR780 (250 μg/ml). $*$ indicates statistical significance ($P \leq 0.05$) compared to the control group. Data represent mean values ± SD of triplicate experiments (n=3).

5.3.6 Combined PDT and SDT Studies

5.3.6.1 Combined PDT and SDT application on *S. aureus*. Figure 5.13 shows the effects of SDT, PDT, and SPDT on *S. aureus* (ATCC 25923). In the three groups, there was a significant decrease in bacterial cell viability with respect to the control group ($P \leq 0.05$). When exposed to SDT followed by PDT, about 47% of bacteria was killed, as compared to 14% and 44%, when exposed to SDT alone and PDT alone, respectively. There was no statistically significant difference between PDT and SPDT groups, but both were statistically significantly different from SDT group ($P \leq 0.05$).

5.3.6.2 Combined PDT and SDT application on *P. aeruginosa*. When exposed to SDT followed by PDT, about 44% of bacteria was killed, as compared to 18% and 31%, when exposed to SDT alone and PDT alone, respectively. The decrease in bacterial cell viability in any group was statistically significantly different from all other groups ($P \leq 0.05$). The results are shown in figure 5.14.

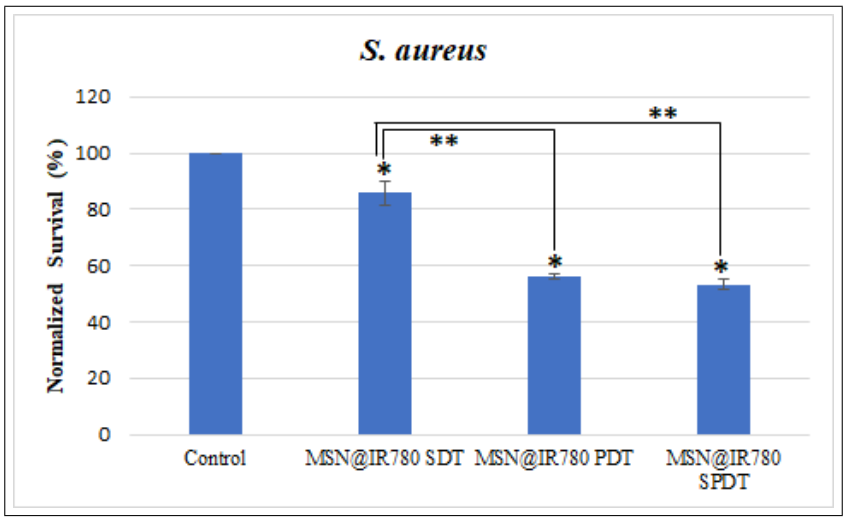

Figure 5.13 Viability of *S. aureus* (ATCC 25923) after combined SDT and PDT using 1-MHz ultrasound unit (1.5 W/cm^2, 50% duty cycle, 3 min), 785 nm diode laser (500 mW/cm^2, 5 min), and MSN@IR780 (150 μg/ml). SPDT: SDT followed by PDT. $*$ indicates statistical significance ($P \leq 0.05$) compared to the control group. $**$ indicates statistical significance ($P \leq 0.05$) compared to SDT group. Data represent mean values ± SD of triplicate experiments (n=3).

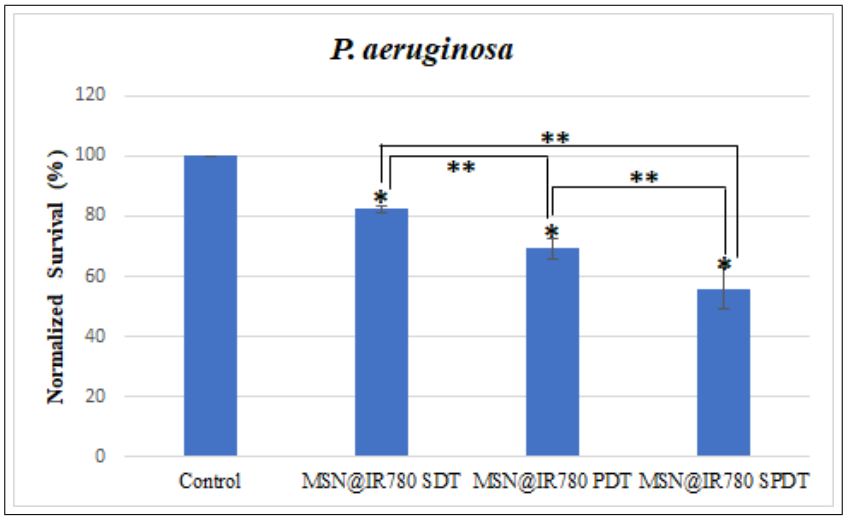

Figure 5.14 Viability of *P. aeruginosa* (ATCC 27853) after combined SDT and PDT using 1-MHz ultrasound unit (1.5 W/cm^2, 50% duty cycle, 3 min),785 nm diode laser (500 mW/cm^2, 5 min), and MSN@IR780 (250 μg/ml). SPDT: SDT followed by PDT. $*$ indicates statistical significance ($P \leq 0.05$) compared to the control group. $**$ indicates statistical significance ($P \leq 0.05$) between the two related groups. Data represent mean values ± SD of triplicate experiments (n=3).

5.3.6.3 Combined PDT and SDT application on MRSA.

For MRSA, almost all bacteria in PDT and SPDT groups were killed. In SPDT group, there was a 4.1-log reduction in bacterial cell viability (99.99% decrease), while in PDT group, there was a 3-log reduction in bacterial cell viability (99.90% decrease). However, there was no statistically significant difference between the two groups ($P > 0.05$).

SDT caused a 21% decrease in bacterial cell viability with respect to the control group ($P \leq 0.05$). The results are shown in figure 5.15.

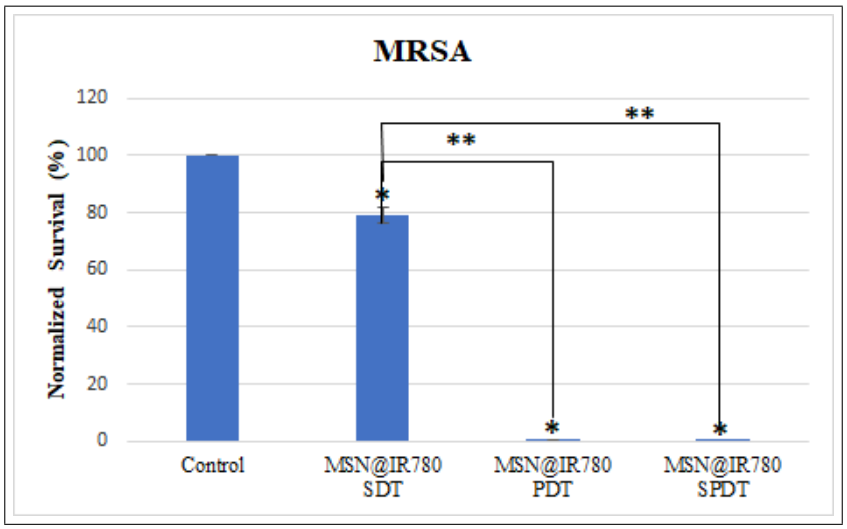

Figure 5.15 Viability of MRSA after combined SDT and PDT using 1-MHz ultrasound unit (1.5 W/cm^2, 50% duty cycle, 3 min), 785 nm diode laser (500 mW/cm^2, 5 min), and MSN@IR780 (150 μg/ml). SPDT: SDT followed by PDT. $*$ indicates statistical significance ($P \leq 0.05$) compared to the control group. $**$ indicates statistical significance ($P \leq 0.05$) compared to SDT group. Data represent mean values ± SD of triplicate experiments (n=3).

5.3.6.4 Combined PDT and SDT application on MDR *P. aeruginosa*. Figure 5.16 shows the effects of SDT, PDT, and SPDT on MDR Pa. aeruginosa. In the three groups, there was a significant decrease in bacterial cell viability with respect to the control group ($P \leq 0.05$). When exposed to SDT followed by PDT, about 45% of bacteria was killed, as compared to 14% and 30%, when exposed to SDT alone and PDT alone, respectively. The decrease in bacterial cell viability in any group was statistically significantly different from all other groups ($P \leq 0.05$).

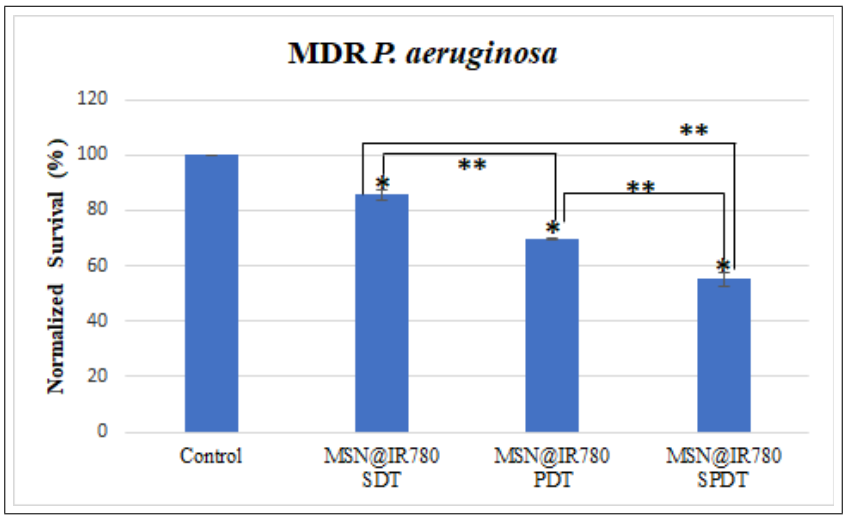

Figure 5.16 Viability of MDR *P. aeruginosa* after combined SDT and PDT using 1-MHz ultrasound unit (1.5 W/cm^2, 50% duty cycle, 3 min),785 nm diode laser (500 mW/cm^2, 5 min), and MSN@IR780 (250 μg/ml). SPDT: SDT followed by PDT. $*$ indicates statistical significance ($P \leq 0.05$) compared to the control group. $**$ indicates statistical significance ($P \leq 0.05$) between the two related groups. Data represent mean values $\pm$ SD of triplicate experiments (n=3).

5.3.7 Bacterial Cell Viability in the Presence of ROS Quenchers

The effects of the presence of NaN3, as a singlet oxygen quencher, on bacterial cell viability with or without MSN@IR780 are shown in Figure 5.17 for MRSA, and Figure 5.18 for MDR *P. aeruginosa*. Control groups involve bacterial cells incubated with 0 or 50 mM of NaN3 for 30 min, to test for its toxicity (without laser or US irradiation). No decrease in cell viability associated with NaN3 dissolved in PBS (pH 7.4), was observed.

For MRSA, the second cluster of bars in figur 5.17 corresponds to the groups incubated with 150 μg/ml of MSN@IR780 iodide, with 0 or 50 mM of NaN3 for 30 min, before US irradiation. The third cluster of bars corresponds to the groups incubated with 150 μg/ml of MSN@IR780 iodide with 0 or 50 mM of NaN3 for 30 min, before laser light irradiation. The fourth cluster of bars corresponds to the groups incubated with 150 μg/ml of MSN@IR780 iodide with 0 or 50 mM of NaN3 for 30 min, before US irradiation followed by laser light irradiation. Addition of NaN3 showed a significant increase in bacterial cell viability due to US, laser, and US followed by laser irradiations,

compared to SDT, PDT, and SPDT groups without the addition of NaN3 ($P \leq 0.05$).

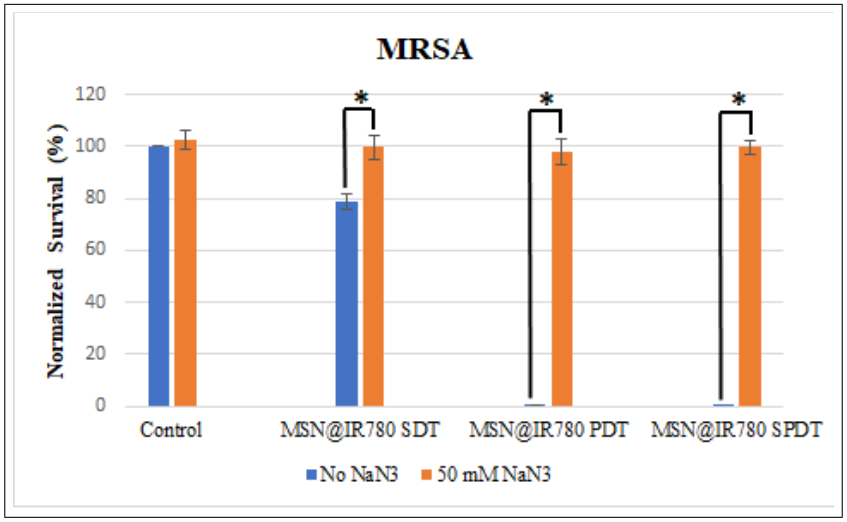

Figure 5.17 Viability of MRSA after combined SDT and PDT using 1-MHz ultrasound unit (1.5 W/cm^2, 50% duty cycle, 3 min), 785 nm diode laser (500 mW/cm^2, 5 min), and MSN@IR780 (150 μg/ml) in the presence and absence of NaN3 (50 mM). $*$ indicates statistical significance ($P \leq 0.05$) compared to the control group. Data represent mean values ± SD of triplicate experiments (n=3).

For MDR *P. aeruginosa*, the second cluster of bars in figure 5.18 corresponds to the groups incubated with 250 μg/ml of MSN@IR780 iodide with 0 or 50 mM of NaN3 for 30 min, before US irradiation. The third cluster of bars corresponds to the groups incubated with 250 μg/ml of MSN@IR780 iodide with 0 or 50 mM of NaN3 for 30 min, before laser light irradiation. The fourth cluster of bars corresponds to the groups incubated with 250 μg/ml of MSN@IR780 iodide with 0 or 50 mM of NaN3 for 30 min, before US irradiation followed by laser light irradiation. Addition of NaN3 showed a significant increase in bacterial cell viability due to US, laser, and US followed by laser irradiations, compared to SDT, PDT, and SPDT groups without the addition of NaN3 ($P \leq 0.05$).

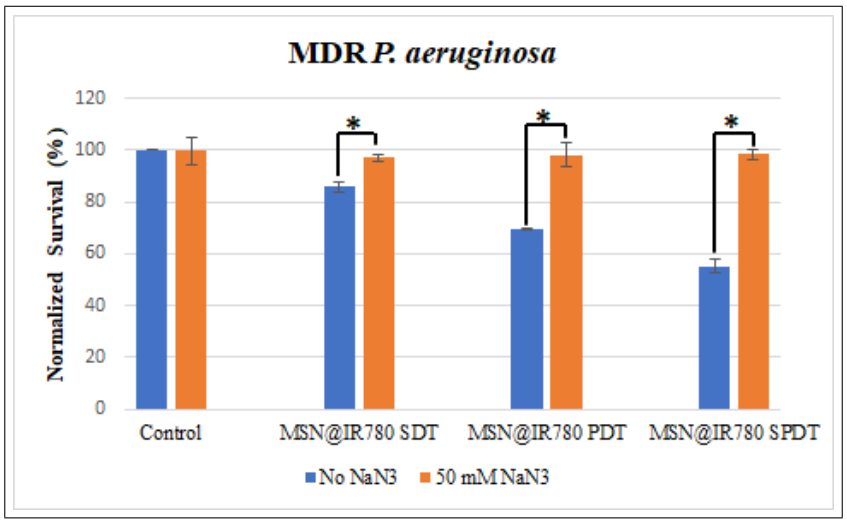

Figure 5.18 Viability of MDR *P. aeruginosa* after combined SDT and PDT using 1-MHz ultrasound unit (1.5 W/cm^2, 50% duty cycle, 3 min), 785 nm diode laser (500 mW/cm^2, 5 min), and MSN@IR780 (250 μg/ml) in the presence and absence of NaN3 (50 mM). $*$ indicates statistical significance ($P \leq 0.05$) compared to the control group. Data represent mean values $\pm$ SD of triplicate experiments (n=3).

5.3.8 Temperature Measurements

Thermal changes of MSN@ IR780 solutions (250 μg/ml) during 785 nm laser irradiation (500 mW/cm^2, 5 min), and US irradiation (1.5 W/cm^2, 50% duty cycle, 3 min) were recorded. For laser irradiation, the increase in temperature after 5 min irradiation of MSN@ IR780 (250 μg/ml) and PBS (control), was about 1.7 $^{\circ}C$ and 2 $^{\circ}C$, respectively. The results are plotted in Figure 5.19. For US irradiation, the increase in temperature after 3 min irradiation of MSN@ IR780 (250 μg/ml) and PBS (control), was about 5.8 $^{\circ}C$ and 7.3 $^{\circ}C$, respectively. The results are plotted in Figure 5.20.

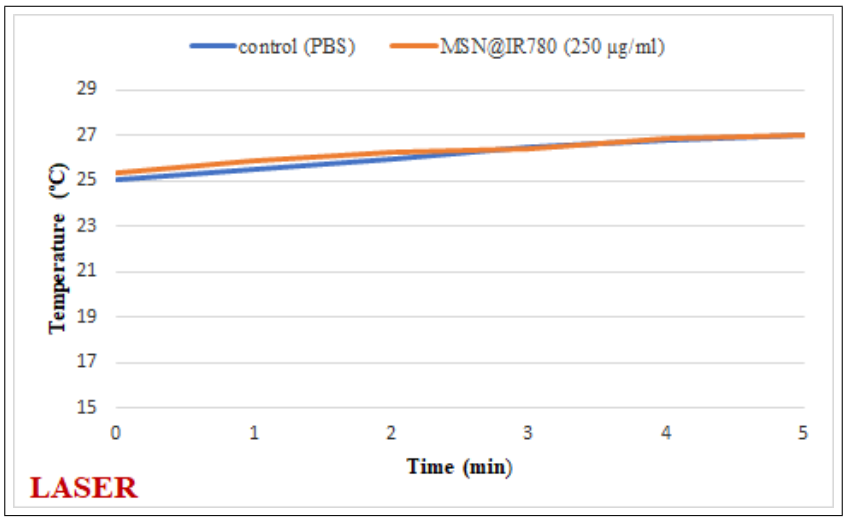

Figure 5.19 Thermal change analysis obtained using an infrared thermal camera for the control (PBS, pH 7.4) and MSN@IR780 (250 μg/ml), under 785 nm laser light irradiation (500 mW/cm^2, 5 min). Data represent mean values of triplicate experiments (n=3).

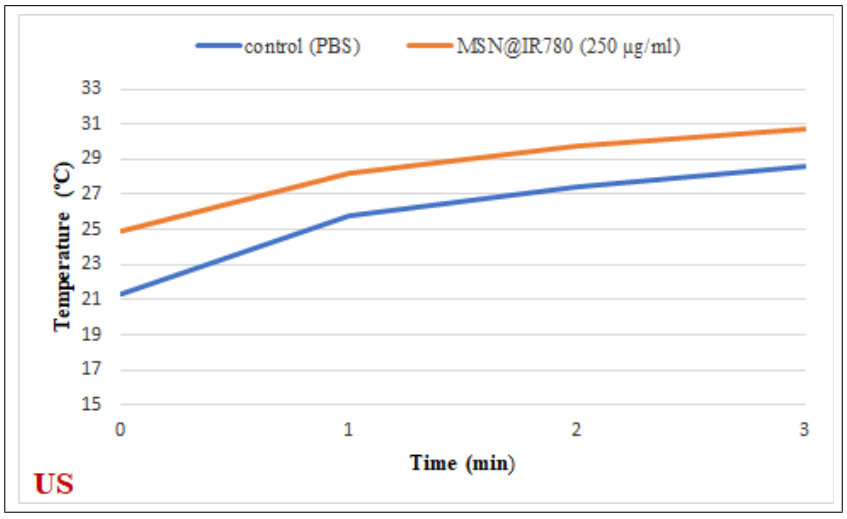

Figure 5.20 Thermal change analysis obtained using an infrared thermal camera for the control (PBS, pH 7.4) and MSN@IR780 (250 μg/ml), 1-MHz US irradiation (1.5 W/cm^2, 50% duty cycle, 3 min). Data represent mean values of triplicate experiments (n=3).

These results are consistent with the results obtained using an infrared thermal thermometer before and after each laser and US application in PDT and SDT experiments. The results are shown in Figure 5.21 for PDT, and Figure 5.22 for SDT.

As can be seen in Figure 5.21, the maximum temperature increase during PDT was about 2 $°C$, and there was no statistically significant difference between the different bacterial strains examined ($P > 0.05$).

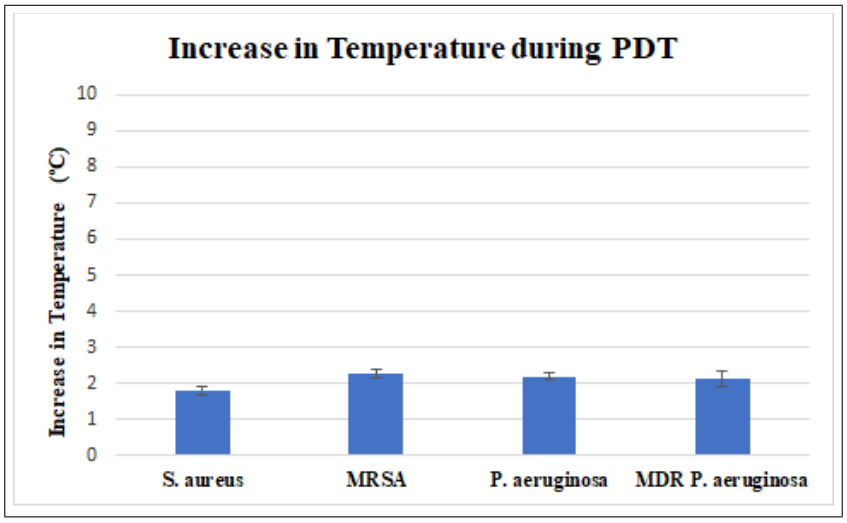

Figure 5.21 Thermal change during PDT (785 nm laser light, 500 mW/cm^2, 5 min), for the different tested bacterial strains, obtained using an infrared thermal thermometer. MSN@IR780 concentrations used were 150 μg/ml for *S. aureus* (ATCC 25923) and MRSA, and 250 μg/ml for *P. aeruginosa* (ATCC 27853) and MDR *P. aeruginosa*. Data represent mean values ± SD of triplicate experiments (n=3).

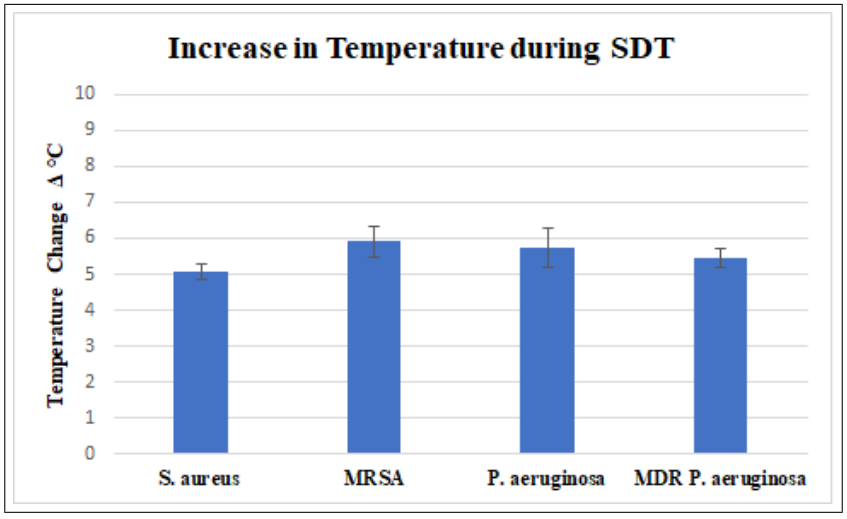

Figure 5.22 Thermal change during SDT (1.5 W/cm^2, 50% duty cycle, 3 min), for the different tested bacterial strains, obtained using an infrared thermal thermometer. MSN@IR780 concentrations used were 150 μg/ml for *S. aureus* (ATCC 25923) and MRSA, and 250 μg/ml for *P. aeruginosa* (ATCC 27853) and MDR *P. aeruginosa*. Data represent mean values ± SD of triplicate experiments (n=3).

As can be seen in Figure 5.22, the maximum temperature increase during SDT was about 6 $°C$, and there was no statistically significant difference between the different bacterial strains examined ($P > 0.05$).

5.3.9 Reactive Oxygen Species (ROS) Production

DPBF reacts with ROS causing absorbance bleaching of the probe near 410 nm, and the change in the absorbance can be measured using a spectrophotometer [89]. By utilizing this method, the ability of MSN@IR780 to generate ROS under 785 nm laser light irradiation (500 mW/cm^2), and US (1.5 W/cm^2, 50% duty cycle), was monitored via absorption reduction of DPBF at 410 nm. For laser irradiation, the absorbance intensity of DPBF was observed over a period of 5 min, and the decrease in absorbance after every 1 min of laser irradiation, was plotted versus time. For US irradiation, the absorbance intensity of DPBF was observed over a period of 3 min, and the decrease in absorbance, , after every 1 min of US irradiation, was plotted versus time. As can be seen from Figure 5.23 and Figure 5.24, MSN@IR780 caused significant DPBF bleaching (reduction in absorbance intensity) under laser and US irradiations, indicating ROS production. Increasing the concentration of MSN@IR780 from 150 μg/ml to 250 μg/ml, had negligible effect on DPBF bleaching. The figures also show that the bleaching caused under laser irradiation (45%) was more than the bleaching caused under US irradiation (15

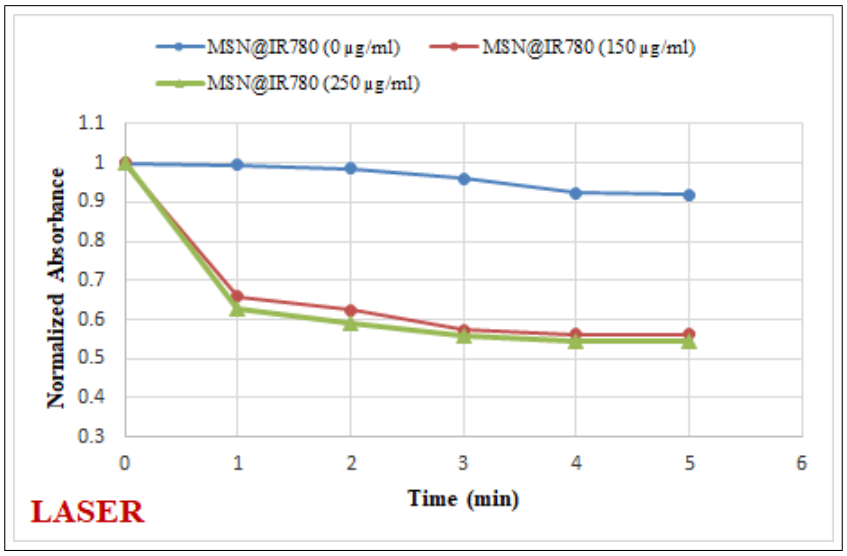

Figure 5.23 ROS production shown as a decrease in DPBF absorbance at 410 nm under 785 nm laser light irradiation (500 mW/cm^2) for a duration of 5 min, in the presence of MSN@IR780 (0, 150 and 250 μg/ml). Data represent mean values ± SD of triplicate experiments (n=3).

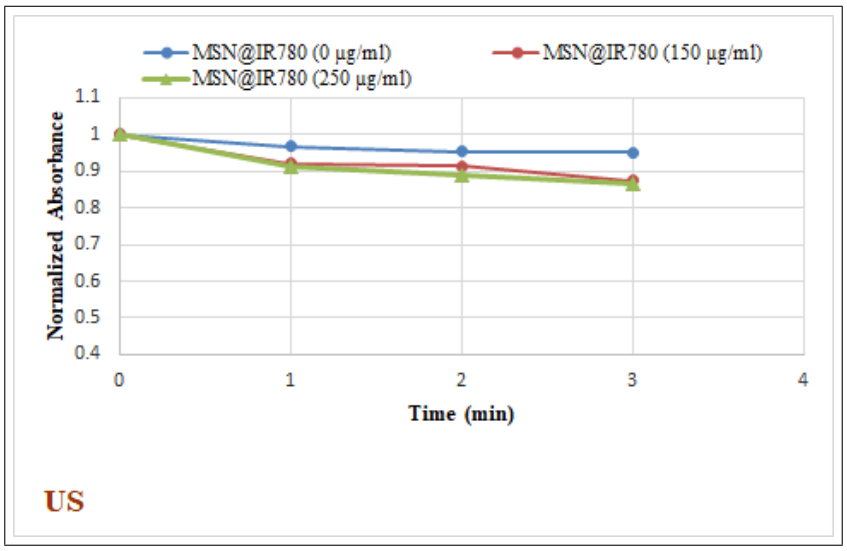

Figure 5.24 ROS production shown as a decrease in DPBF absorbance at 410 nm US irradiation (1.5 W/cm^2, 50% duty cycle) for a duration of 3 min, in the presence of MSN@IR780 (0, 150 and 250 μg/ml). Data represent mean values ± SD of triplicate experiments (n=3).

5.3.10 Post-treatment Biofilm Formation Assay

Biofilm formation of resistant strains of *S. aureus* and *P. aeruginosa* (MRSA and MDR *P. aeruginosa*) post PDT, SDT, and SPDT was assessed by CV assay, 24 h after the treatments. For MRSA, optical density (OD_{570}) measurements demonstrated that sonodynamic treatment with MSN@IR780 decreased the biofilm formation by 7% compared to the untreated control group, but the difference was not statistically significant ($P > 0.05$). In PDT and SPDT groups, there was a significant decrease (45%) in biofilm formation compared to the untreated control group ($P \leq 0.05$). There was no statistically significant difference between PDT and SPDT groups ($P > 0.05$). The results are shown in Figure 5.25 normalized to the untreated control group. For MDR *P. aeruginosa*, optical density (OD_{570}) measurements demonstrated that there was no statistically significant difference in biofilm formation between the treated SDT, PDT, and SPDT groups, and the untreated control group ($P > 0.05$). The results are shown in Figure 5.26 normalized to the control group.

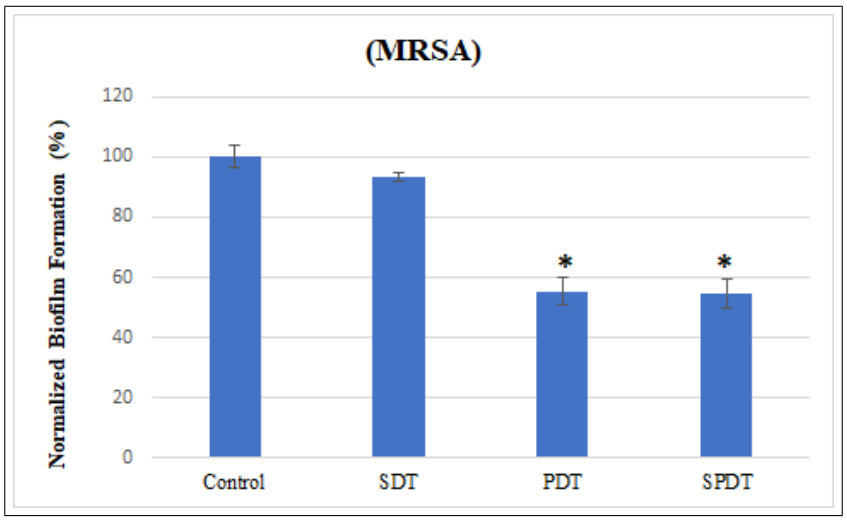

Figure 5.25 Post-treatment biofilm formation by MRSA, assessed by CV assay 24 h post treatments: Control; no laser and no nanoparticles, SDT; MSN@IR780 (150 μg/ml) with US (1.5 W/cm^2, 50% duty cycle, 3 min), PDT; MSN@IR780 (150 μg/ml) with laser light (500 mW/cm^2, 5 min); SPDT; SDT followed by PDT. $*$ indicates statistical significance ($P \leq 0.05$) compared to the control group. Data represent mean values $\pm$ SD of triplicate experiments (n=3).

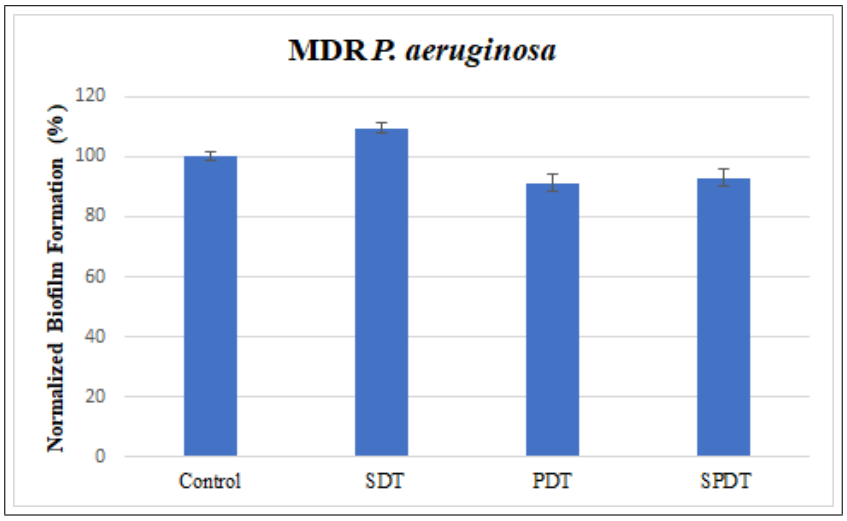

Figure 5.26 Post-treatment biofilm formation by MDR *P. aeruginosa*, assessed by CV assay 24 h post treatments: Control; no laser and no nanoparticles, SDT; MSN@IR780 (250 μg/ml) with US (1.5 W/cm^2, 50% duty cycle, 3 min), PDT; MSN@IR780 (250 μg/ml) with laser light (500 mW/cm^2, 5 min); SPDT; SDT followed by PDT. Data represent mean values $\pm$ SD of triplicate experiments (n=3).

5.3.11 SEM Examination of Post-treatment Biofilms

The SEM images shown in Figure 5.27 were obtained for the control, SDT, PDT, and SPDT groups of MRSA, 72 h post-treatments, to visualize the extent of biofilm formation. Significant reduction of recurrent MRSA biofilm was observed in PDT and

SPDT groups compared to the untreated control group. In SDT group, there was only a slight reduction in biofilm formation compared to the control group, as can be seen in Figure 5.27B.

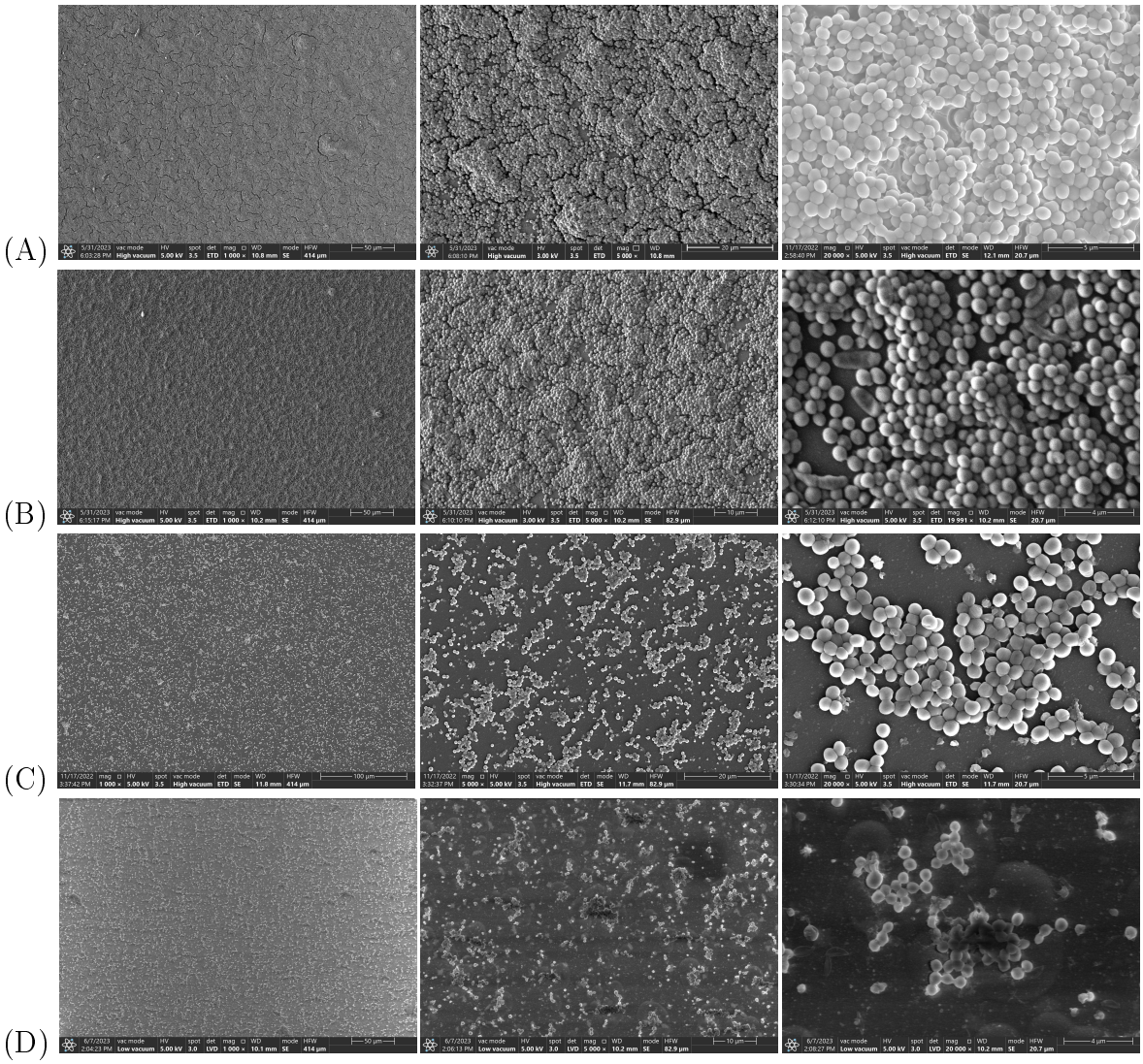

Figure 5.27 SEM images of MRSA biofilms 72 h post treatments: (A) Control; no laser, no US, and no nanoparticles. (B) MSN@IR780 SDT; MSN@IR780 (150 μg/ml) with US (1.5 W/cm^2, 50% duty cycle, 3 min). (C) MSN@IR780 PDT; MSN@IR780 (150 μg/ml) with laser light (500 mW/cm^2, 5 min). (D) MSN@IR780 SPDT; SDT followed by PDT. Left column (1000x), middle column (5000x), right column (20 000x).

The SEM images shown in Figure 5.28 were obtained for the control, SDT, PDT, and SPDT groups of MDR *P. aeruginosa*, 72 h post-treatments, to visualize the extent of biofilm formation. No difference can be seen between SDT and the control groups which is consistent with CV assay results. In PDT group, there is only a slight reduction in biofilm formation compared to the control and SDT groups. Less recurrent

biofilm is observed in SPDT group compared to the control, SDT and PDT groups, although the CV assay revealed that there was no statistically significant difference between these groups.

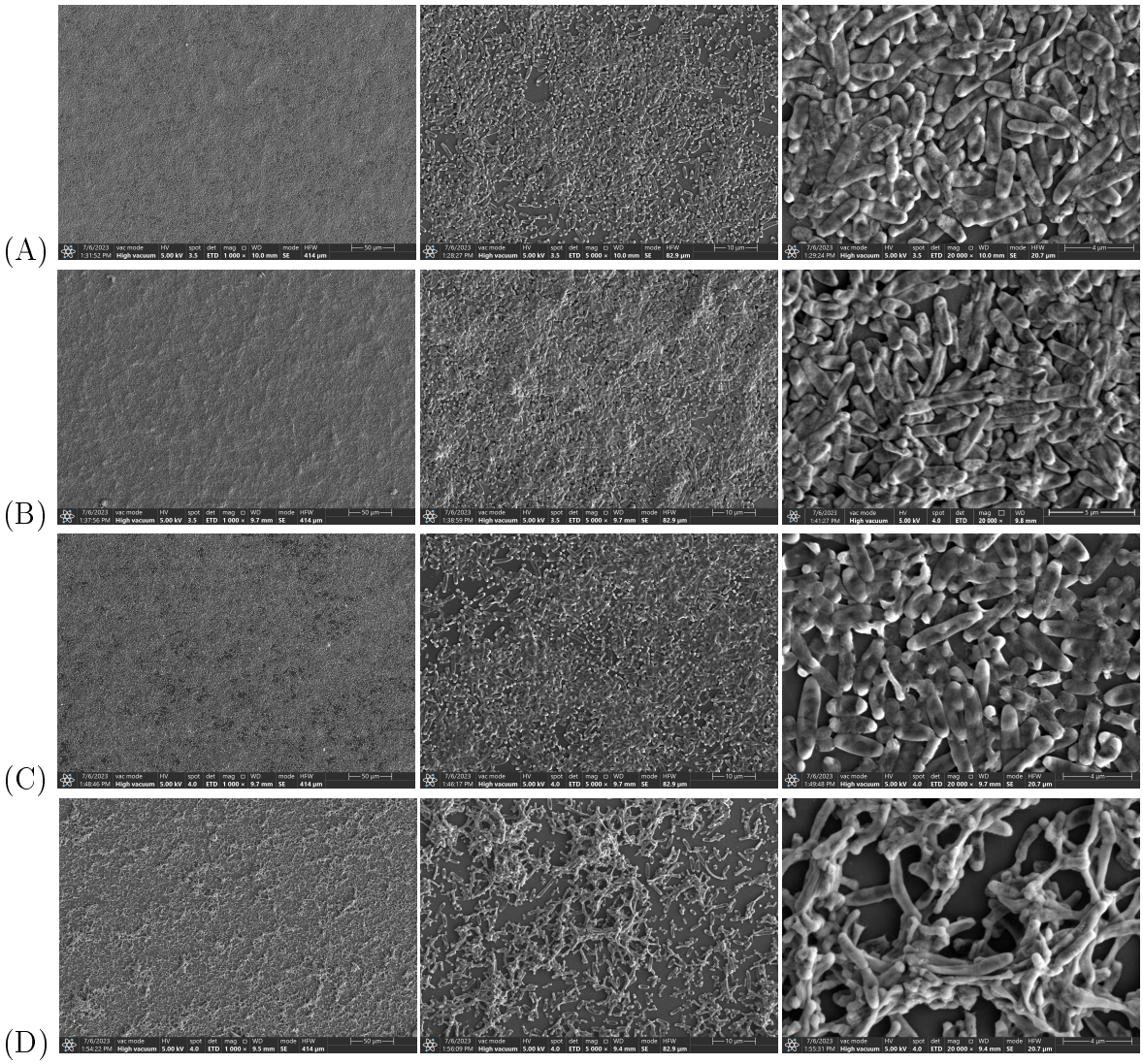

Figure 5.28 SEM images of MDR *P. aeruginosa* biofilms 72 h post treatments: (A) Control; no laser, no US, and no nanoparticles. (B) MSN@IR780 SDT; MSN@IR780 (250 μg/ml) with US (1.5 W/cm^2, 50% duty cycle, 3 min). (C) MSN@IR780 PDT; MSN@IR780 (250 μg/ml) with laser light (500 mW/cm^2, 5 min). (D) MSN@IR780 SPDT; SDT followed by PDT. Left column (1000x), middle column (5000x), right column (20 000x).

A summary of the results obtained in PDT, SDT, and SPDT studies using MSN@IR780, is presented in Table 5.2.

Table 5.2

Summary of the results obtained in PDT, SDT, and SPDT studies using MSN@IR780. SDT; MSN@IR780 with US (1.5 W/cm^2, 50% duty cycle, 3 min), PDT; MSN@IR780 with laser light (500 mW/cm^2, 5 min); SPDT; SDT followed by PDT. MSN@IR780 concentrations used were 150 μg/ml for *S. aureus* and MRSA, and 250 μg/ml for *P. aeruginosa* and MDR *P. aeruginosa*. Temperature measurements were obtained using an infrared thermal thermometer. Biofilm formation was assessed by CV assay 24 h post treatments. Data represent mean values ± SD of triplicate experiments (n = 3).

Normalized survival of planktonic bacteria with respect to the control group % (control =100%)						
	SDT	**PDT**	**SPDT**	**SDT+NaN3**	**PDT+NaN3**	**SPDT+NaN3**
***S. aureus* (ATCC 25923)**	85.87±4.35	55.94±0.93	53.40±1.74	-	-	-
***P. aeruginosa* (ATCC 27853)**	82.28±1.07	69.14±3.39	55.84±6.77	-	-	-
MRSA	79.05±3.02	0.1±0.09	0.01±0.01	99.67±4.87	97.9±4.81	99.66±2.77
MDR *P. aeruginosa*	85.74±1.84	69.66±0.51	55.20±2.50	97.18±1.41	98.24±4.52	98.34±1.72
Increase in Temperature $\Delta\ ^\circ C$						
	SDT	**PDT**				
***S. aureus* (ATCC 25923)**	5.09±0.21	1.80±0.12				
***P. aeruginosa* (ATCC 27853)**	5.72±0.55	2.20±0.10				
MRSA	5.91±0.44	2.27±0.12				
MDR *P. aeruginosa*	5.43±0.26	2.13±0.23				
Normalized biofilm formation with respect to the control group % (control =100%)						
	SDT	**PDT**	**SPDT**			
MRSA	93.09±1.42	55.37±4.46	54.65±4.63			
MDR *P. aeruginosa*	109.54±1.73	91.12±2.80	93.03±2.85			

5.4 Discussion

The aim of this study was to overcome the limitations of toxicity and hydrophobicity of IR780 iodide, by encapsulating it into mesoporous silica nanoparticles, and to investigate the photodynamic, sonodynamic, and combined photodynamic and sonodynamic potentials of these loaded nanoparticles on reference and resistant strains of gram-positive and gram-negative bacteria. At first, MSN were synthesized and loaded with IR780 iodide. STEM images indicated successful synthesis of spherical MSN with a diameter of around 60 nm. UV-VIS spectrum confirmed the loading of IR780 iodide into MSN. The loading efficiency was high (95%).

The results of PDT on planktonic bacteria, suggest that MSN@IR780 effectively reduced the number of living bacterial cells after irradiation with 785 nm laser light (500 mW/cm^2, 5 min), for all the tested strains. The killing was mainly due to photodynamic and not photothermal effect, as confirmed by temperature, and DPBF bleaching measurement results. The ability of MSN@IR780 to generate ROS under laser irradiation was confirmed by the decrease in absorbance intensity of DPBF at 410 nm after laser irradiation. Temperature measurements showed no significant change in temperature in MSN@IR780 PDT groups for all the tested strains, indicating that MSN@IR780 have no photothermal effect. This was also confirmed by the results obtained from testing the photodynamic effect of MSN@IR780 in the presence of NaN3, as a singlet oxygen quencher, on MRSA and MDR *P. aeruginosa*. The addition of NaN3 caused a significant increase in bacterial cell viability, compared to PDT groups without the addition of NaN3 for both strains, excluding any photothermal effect involved. The results also indicate that the killing was caused specifically by singlet oxygen ($^1O_2$).

For the same laser dose and MSN@IR780 dose, it was found that resistant strains of *S. aureus* and *P. aeruginosa* (MRSA and MDR *P. aeruginosa*) were more sensitive to PDT than their reference strains (ATCC 25923 and ATCC 27853). These results are consistent with previous studies [19],[96]. Topaloğlu et al. showed that ICG-PDT was more effective on resistant strains of *S. aureus* and *P. aeruginosa*, than on their reference wild type strains for the same laser energy and ICG doses [19]. Similarly,

Tang et al. found that MRSA strain was more sensitive to pL-ce6 and TBO mediated PDT than *S. aureus* (ATCC 25923) strain [96]. The increased susceptibility of resistant strains, compared to their reference strains, might be due to the variation in their cell wall structures, which might possibly affect the binding and uptake of photosensitizers [19]. Tang et al. suggested that MRSA has a more permeable cell wall than *S. aureus* (ATCC 25923) strain, and this altered architectural structure in MRSA may favor the penetration of photosensitizers across the cell wall, resulting in higher killing of MRSA due to PDT [96].

MSN@IR780 -mediated PDT was more effective on gram-positive strains than on gram-negative strains. The increased susceptibility of gram-positive bacteria compared to gram-negative bacteria can be explained by the difference in cell envelope constituents between the two types. Gram-positive bacteria have a simpler and relatively porous peptidoglycan layer surrounding the cytoplasmic membrane, compared to the complex double lipid bilayer cell envelope structure surrounding the cytoplasmic membrane of gram-negative bacteria [97], which may restrict the entry and internalization of photosensitizers in gram-negative bacteria compared to gram-positive bacteria [19],[71],[98],[99].

SDT was less effective than PDT for all the tested strains. These results are similar to the results obtained from IR780 iodide studies, and are consistent with previous studies [28],[86]. The reason for that can be explained by less ROS production in SDT compared to PDT, as was confirmed by DPBF bleaching results, which showed that ROS production in response to US, was less than ROS production in response to laser light.

The reduction in bacterial cell viability due to SDT ranged between 15 and 21% for the different tested strains. The killing was mainly due to sonodynamic effect with no thermal effect involved. This was confirmed by the results obtained from testing the sonodynamic effect of MSN@IR780, in the presence of NaN3, as a singlet oxygen quencher, on MRSA and MDR *P. aeruginosa*. The addition of NAN3 caused a significant increase in bacterial cell viability compared to SDT groups without the

addition of NaN3 for both strains, excluding any thermal effect involved. The results also indicate that the killing was caused specifically by singlet oxygen ($^1O_2$), which is consistent with the study conducted by Huang et al. [50].

The combined treatment of SDT and PDT, resulted in enhanced reduction in bacterial cell viability compared to SDT and PDT. For MRSA, SPDT caused a 4.1-log reduction in bacterial cell viability, compared to a 3-log reduction caused by PDT, but the difference between the two groups was not statistically significant. For *P. aeruginosa* and MDR *P. aeruginosa*, the enhanced killing effect by SPDT was statistically significant than SDT and PDT, which is expected and consistent with previous studies [86],[87],[88].

A successful antimicrobial treatment should not only be able to inactivate planktonic bacteria, but also be able to inhibit biofilm formation. Biofilms show stronger resistance to antibiotics due to their sophisticated matrix [99], and therefore, combating them is of great concern when dealing with bacterial infections. Post treatment biofilm analysis of MRSA and MDR *P. aeruginosa* was carried out. For MRSA, CV assay revealed that PDT and SPDT inhibited the formation of biofilms by almost 45%. No statistically significant difference was found between the two groups similar to the results of planktonic cells. This reduction in post treatment biofilm formation is probably a result of less bacteria being present in the treated PDT and SPDT groups compared to the control group [100], due to the antimicrobial effect of MSN@IR780. SDT caused a slight reduction in post treatment biofilm formation (7%). This was expected, since the reduction in bacterial cell viability due to SDT was only 15%, which means that there was a lot of bacteria present in SDT group that formed the biofilm afterwards. SEM images confirmed the results of CV assay. They clearly show less developed biofilms in PDT and SPDT groups, while only a slight reduction in the developed biofilm in SDT group, compared to the control group.

For MDR *P. aeruginosa*, although the SEM images showed some reduction in SPDT and PDT groups compared to the control group, CV assay didn't reveal any statistically significant difference between the treated groups and non-treated control

group. Similar to SDT of MRSA, this is probably due the presence of significant number of bacteria in the treated groups, that were able to develop the biofilms.

5.5 Conclusion

The present study shows that IR780 iodide loaded mesoporous silica nanoparticles have photodynamic and sonodynamic potentials for the inactivation of resistant strains of gram-positive and gram-negative bacteria. The photodynamic potential was superior to the sonodynamic potential, and gram-positive bacteria were more susceptible to the treatments than gram-negative bacteria. IR780 iodide loaded mesoporous silica nanoparticles also showed a potential to inhibit post treatment biofilm formation, especially for MRSA. Future work will focus on improving the therapeutic output of sonodynamic therapy using these nanoparticles, and on enhancing the anti-biofilm capability of these nanoparticles.

6. OVERALL DISCUSSION AND CONCLUSION

The rapid spread of antimicrobial resistance has become a serious threat to global health [101]. Therefore, alternative treatments to conventional antibiotics are urgently needed. Photodynamic therapy (PDT) is a promising approach. The killing caused by PDT is entirely based on the generation of ROS by light activated photosensitizers. ROS act on nonspecific targets within a microbe, so it is unlikely that resistance to PDT could be developed [102]. The main limitation of PDT is the limited penetration depth of visible light needed to activate most of the common photosensitizers, limiting the therapeutic potential to superficial areas [23]. Identifying and developing novel photosensitizers that can absorb NIR light, is one possible approach to increase the targeted depth in tissue. Researchers also developed sonodynamic therapy (SDT) as a complementary or alternative therapy to PDT, to overcome the light penetration depth limitation, by using ultrasound to excite the photosensitizers, as it has superior tissue penetration compared to light [24]. Due to the similarities between PDT and SDT, investigation of the combined effect has been a trend in research, especially for the treatment of cancer [81],[82],[83],[84],[85], and recently for the treatment of microbial infections [86],[87],[88].

The aim of this study was to develop a combined PDT and SDT for the treatment of microbial infections caused by resistant bacterial strains. Identifying and developing a novel photo/sonosensitizer was the main factor to consider in order to achieve this aim. IR780 iodide was chosen because it is a NIR dye with a peak absorption of 780 nm, which coincides with the therapeutic window (600-1000 nm) [38], allowing relatively deeper tissue penetration. Moreover, it has a capability of producing ROS, which makes it a good candidate for being used as a photo/sonosensitizer. In addition to that, and to our best knowledge, it was not investigated as a photo/sonosensitizer for the treatment of bacterial infections.

At first, preliminary studies were conducted to find the optimal laser and ultra-

sound parameters. After that, investigation of the photodynamic, sonodynamic, and combined photodynamic and sonodynamic potentials of IR780 iodide on gram-positive *S. aureus* and MRSA, and gram-negative *P. aeruginosa* and MDR *P. aeruginosa* was carried out *in vitro*. The results of PDT showed that IR780 iodide inactivated all the tested strains after being irradiated with a low dose of 785 laser light (500 mW/cm^2, 5 min). It is suggested that the cationic nature of IR780 iodide makes it as effective in inactivating gram-negative *P. aeruginosa*, as it is on gram-positive *S. aureus*. The results also showed that IR780 iodide can function as a sonosensitizer in SDT. However, SDT was less effective than PDT, due to lower ROS production in response to US compared to ROS production in response to laser light, for the same IR780 iodide concentration. Due to the low efficacy of SDT, the combined therapy of SDT and PDT didn't result in a significant enhancement in bacterial inactivation compared to PDT alone.

It is expected that higher concentrations of IR780 iodide would result in higher ROS production, and hence, better PDT, SDT, and combined therapy efficacy. However, the concentrations used in this study were the highest non-toxic concentrations (no dark toxicity) that could be used. As a solution to this problem, encapsulating IR780 iodide into nanoparticles was suggested, as it would result in increasing the amount of IR780 iodide that can be delivered to bacterial cells, due to the large surface to volume ratios of the nanoparticles. Moreover, it could overcome the hydrophobicity drawback of IR780 iodide which could limit its clinical application [44],[45].

Mesoporous silica nanoparticles (MSN) were chosen to be the nanocarriers for IR780 iodide, due to their unique properties such as ease of synthesis, controllable particle size, good biocompatibility, easy functionalization, and large specific surface area and pore volume, enabling high loading capacity of drugs [60],[61],[62],[63],[64],[65].

MSN were successfully synthesized and loaded with IR780 iodide, and their potentials for PDT and SDT were studied. The results of PDT revealed that MSN@IR780 inactivated bacterial cells after irradiation with 785 nm laser light (500 mW/cm^2, 5 min), for all the tested strains. The degree of inactivation was found to be strain

dependent. MRSA showed the best results where almost all bacteria were killed after PDT. Overall, gram-positive and resistant strains were more sensitive to PDT than gram-negative and reference strains, which is consistent with previous studies [19],[71],[98],[99]. Structural differences between the different strains affect the binding and uptake of the photosensitizers, which affect the susceptibility of the different strains to PDT. For example, gram-positive bacteria have a simpler and relatively porous peptidoglycan layer surrounding the cytoplasmic membrane, which allows photosensitizers to enter bacterial cells more easily than in gram-negative bacteria, which have a complex double lipid bilayer cell envelope structure surrounding the cytoplasmic membrane, which may restrict the entry and internalization of photosensitizers, resulting in less susceptibility to PDT.

Similar to the results obtained from free IR780 iodide studies, SDT was less effective than PDT for all the tested strains. This can be explained by DPBF bleaching results, which showed that ROS production in response to US, was less than ROS production in response to laser light, for the same MSN@IR780 concentrations.

The combined treatment of SDT and PDT, resulted in enhanced reduction in bacterial cell viability compared to SDT and PDT. For MRSA, SPDT caused a 4.1-log reduction in bacterial cell viability, compared to a 3-log reduction caused by PDT. For *P. aeruginosa* and MDR *P. aeruginosa*, the enhanced killing by SPDT was statistically significant from SDT and PDT, which is expected and consistent with previous studies [86],[87],[88].

In order to investigate if there was any thermal effect involved in the killing caused by MSN@IR780-mediated PDT, SDT, and SPDT, the experiments were conducted in the presence of NaN3, as a singlet oxygen quencher, on MRSA and MDR *P. aeruginosa*. The addition of NAN3 caused a significant increase in bacterial cell viability, compared to PDT, SDT, and SPDT groups without the addition of NaN3, for both strains, excluding any thermal effect involved. The results also indicate that the killing was caused specifically by singlet oxygen ($^1O_2$).

Since combating biofilms is of great concern when dealing with bacterial infections, the ability of MSN@IR780-mediated PDT, SDT, and SPDT to inhibit post-treatment biofilm formation of MRSA and MDR *P. aeruginosa* was investigated via CV assay and SEM images. For MRSA, both methods revealed that PDT and SPDT inhibited the formation of biofilms by almost 45%, while SDT caused a slight reduction in post treatment biofilm formation (7%). For MDR *P. aeruginosa*, MSN@IR780-mediated PDT, SDT, and SPDT were not able to inhibit post-treatment biofilm formation, probably due the presence of significant amount of bacteria in the treated groups, that were able to develop the biofilms.

In summary, both IR780 iodide and MSN@IR780 have potentials for PDT and SDT of bacterial infections. The results revealed that designing a successful combined therapy depends on many factors, such as the concentration of the photo/sonosensitizer, the nature of the photo/sonosensitizer (i.e., cationic or anionic), the strain being treated, and the laser and US parameters. The best results obtained were for MRSA, where the combined treatment (SPDT) using MSN@IR780 caused a 4.1-log reduction in bacterial cell viability, and inhibited post-treatment biofilm formation by 45%. For the remaining tested strains, IR780 iodide-mediated PDT and combined PDT and SDT, were more efficient in reducing the bacterial cell viability, compared to MSN@IR780-mediated PDT, SDT, and SPDT, which could be due to the cationic nature of IR780, which facilitated the uptake of IR780 iodide into bacterial cells. MSN@IR780 surface charge was not tested, but probably it is less cationic than IR780 iodide, and thereby affected the uptake of MSN@IR780 by bacterial cells. Despite this, encapsulating IR780 iodide in MSN has many advantages over using IR780 iodide in free form, such as overcoming its hydrophobicity and increasing its stability, which will make it more suitable for clinical application.

Future work will focus on the functionalization of MSN@IR780 to enhance their uptake by bacteria. This may include modifying their surface charge, conjugating them with antimicrobial peptides and/or targeting entities, which is expected to result in enhanced PDT and SDT results, and enhanced anti-biofilm capability of these nanoparticles. In addition to that, further studies will be conducted to study the up-

take of MSN@IR780 by bacteria, to examine the leakage of IR780 iodide from MSN, to assess the photostability of the nanoparticles, and to understand the bacterial cell death mechanisms by MSN@IR780-mediated PDT and SDT.

6.1 List of Publications Produced from the Thesis

1. Inactivation of planktonic cells and inhibitory effect on post-treatment biofilm formation of methicillin-resistant *Staphylococcus aureus* by photodynamic treatment with IR780 iodide loaded mesoporous silica nanoparticles and near infrared light H. Z. Alagha, M. Gülsoy, *Journal of Microbiological Methods*, Vol. 211, pp. 106773, 2023.

REFERENCES

1. Murray, C. J., K. S. Ikuta, F. Sharara, L. Swetschinski, *et al.*, "Global burden of bacterial antimicrobial resistance in 2019: a systematic analysis," *The Lancet*, Vol. 399, pp. 629–655, Feb 2022.

2. Pulingam, T., T. Parumasivam, A. M. Gazzali, A. M. Sulaiman, *et al.*, "Antimicrobial resistance: Prevalence, economic burden, mechanisms of resistance and strategies to overcome," *European Journal of Pharmaceutical Sciences*, Vol. 170, p. 106103, Mar 2022.

3. Zhu, Y., W. E. Huang, and Q. Yang, "Clinical perspective of antimicrobial resistance in bacteria," *Infection and Drug Resistance*, pp. 735–746, Dec 2022.

4. Maisch, T., "Resistance in antimicrobial photodynamic inactivation of bacteria," *Photochemical & Photobiological Sciences*, Vol. 14, pp. 1518–1526, Aug 2015.

5. Behzadpour, N., N. Sattarahmady, and N. Akbari, "Antimicrobial photothermal treatment of pseudomonas aeruginosa by a carbon nanoparticles-polypyrrole nanocomposite," *Journal of Biomedical Physics & Engineering*, Vol. 9, p. 661, Dec 2019.

6. Xu, Q., W. Xiu, Q. Li, Y. Zhang, *et al.*, "Emerging nanosonosensitizers augment sonodynamic-mediated antimicrobial therapies," *Materials Today Bio*, p. 100559, Apr 2023.

7. Dai, T., Y.-Y. Huang, and M. R. Hamblin, "Photodynamic therapy for localized infections—state of the art," *Photodiagnosis and Photodynamic Therapy*, Vol. 6, pp. 170–188, Sep-Dec 2009.

8. Lee, A. S., H. De Lencastre, J. Garau, J. Kluytmans, *et al.*, "Methicillin-resistant staphylococcus aureus," *Nature Reviews Disease Primers*, Vol. 4, pp. 1–23, May 2018.

9. Enright, M. C., D. A. Robinson, G. Randle, E. J. Feil, *et al.*, "The evolutionary history of methicillin-resistant staphylococcus aureus (mrsa)," *Proceedings of the National Academy of Sciences*, Vol. 99, pp. 7687–7692, May 2002.

10. Aloush, V., S. Navon-Venezia, Y. Seigman-Igra, S. Cabili, *et al.*, "Multidrug-resistant pseudomonas aeruginosa: risk factors and clinical impact," *Antimicrobial Agents and Chemotherapy*, Vol. 50, pp. 43–48, Jan 2006.

11. Driscoll, J. A., S. L. Brody, and M. H. Kollef, "The epidemiology, pathogenesis and treatment of pseudomonas aeruginosa infections," *Drugs*, Vol. 67, pp. 351–368, Feb 2007.

12. Matos, E. C. O. d., R. B. Andriolo, Y. C. Rodrigues, P. D. L. d. Lima, *et al.*, "Mortality in patients with multidrug-resistant pseudomonas aeruginosa infections: a meta-analysis," *Revista da Sociedade Brasileira de Medicina Tropical*, Vol. 51, pp. 415–420, Jul-Aug 2018.

13. *Multidrug-resistant Pseudomonas aeruginosa*, CDC, 2022. Available: https://arpsp.cdc.gov/profile/antibiotic-resistance/mdr-pseudomonas-aeruginosa?redirect=true.

14. Cieplik, F., D. Deng, W. Crielaard, and W. a. Buchalla, "Antimicrobial photodynamic therapy–what we know and what we don't," *Critical Reviews in Microbiology*, Vol. 44, pp. 571–589, Sep 2018.

15. Kessel, D., "Photodynamic therapy: from the beginning," *Photodiagnosis and Photodynamic Therapy*, Vol. 1, pp. 3–7, May 2004.

16. Jori, G., C. Fabris, M. Soncin, S. Ferro, *et al.*, "Photodynamic therapy in the treatment of microbial infections: basic principles and perspective applications," *Lasers in Surgery and Medicine: The Official Journal of the American Society for Laser Medicine and Surgery*, Vol. 38, pp. 468–481, Jun 2006.

17. Rosa, L. P., and F. C. da Silva, "Antimicrobial photodynamic therapy: a new therapeutic option to combat infections," *Journal of Medical Microbiology & Diagnosis*, Vol. 3, p. 1, Aug 2014.

18. Fu, X.-j., Y. Fang, M. Yao, *et al.*, "Antimicrobial photodynamic therapy for methicillin-resistant staphylococcus aureus infection," *BioMed Research International*, Vol. 2013, Feb 2013.

19. Topaloglu, N., M. Gulsoy, and S. Yuksel, "Antimicrobial photodynamic therapy of resistant bacterial strains by indocyanine green and 809-nm diode laser," *Photomedicine and Laser Surgery*, Vol. 31, pp. 155–162, Apr 2013.

20. Songca, S. P., O. S. Oluwafemi, and A. T. Bamidele, "Application of porphyrins in antibacterial photodynamic therapy," *Free Radical Biology and Medicine*, Vol. 100, p. S194, Nov 2016.

21. Kashef, N., and M. R. Hamblin, "Can microbial cells develop resistance to oxidative stress in antimicrobial photodynamic inactivation?," *Drug Resistance Updates*, Vol. 31, pp. 31–42, Mar 2017.

22. Quirk, B. J., G. Brandal, S. Donlon, J. C. Vera, *et al.*, "Photodynamic therapy (pdt) for malignant brain tumors–where do we stand?," *Photodiagnosis and Photodynamic Therapy*, Vol. 12, pp. 530–544, Sep 2015.

23. *Photodynamic Therapy to Treat Cancer*, National Cancer Institute, 2021. Available: https://www.cancer.gov/about-cancer/treatment/types/photodynamic-therapy.

24. Rosenthal, I., J. Z. Sostaric, and P. Riesz, "Sonodynamic therapy—-a review of the synergistic effects of drugs and ultrasound," *Ultrasonics Sonochemistry*, Vol. 11, pp. 349–363, Sep 2004.

25. Kuroki, M., K. Hachimine, H. Abe, H. Shibaguchi, *et al.*, "Sonodynamic therapy of cancer using novel sonosensitizers," *Anticancer Research*, Vol. 27, pp. 3673–3677, Nov 2007.

26. Serpe, L., and F. Giuntini, "Sonodynamic antimicrobial chemotherapy: First steps towards a sound approach for microbe inactivation," *Journal of Photochemistry and Photobiology B: Biology*, Vol. 150, pp. 44–49, SEP 2015.

27. Xu, H., X. Zhang, R. Han, P. Yang, *et al.*, "Nanoparticles in sonodynamic therapy: state of the art review," *RSC Advances*, Vol. 6, pp. 50697–50705, MAy 2016.

28. Nakonechny, F., M. Nisnevitch, Y. Nitzan, M. Nisnevitch, *et al.*, "Sonodynamic excitation of rose bengal for eradication of gram-positive and gram-negative bacteria," *BioMed Research International*, Vol. 2013, May 2013.

29. Harris, F., S. R. Dennison, and D. A. Phoenix, "Using sound for microbial eradication–light at the end of the tunnel?," *FEMS Microbiology Letters*, Vol. 356, pp. 20–22, Jul 2014.

30. Zhuang, D., C. Hou, L. Bi, J. Han, *et al.*, "Sonodynamic effects of hematoporphyrin monomethyl ether on staphylococcus aureus in vitro," *FEMS Microbiology Letters*, Vol. 361, pp. 174–180, Dec 2014.

31. Wang, X., M. Ip, A. W. Leung, and C. Xu, "Sonodynamic inactivation of methicillin-resistant staphylococcus aureus in planktonic condition by curcumin under ultrasound sonication," *Ultrasonics*, Vol. 54, pp. 2109–2114, Dec 2014.

32. Wang, X., M. Ip, A. W. Leung, Z. Yang, *et al.*, "Sonodynamic action of curcumin on foodborne bacteria bacillus cereus and escherichia coli," *Ultrasonics*, Vol. 62, pp. 75–79, Sep 2015.

33. Wang, X., A. W. Leung, H. Hua, C. Xu, *et al.*, "Sonodynamic action of hypocrellin b on biofilm-producing staphylococcus epidermidis in planktonic condition," *The Journal of the Acoustical Society of America*, Vol. 138, pp. 2548–2553, Oct 2015.

34. Roy, J., V. Pandey, I. Gupta, and H. Shekhar, "Antibacterial sonodynamic therapy: current status and future perspectives," *ACS Biomaterials Science & Engineering*, Vol. 7, pp. 5326–5338, Dec 2021.

35. Wang, R., Q. Liu, A. Gao, N. Tang, *et al.*, "Recent developments of sonodynamic therapy in antibacterial application," *Nanoscale*, Vol. 14, pp. 12999–13017, Sep 2022.

36. Allison, R. R., G. H. Downie, R. Cuenca, X.-H. Hu, *et al.*, "Photosensitizers in clinical pdt," *Photodiagnosis and Photodynamic Therapy*, Vol. 1, pp. 27–42, May 2004.

37. Kudinova, N. V., and T. T. Berezov, "Photodynamic therapy of cancer: Search for ideal photosensitizer," *Biochemistry (Moscow) Supplement Series B: Biomedical Chemistry*, Vol. 4, pp. 95–103, Mar 2010.

38. Higgins, S. L. H., and K. J. Brewer, "Designing red-light-activated multifunctional agents for the photodynamic therapy," *Angew. Chem. Int. Ed Engl.*, Vol. 51, pp. 11420–11422, Nov 2012.

39. Zhang, C., T. Liu, Y. Su, S. Luo, *et al.*, "A near-infrared fluorescent heptamethine indocyanine dye with preferential tumor accumulation for in vivo imaging," *Biomaterials*, Vol. 31, pp. 6612–6617, Sep 2010.

40. Yang, Y., and C. Yu, "Advances in silica based nanoparticles for targeted cancer therapy," *Nanomedicine: Nanotechnology, Biology and Medicine*, Vol. 12, pp. 317–332, Feb 2016.

41. Wang, Y., T. Liu, E. Zhang, S. Luo, *et al.*, "Preferential accumulation of the near infrared heptamethine dye ir-780 in the mitochondria of drug-resistant lung cancer cells," *Biomaterials*, Vol. 35, pp. 4116–4124, Apr 2014.

42. Yue, C., P. Liu, M. Zheng, P. Zhao, *et al.*, "Ir-780 dye loaded tumor targeting theranostic nanoparticles for nir imaging and photothermal therapy," *Biomaterials*, Vol. 34, pp. 6853–6861, Sep 2013.

43. Wang, K., Y. Zhang, J. Wang, A. Yuan, *et al.*, "Self-assembled ir780-loaded transferrin nanoparticles as an imaging, targeting and pdt/ptt agent for cancer therapy," *Scientific Reports*, Vol. 6, p. 27421, Jun 2016.

44. Tran, T. H., H. T. Nguyen, T. T. Phuong Tran, S. K. Ku, *et al.*, "Combined photothermal and photodynamic therapy by hyaluronic acid-decorated polypyrrole nanoparticles," *Nanomedicine*, Vol. 12, pp. 1511–1523, Jun 2017.

45. Nagy-Simon, T., M. Potara, A.-M. Craciun, E. Licarete, *et al.*, "Ir780-dye loaded gold nanoparticles as new near infrared activatable nanotheranostic agents for simultaneous photodynamic and photothermal therapy and intracellular tracking by surface enhanced resonant raman scattering imaging," *Journal of Colloid and Interface Science*, Vol. 517, pp. 239–250, May 2018.

46. Li, Y., Q. Zhou, Z. Deng, M. Pan, *et al.*, "Ir-780 dye as a sonosensitizer for sonodynamic therapy of breast tumor," *Scientific Reports*, Vol. 6, p. 25968, May 2016.

47. Jiang, C., H. Cheng, A. Yuan, X. Tang, *et al.*, "Hydrophobic ir780 encapsulated in biodegradable human serum albumin nanoparticles for photothermal and photodynamic therapy," *Acta Biomaterialia*, Vol. 14, pp. 61–69, Mar 2015.

48. Chen, Y., Z. Li, H. Wang, Y. Wang, *et al.*, "Ir-780 loaded phospholipid mimicking homopolymeric micelles for near-ir imaging and photothermal therapy of pancreatic cancer," *ACS Applied Materials & Interfaces*, Vol. 8, pp. 6852–6858, Mar 2016.

49. Chen, J., H. Luo, Y. Liu, W. Zhang, *et al.*, "Oxygen-self-produced nanoplatform for relieving hypoxia and breaking resistance to sonodynamic treatment of pancreatic cancer," *ACS Nano*, Vol. 11, pp. 12849–12862, Dec 2017.

50. Huang, B., L. Wang, K. Tang, S. Chen, *et al.*, "Ir780 based sonotherapeutic nanoparticles to combat multidrug-resistant bacterial infections," *Frontiers in Chemistry*, Vol. 10, Jan 2022.

51. Xu, T., W. Liu, Z. Li, B. Wang, *et al.*, "Photothermal and selective microbial inactivation behaviors of gluconamide-coated ir780 nanoparticles," *Colloids and Surfaces B: Biointerfaces*, Vol. 222, p. 113126, Feb 2023.

52. Lucky, S. S., K. C. Soo, and Y. Zhang, "Nanoparticles in photodynamic therapy," *Chemical Reviews*, Vol. 115, pp. 1990–2042, Feb 2015.

53. Bekmukhametova, A., H. Ruprai, J. M. Hook, D. Mawad, *et al.*, "Photodynamic therapy with nanoparticles to combat microbial infection and resistance," *Nanoscale*, Vol. 12, pp. 21034–21059, Oct 2020.

54. Ghasemi, M., K. Khorsandi, and Z. Kianmehr, "Photodynamic inactivation with curcumin and silver nanoparticles hinders pseudomonas aeruginosa planktonic and biofilm formation: evaluation of glutathione peroxidase activity and ros production," *World Journal of Microbiology and Biotechnology*, Vol. 37, p. 149, Aug 2021.

55. Silvestre, A. L. P., L. D. Di Filippo, J. F. Besegato, S. R. de Annunzio, *et al.*, "Current applications of drug delivery nanosystems associated with antimicrobial photodynamic therapy for oral infections," *International Journal of Pharmaceutics*, Vol. 592, p. 120078, Jan 2021.

56. Ferrisse, T. M., L. M. Dias, A. B. de Oliveira, C. C. Jordão, *et al.*, "Efficacy of antimicrobial photodynamic therapy mediated by photosensitizers conjugated with inorganic nanoparticles: Systematic review and meta-analysis," *Pharmaceutics*, Vol. 14, p. 2050, Sep 2022.

57. Badran, Z., B. Rahman, P. De Bonfils, P. Nun, *et al.*, "Antibacterial nano-photosensitizers in photodynamic therapy: an update," *Drug Discovery Today*, p. 103493, Apr 2023.

58. Fabio, G. B., B. A. Martin, L. F. Dalmolin, and R. F. V. Lopez, "Antimicrobial photodynamic therapy and the advances impacted by the association with nanoparticles," *Journal of Drug Delivery Science and Technology*, p. 104147, Feb 2023.

59. Garapati, C., S. H. Boddu, S. Jacob, K. M. Ranch, *et al.*, "Photodynamic therapy: A special emphasis on nanocarrier-mediated delivery of photosensitizers in antimicrobial therapy," *Arabian Journal of Chemistry*, p. 104583, Apr 2023.

60. Tang, F., L. Li, and D. Chen, "Mesoporous silica nanoparticles: synthesis, biocompatibility and drug delivery," *Advanced Materials*, Vol. 24, pp. 1504–1534, Mar 2012.

61. Mamaeva, V., C. Sahlgren, and M. Lindén, "Mesoporous silica nanoparticles in medicine—recent advances," *Advanced Drug Delivery Reviews*, Vol. 65, pp. 689–702, May 2013.

62. Tarn, D., C. E. Ashley, M. Xue, E. C. Carnes, *et al.*, "Mesoporous silica nanoparticle nanocarriers: biofunctionality and biocompatibility," *Accounts of Chemical Research*, Vol. 46, pp. 792–801, Mar 2013.

63. Wang, Y., Q. Zhao, N. Han, L. Bai, *et al.*, "Mesoporous silica nanoparticles in drug delivery and biomedical applications," *Nanomedicine: Nanotechnology, Biology and Medicine*, Vol. 11, pp. 313–327, Feb 2015.

64. Ahmed, H., S. S. Gomte, A. Prabakaran, M. Agrawal, *et al.*, "Biomedical applications of mesoporous silica nanoparticles as a drug delivery carrier," *Journal of Drug Delivery Science and Technology*, p. 103729, Oct 2022.

65. Xu, Q., Y. Yang, J. Lu, Y. Lin, *et al.*, "Recent trends of mesoporous silica-based nanoplatforms for nanodynamic therapies," *Coordination Chemistry Reviews*, Vol. 469, p. 214687, Oct 2022.

66. Planas, O., R. Bresolí-Obach, J. Nos, T. Gallavardin, *et al.*, "Synthesis, photophysical characterization, and photoinduced antibacterial activity of methylene blue-loaded amino-and mannose-targeted mesoporous silica nanoparticles," *Molecules*, Vol. 20, pp. 6284–6298, Apr 2015.

67. Yang, Y., and C. Yu, "Advances in silica based nanoparticles for targeted cancer therapy," *Nanomedicine: Nanotechnology, Biology and Medicine*, Vol. 12, pp. 317–332, Feb 2016.

68. Castillo, R. R., M. Colilla, and M. Vallet-Regí, "Advances in mesoporous silica-based nanocarriers for co-delivery and combination therapy against cancer," *Expert Opinion on Drug Delivery*, Vol. 14, pp. 229–243, Feb 2017.

69. Bayir, S., A. Barras, R. Boukherroub, S. Szunerits, *et al.*, "Mesoporous silica nanoparticles in recent photodynamic therapy applications," *Photochemical & Photobiological Sciences*, Vol. 17, pp. 1651–1674, Nov 2018.

70. Paramanantham, P., B. Siddhardha, S. L. Sb, A. Sharan, *et al.*, "Antimicrobial photodynamic therapy on staphylococcus aureus and escherichia coli using malachite green encapsulated mesoporous silica nanoparticles: An in vitro study," *PeerJ*, Vol. 7, p. e7454, Sep 2019.

71. Parasuraman, P., A. P. Antony, A. Sharan, B. Siddhardha, *et al.*, "Antimicrobial photodynamic activity of toluidine blue encapsulated in mesoporous silica nanoparticles against pseudomonas aeruginosa and staphylococcus aureus," *Biofouling*, Vol. 35, pp. 89–103, Jan 2019.

72. Mirzahosseinipour, M., K. Khorsandi, R. Hosseinzadeh, M. Ghazaeian, *et al.*, "Antimicrobial photodynamic and wound healing activity of curcumin encapsulated in silica nanoparticles," *Photodiagnosis and Photodynamic Therapy*, Vol. 29, p. 101639, Mar 2020.

73. Barkat, A., S. Beg, S. K. Panda, K. S. Alharbi, *et al.*, "Functionalized mesoporous silica nanoparticles in anticancer therapeutics," in *Seminars in Cancer Biology*, Vol. 69, pp. 365–375, Feb 2021.

74. Er, H., E. Bakay, A. Pamukçu, D. Ş. Karaman, *et al.*, "Antibiofilm activity of photodynamic therapy with a novel dual photosensitizer incorporated mesoporous silica nanoparticle and laser system," in *European Conference on Biomedical Optics*, pp. EW1A–4, Optica Publishing Group, 2021.

75. Bakay, E., A. Pamukçu, Ö. Yıldız, D. S. Karaman, *et al.*, "The effect of photodynamic therapy mediated by mesoporous silica nanoparticles containing chlorin e6 and indocyanine green on 3d prostate cancer model," in *2022 Medical Technologies Congress (TIPTEKNO)*, pp. 1–4, IEEE, 2022.

76. Busa, P., R. K. Kankala, J.-P. Deng, C.-L. Liu, and C.-H. Lee, "Conquering cancer multi-drug resistance using curcumin and cisplatin prodrug-encapsulated mesoporous silica nanoparticles for synergistic chemo-and photodynamic therapies," *Nanomaterials*, Vol. 12, p. 3693, Oct 2022.

77. Slapak, E. J., M. El Mandili, M. F. Bijlsma, and C. A. Spek, "Mesoporous silica nanoparticle-based drug delivery systems for the treatment of pancreatic cancer: a systematic literature overview," *Pharmaceutics*, Vol. 14, p. 390, Feb 2022.

78. Yu, X., X. Wang, and A. Yamazaki, "Mn-si-based nanoparticles-enhanced inhibitory effect on tumor growth and metastasis in photo-immunotherapy," *Colloids and Surfaces B: Biointerfaces*, Vol. 226, p. 113314, Jun 2023.

79. Wang, J., Y. Jiao, and Y. Shao, "Mesoporous silica nanoparticles for dual-mode chemo-sonodynamic therapy by low-energy ultrasound," *Materials*, Vol. 11, p. 2041, Oct 2018.

80. Guo, J., Y. Xu, M. Liu, J. Yu, *et al.*, "An msn-based synergistic nanoplatform for root canal biofilm eradication via fenton-enhanced sonodynamic therapy," *Journal of Materials Chemistry B*, Vol. 9, pp. 7686–7697, Sep 2021.

81. Jin, Z.-h., N. Miyoshi, K. Ishiguro, S.-i. Umemura, *et al.*, "Combination effect of photodynamic and sonodynamic therapy on experimental skin squamous cell carcinoma in c3h/hen mice," *The Journal of Dermatology*, Vol. 27, pp. 294–306, May 2000.

82. Kolarova, H., K. Tomankova, R. Bajgar, P. Kolar, and R. Kubinek, "Photodynamic and sonodynamic treatment by phthalocyanine on cancer cell lines," *Ultrasound in Medicine & Biology*, Vol. 35, pp. 1397–1404, Aug 2009.

83. Wang, X., W. Zhang, Z. Xu, Y. Luo, *et al.*, "Sonodynamic and photodynamic therapy in advanced breast carcinoma: a report of 3 cases," *Integrative Cancer Therapies*, Vol. 8, pp. 283–287, Sep 2009.

84. Tserkovsky, D., E. Alexandrova, V. Chalau, and Y. P. Istomin, "Effects of combined sonodynamic and photodynamic therapies with photolon on a glioma c6 tumor model," *Experimental Oncology*, Dec 2012.

85. Li, Q., X. Wang, P. Wang, K. Zhang, *et al.*, "Efficacy of chlorin e6-mediated sonophotodynamic therapy on 4t1 cells," *Cancer Biotherapy and Radiopharmaceuticals*, Vol. 29, pp. 42–52, Feb 2014.

86. Xu, F., M. Hu, C. Liu, and S. K. Choi, "Yolk-structured multifunctional up-conversion nanoparticles for synergistic photodynamic–sonodynamic antibacterial resistance therapy," *Biomaterials Science*, Vol. 5, pp. 678–685, Mar 2017.

87. Alves, F., G. Gomes Guimaraes, N. Mayumi Inada, S. Pratavieira, *et al.*, "Strategies to improve the antimicrobial efficacy of photodynamic, sonodynamic, and sonophotodynamic therapies," *Lasers in Surgery and Medicine*, Vol. 53, pp. 1113–1121, Oct 2021.

88. Ziental, D., M. Wysocki, M. Michalak, J. Dlugaszewska, *et al.*, "The dual synergy of photodynamic and sonodynamic therapy in the eradication of methicillin-resistant staphylococcus aureus," *Applied Sciences*, Vol. 13, p. 3810, Mar 2023.

89. Entradas, T., S. Waldron, and M. Volk, "The detection sensitivity of commonly used singlet oxygen probes in aqueous environments," *Journal of Photochemistry and Photobiology B: Biology*, Vol. 204, p. 111787, Mar 2020.

90. Dahl, T., W. R. Midden, and D. Neckers, "Comparison of photodynamic action by rose bengal in gram-positive and gram-negative bacteria," *Photochemistry and Photobiology*, Vol. 48, pp. 607–612, Nov 1988.

91. Usacheva, M. N., M. C. Teichert, and M. A. Biel, "Comparison of the methylene blue and toluidine blue photobactericidal efficacy against gram-positive and gram-negative microorganisms," *Lasers in Surgery and Medicine: The Official Journal of the American Society for Laser Medicine and Surgery*, Vol. 29, pp. 165–173, Aug 2001.

92. George, S., M. R. Hamblin, and A. Kishen, "Uptake pathways of anionic and cationic photosensitizers into bacteria," *Photochemical & Photobiological Sciences*, Vol. 8, pp. 788–795, Jun 2009.

93. Pál, C., B. Papp, and V. Lázár, "Collateral sensitivity of antibiotic-resistant microbes," *Trends in Microbiology*, Vol. 23, pp. 401–407, July 2015.

94. Costley, D., H. Nesbitt, N. Ternan, J. Dooley, *et al.*, "Sonodynamic inactivation of gram-positive and gram-negative bacteria using a rose bengal–antimicrobial peptide conjugate," *International Journal of Antimicrobial Agents*, Vol. 49, pp. 31–36, Jan 2017.

95. Lin, Y.-S., and C. L. Haynes, "Impacts of mesoporous silica nanoparticle size, pore ordering, and pore integrity on hemolytic activity," *Journal of the American Chemical Society*, Vol. 132, pp. 4834–4842, Apr 2010.

96. Tang, H. M., M. R. Hamblin, and C. M. Yow, "A comparative in vitro photoinactivation study of clinical isolates of multidrug-resistant pathogens," *Journal of Infection and Chemotherapy*, Vol. 13, pp. 87–91, Apr 2007.

97. Silhavy, T. J., D. Kahne, and S. Walker, "The bacterial cell envelope," *Cold Spring Harbor perspectives in Biology*, Vol. 2, p. a000414, May 2010.

98. Sahu, K., H. Bansal, C. Mukherjee, M. Sharma, *et al.*, "Atomic force microscopic study on morphological alterations induced by photodynamic action of toluidine blue o in staphylococcus aureus and escherichia coli," *Journal of photochemistry and Photobiology B: Biology*, Vol. 96, pp. 9–16, Jul 2009.

99. Usacheva, M., B. Layek, S. S. Rahman Nirzhor, S. Prabha, *et al.*, "Nanoparticle-mediated photodynamic therapy for mixed biofilms," *Journal of Nanomaterials*, Vol. 2016, Aug 2016.

100. Ghaffari, S., A. S. K. Sarp, D. Lange, and M. Gülsoy, "Potassium iodide potentiated photodynamic inactivation of enterococcus faecalis using toluidine blue: Comparative analysis and post-treatment biofilm formation study," *Photodiagnosis and Photodynamic Therapy*, Vol. 24, pp. 245–249, Dec 2018.

101. Hu, X.-Y., M. Logue, and N. Robinson, "Antimicrobial resistance is a global problem–a uk perspective," *European Journal of Integrative Medicine*, Vol. 36, p. 101136, Jun 2020.

102. Sehmi, S. K., S. Noimark, S. D. Pike, J. C. Bear, *et al.*, "Enhancing the antibacterial activity of light-activated surfaces containing crystal violet and zno nanoparticles: investigation of nanoparticle size, capping ligand, and dopants," *ACS Omega*, Vol. 1, pp. 334–343, Sep 2016.